2017

Evaluation of Compositional Effects on Gas-Oil Miscibility and Gas-Assisted Gravity Drainage (GAGD) EOR Process

Mohamed Al Riyami
Louisiana State University and Agricultural and Mechanical College

EVALUATION OF COMPOSITIONAL EFFECTS ON GAS-OIL MISCIBILITY AND GAS-ASSISTED GRAVITY DRAINAGE (GAGD) EOR PROCESS

A Dissertation

Submitted to the Graduate Faculty of the
Louisiana State University and
Agricultural and Mechanical College
in partial fulfillment of the
requirements for the degree of
Doctor of Philosophy

in

The Craft & Hawkins Department of Petroleum Engineering

by
Mohamed N. Al Riyami
B.Sc (Physics), Leeds University, UK, 2002
M.Sc (Petroleum Engineering), Imperial College, UK, 2004
May 2017

This dissertation is dedicated ..

To my loving parents, Latifa and Nasser Al Riyami whose words of encouragement and push for tenacity ring in my ears.

To my lovely wife Hala and my daughters Jude and Siba, for supporting me during my time in LSU.

To my my brothers and sisters Mundeer, Ahmed, Houmud, Moza and Sakina for believing in me.

Acknowledgments

I would like to thank Dr. Dandina Rao for his guidance and mentorship throughout my PhD journey. I thank him for encouraging me to explore different horizons and believe in what I do.

I would like to recognize the impact Dr. N Kumar had in me. I thank him for teaching me to go back to fundamentals and understand the root of any problem.

I would like to thank my committee members, Dr. T. Karsten and Dr. Sears , who agreed to serve as my committee members. I thank them for providing the support and recommendations to complete this study.

Thank you to all my amazing friends in Louisiana for making my stay pleasant and memorable. Special acknowledgment goes to my fellow graduate students who helped me with this work: Paulina Mwangi, Sandeep Gubta, Foad Haeri, Bikash Saikia and Mohamed Abdul Rahim.

I would like also to acknowledge the following: Fulbright, Ministry of Higher Education (MOHE)Oman, Petroleum Development Oman (PDO) and Louisiana State University (LSU) for providing financial assistance during my PhD in LSU.

Finally I would like to thank my inspirational parents for their sacrifice and unconditional love, my loving wife for her support and my siblings for their encouragement.

Table of Contents

List of Tables

List of Figures

Abstract

The Vanishing interface technique (VIT), offers fast and accurate determination of minimum miscibility pressure (MMP) between the reservoir crude oil and the various gases injected for enhancing oil recovery (EOR). The technique is based on miscibility being the condition where an interface between the injected fluid and the reservoir crude oil vanishes. This research has evaluated the effect of the gas-oil ratio on zero-IFT pressure. VIT experiments were simulated using an equation of state (EOS) and the Parachor model. This work proves the robustness of VIT in estimating miscibility pressures for gas injection EOR projects.

Also this work presents a simple method for estimating near-miscibility pressures (NMP) that are based on a gas-oil interfacial tension (IFT) calculation procedure. The method evaluates near miscibility conditions at low (as against zero) IFT and relies only on using EOS and the Parachor model. The results show that NMP estimation method is reasonably accurate, MMPs agreed with slim tube MMPs within 7 %.

In recent years CO_2- based EOR projects have been steadily gaining ground over all other EOR processes. However, due to limited supply of pure CO_2 availability, an alternative option is to utilize emitted flue gas. Miscibility pressures were successfully determined using VIT of different gas mixtures with n-decane (nC_{10}), namely CO_2, N_2, CO_2 - N_2 (85 %- 15 %) and CO_2- N_2 (15 %- 85 %). This proves the ease of applicability of VIT to evaluate the effect of injected gas type and composition on gas-oil miscibility.

Earlier reported Gas-Assisted Gravity Drainage (GAGD) work using CO_2 for gas injection resulted in good oil recoveries. To expand the applicability of using GAGD in areas where there is limited CO_2, an experimental study was conducted to examine the effect of using different gases on GAGD performance. CO_2, N_2 and flue gas were used with nC_{10} as the oil phase, in conducting high-pressure corefloods. The floods

resulted in oil recoveries in the range of 30-49 % (immiscible mode) of remaining oil after water floods. This work has demonstrated the superiority of GAGD over the other gas injection methods currently practiced, such as WAG and CGI, using CO_2 or any other gas.

Chapter 1
Introduction

This chapter describes the motivation behind the present study, the proposed research objectives and the structure of this dissertation. The subsequent chapters will discuss the topics in depth.

1.1 Description of the Problem

Enhanced oil recovery is referred to the methods/processes that involve injecting flueids to complement the natural energy in the reservoir to displace the remaining oil in place (Walsh and Lake 2008). Improved oil recovery on the other hand includes EOR methods, new drilling, well technologies and smart reservoir management (Rao 2001).

They are three major categories of EOR process reported in the literature: Thermal recovery, gas injection and chemical injection (Walsh and Lake 2008). Thermal recovery, applies to heavy oil, where the process is based on increasing the temperature to reduce the viscosity of the hydrocarbon. Gas injection, is a fluid injection method that recovers oil via displacement involving mass transfer mechanisms. Chemical recovery methods, either increase capillary number though IFT reduction or change the mobility ratio through polymer or alkaline or surfactant flooding.

According to Vladimir and Eduardo (2010) EOR by gas injection projects exhibited a growth in trend since year 2000, mainly due to increase in CO_2 injection projects. CO_2 injection process is mainly depends on interaction between the gas (CO_2)with the crude oil. It is also important to highlight that Carbon dioxide (CO_2) is not directly miscible on first contact with most crude oils at reservoir conditions. However,

through continuous interaction with reservoir oil and choosing the right operating conditions, such as pressure above minimum miscibility pressure (MMP), miscibility can be achieved.

MMP condition can be determined experimentally using methods such as slim tube (ST) and rising bubble (RB). Slim tube method is based on injecting a gas in a narrow tube packed with sand or glass beads, saturated with oil at reservoir temperature and recording oil recovery. Then MMP is determined by identifying the break point on the slope of the oil vs. pressure plot (Stalkup 1983). As for the rising bubble method, it depends on observing the shape of the bubbles of injected gas in a visual high pressure cell filled with reservoir crude oil. The pressure at which a rising bubble vanishes in a column of oil is known as the MMP (Elsharkawy, Poettmann, and Christiansen 1996). These techniques mentioned above are widely used, and produce reasonable results but with limitations (Rao 1997).

Rao (1997) proposed a technique known as vanishing interface technique (VIT). The technique relates miscibility to the point of vanishing interfacial tension, by measuring gas-oil interfacial surface tension (IFT) as a function of pressure and extrapolating the plot to zero IFT to determine MMP. The technique allows fast and cost effective determination of minimum miscibility pressure (MMP) and minimum miscibility enrichment (MME). Although technique is promising and number of experiments proved the practicality of the technique and credibility of the results, it needs to address few concerns that were raised by other researchers.

In gas injection process, large density difference between the injected gas and the reservoir crude oil results in gravity segregation. The adverse mobility ratio due to large viscosity differences between oil and gas in all gas injection processes results in poor sweep efficiencies. A process of water-alternating-gas (WAG) was proposed (Christensen, stenby, and Skauge 2001) to solve the sweep problem, where gas is generally

injected in discrete slugs with intermittent slugs of water. This process demonstrated promising results in the laboratory but yielded disappointing performance when applied on a reservoir scale. As an alternative process Gas Assisted Gravity Drainage (GAGD) was proposed by Rao (2004). The method takes an advantage of natural segregation of injected gas from crude oil in the reservoir. It involves injection gas from the top of the reservoir and producing from the bottom of the reservoir through horizontal wells. Previous reported work have investigated the effect of wettability, fractures, gravity, injection depth and injection rate on GAGD. Although GAGD is a promising method, further work need to be done in assessing the effect of other factors such as different gas types, different rock type, fractured medium and wider range of kv and kh permeability on GAGD process.

Based on the discussion above and recognizing the importance of the gas injection in recovering remaining oil in place, the following can be summarized:

1. MMP is an important condition for gas miscible injection process.

2. There are some disagreements on the type of method used to measure or calculate MMP (Elsharkawy, Poettmann, and Christiansen 1996; Ayirala 2005; Orr and Jessen 2007).

3. Vanishing Interface Technique and its connection to miscibility pressure is an interesting concept that was proved to offer cheap and fast option to measure MMP or MME.

4. There is a lack of computational model that is based on IFT to determine miscibility pressure.

5. There is no study/evaluation based on coreflood on different gas type, especially flue gas on the performance of GAGD.

Therefore this research seeks to address some of the aspects mentioned earlier and evaluate flue gas on the performance of GAGD to improve gas injection recoveries.

1.2 Research Objectives

Miscibility pressure is an important parameter for EOR gas injection, therefore this dissertation addresses further the area of interfacial tension and miscibility pressure through VIT technique to build up on previous work done in the field. Then, it evaluates different aspect concerning GAGD. The primary objectives of the research are listed below:

1. Model VIT technique experiments and match previous reported data.
2. Assess the effect of gas composition and gas-oil ratio on miscibility pressures.
3. Develop a new calculation method/approach to determine near miscibility pressure (NMP) using interfacial tension.
4. Measure miscibility pressures for four systems, using VIT technique: CO_2-nC_{10}, N_2-nC_{10} ((N_2 15%- CO_2 85%)), CO_2-N_2-nC_{10} ((N_2 85%- $CO_2$15%)), and CO_2-N_2-nC_{10}.
5. Develop a framework for modeling VIT experiments that involve N_2 gas.
6. Evaluate the oil recovery performance of GAGD process using different gases N_2, CO_2 and flue gas.
7. Correlate the measured IFT with the measured oil recoveries from the tertiary GAGD core floods.
8. Compare this study work with other reported studies.

1.3 Methodology

To meet research objectives of this study a combination of computaional and experimental work was performed. To understand VIT method further and to shed clarification to the method, reported experiments were modeled using PR-EOS and Parachor model (Ayirala and Rao 2011; Sequeira). All EOS calculations were performed using a commercial software WinProp (Winprop 2013).

After performing number of IFT prediction using the framework suggested by this study, a new method to predict near miscible pressure based on IFT calculated data was suggested, using EOS, a parchor model and a cut-off IFT value.

To evaluate GAGD performance using different gas types and other factors, two type of experiments were performed:

1. VIT experiments to determine MMP of different gas-oil systems.

2. Gas floods, displacement tests, were conducted at high pressures and fixed temperature.

All VIT experiments were conducted using n-Dedcane and gas(CO_2, N_2 and flue gas). All flood experiments were conducted using n-Dedcane, brine, gas, and core rocks. Volumes, time, rates, pressures, pressure difference, recovery were either measured or determined during corefloods in order to evaluate the performance of GAGD.

1.4 Structure of the Dissertation

This dissertation consists of seven chapters. Chapter 1 is an introduction followed by Chapter 2, literature review and background of MMP, IFT and gas injection methods that relates to this study. Chapter 3, examines further VIT for MMP determination, and the effect of GOR on VIT experiments. Chapter 4 describes the new IFT based

method in calculating near miscbility pressure (NMP). This chapter demonstrates an alternative approach to determine NMP and provides examples of how to use the method and demonstrate the robustness of the method, by testing 12 different fluids and comparing the results to slim tube data. Chapter 5 describes experimental setup and experimental procedures used for measuring MMP via interfacial tension measurement and GAGD core flooding experiments. Also detailed description of VIT method measurements and modeling steps are presented. The experiments described were designed to meet the research objectives mentioned in section 1.2 . Chapter 6 summarizes the results of experiments, VIT and GAGD core floods, and VIT modeling performed in chapter 4. In this chapter the results are analyzed further and compared to earlier work. Chapter 7 summarizes the results of this study and suggests few recommendation for future research.

Chapter 2
Background and Literature Review

This chapter begins with an introduction about miscibility pressure, miscibility pressure measurement and computational methods followed by introduction about interfacial tension and it′s connection to miscibility pressure. Finally the chapter summarizes Gas Assisted Gravity Drainage process (GAGD) reported studies and an overview of some flue gas injection studies that will be used in later chapters.

2.1 Miscibility Pressure

Miscibility between two fluids can be generated by changing pressure or changing composition of a mixture. In petroleum literature, miscibility generated via changing pressure is usually referred as first or single contact miscibility while miscibility generated through changing composition in a displacement process is referred as multi-contact miscibility(Stalkup 1983). First contact miscibility (FCM) is a condition or a process, where the injected solvent/gas is directly miscible and forms a single phase with reservoir oil on first contact. Multiple contact miscibility (MCM) is a process where displacement is initially immiscible, but through multiple contacts of injected phase and oil phase in the reservoir, miscibility is achieved. Moreover, multi-contact miscibility displacement can be classified as vaporization gas drive, condensation gas drive or combined drive. Vaporization gas drive usually occurs at the front of an advancing gas, where the injected gas gets enriched by contacting fresh oil. Condensation gas drive occurs at the injection point, where the oil gets enriched by contacting injected rich gas. As for the combined drive, a condensing process at the front and vaporizing

mechanism at the tail is responsible of creating a critical mixture in the transition zone (Zick 1986; Stalkup 1983) .

2.1.1 Miscibility Pressure Measurement Techniques

There are few miscibility pressure measurement techniques used in the industry and mentioned in literature. However, only the following techniques will be discussed here:

- Slim tube.
- Raising bubble technique.
- Vanishing interface technique.

2.1.1.1 Slim tube

Slim tube is the oldest and most popular among the three techniques. The technique has been discussed comprehensively in literature when it comes to its specification, applicability, limitation and procedures (Ayirala 2005; Elsharkawy, Poettmann, and Christiansen 1996). A brife summary is provided here based on what is reported in litreture (Stalkup 1983; Elsharkawy, Poettmann, and Christiansen 1996; Danesh 1998). Slim tube consists of a long tube that contains either sand or glass beads. The default is the tube to be arranged vertically, usually looped. The tube is used to displace oil with a gas of known composition, and record, pressures (down and upstream), oil and gas recoveries and effluent composition. The typical procedure of slim tube technique is to: 1) Saturate the tube with oil. 2) Inject a gas at particular pressure. 3) Record the effluent composition, density and produced fluids. 4) Repeat the procedure at different pressures. All runs normally are stopped at 1.2 PV. 5) Ultimate oil recovery of different slim tube runs are plotted as a function pf pressure, see Figure 2.1 for atypical slim tube plot. 6) Miscibility pressure is determined at using a specific criteria either 100

%, 98 % recovery or when the plot of recovery vs pressure breaks or levels, see Figure 2.1 for a typical slim tube result plot.

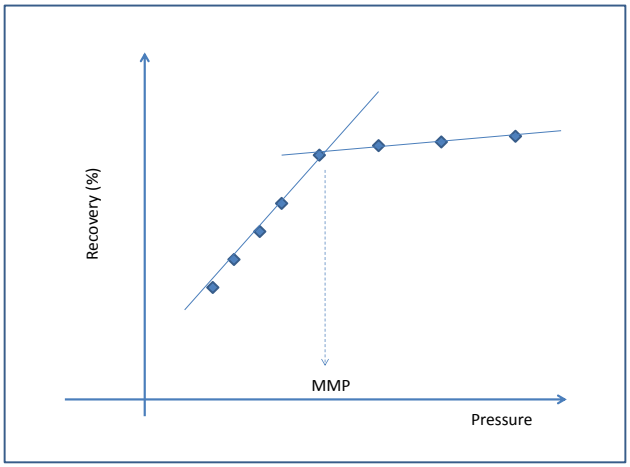

Figure 2.1: Typical slim tube results

Though there is a lot disagreement in terms of slim tube specification and MMP criteria (Ayirala 2005). The following reported to be acceptable parameters can be used. The length of the slim tube is between 10- 40 m, depending on gas used. Though some argue that the injection rates influence the recoveries, it has been recommended to use around 1.5- 2.5 m/hr. MMP is picked to be the pressure at the break over point seen in the recovery vs pressure plot, otherwise a point at 90 -95 % recovery occurs. Slim tube experiment can take anything between 1-3 weeks (Ayirala 2005; Elsharkawy, Poettmann, and Christiansen 1996).

2.1.1.2 Rising Bubble Apparatus (RBA)

Christiansen and Haines (1987) developed the Rising bubble method. The apparatus consist of vertical mounted tube that a bubble of gas can be observed through. Rising Bubble method can measure MMP up to 34-69 MPa and temperatures up to 300 oF

(Christiansen and Haines 1987). The method depends on observing the shape of the bubbles of injected gas in a visual high pressure cell filled with reservoir crude oil. Therefore the typical procedure is as follows: 1) the tube is filled with water then displaced with Oil. 2) A bubble if gas is introduced at the bottom and left to rise. 3) The raising bubble is monitored and recorded. 4) the process is repeated at different pressures and fixed temperature. The pressure at which a rising bubble vanishes in a column of oil is known as the MMP. The Rising Bubble method is cheaper, faster to give an approximate MMP, does not devour much oil, yields a thermodynamic multi-contact MMP and easy to use to correlate the behavior of MMP with other parameters such as temperature. However, MMP via RB is determined qualitatively, and provide no compositional, IFT or density data. Also, according to Zhou and Orr (1998), the method is less accurate with condensing mechanism drive and additional work is needed to test the reliability of the technique for multi-component systems that show condensing /vaporizing behavior.

2.1.1.3 Vanishing Interface Technique

Rao (1997) presented a new technique that is called Vanishing Interface Technique (VIT). The technique is based on measuring interfacial tension as a function of pressure or enrichment levels of injected phase. Typical VIT procedure include: 1) Filling a cell with gas at particular pressure and temperature. 2) Inject a drop of oil from the top of the cell. 3) Take image of the pendent drop after it reaches equilibrium. 4) process the images to determine IFT. 5) Repeat the process for 5-10 oil drops to get average IFT. 6) Repeat everything at different pressures. By extrapolating a plot of interfacial tension against pressure or composition of the injection phase to zero interfacial tension, MMP or MME can be obtained, see Figure 2.2 for an example of VIT plot.

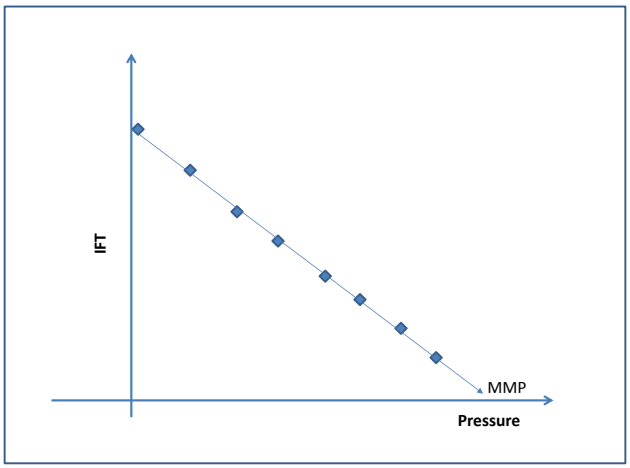

Figure 2.2: Example of VIT, IFT vs pressure plot

2.1.2 Miscibility Pressure Computational Techniques

Computational MMP techniques can be classified as analytical or numerical. The analytical methods provide an alternative to experimental data in determining minimum miscible pressure. Examples of some computational methods for MMP estimation based on Equation of state (EOS): multi-cell algorithm (Metcalf, Fussel, and Shelton 1973; Hearn and Whitson 1995; Ahmadi and Johns 2011), single mixing cell algorithm (Luks, Turek, and Baker 1987; Wang and Orr 1997), one dimensional compositional simulation (Zick 1986; Stalkup 1987), tie line (Nour and Lock 1988; Whitson and Michelsen 1989; Wang and Orr 1997) and tie line algorithm and Method of Characteristic (MOC) model (Dindoruk, Orr, and Johns 1997; Johns and Orr 1996; Wang and Orr 1997).

2.1.2.1 Mixing cell algorithms

this is a computational algorithm which allows the calculation of MMP. These can be classified as one mixing cell or multiple mixing cell. One mixing cell algorithms are based on forward and backward contacts performed in a single cell to calculate MMP

(Ayirala 2005). On the other hand multiple mixing cell algorithms/calculation, are based on multiple contacts in more than one cell.

2.1.2.2 1-D compositional simulation

this method mimics the flow in porous media that occurs in slim tube. A typical procedure involves, using a compositional simulation to predict recoveries of oil displacements by gas at different pressures. Disadvantages include computational time and numerical dispersion(Zick 1986; Stalkup 1983).

2.1.2.3 Tie line algorithm and Method of Characteristic (MOC)

The main principle is that all key tie-lines intersect each other in a multi-component system. Key tie-lines are first determined for various increasing pressures. Then MMP is defined as the pressure at which one of the key tie-lines becomes a critical tie- line, that is, a tangential tie- line of zero length to the critical locus. The main advantage of this method is that the computed MMEs and MMPs are dispersion-free. However the technique requires a well characterized equation of state (Ayirala 2005). .

2.2 Interfacial Tension

Interfacial tension (IFT) between phases at ambient and reservoir conditions are measured using different techniques, for example: pendent drop method, capillary rise technique and sessile drop method. These techniques are discussed in depth elsewhere (Ayirala 2005).

2.2.1 Interfacial Tension Prediction Models

Several models or correlations have been proposed to predict interfacial tension, for example, Parachor model (Schechter and Guo 1998), gradient theory (Xiang and Stenby. 1997), scaling law and mechanistic Parachor model (Ayirala 2005). However, several of these models suffer limitations (Ayirala 2005). The following are some IFT prediction models that are used in petroleum industry:

2.2.1.1 Parachor Model

Macleod (1923) suggested the following relation between gas-oil interfacial tension and pure component density phase difference as follows:

$$\sigma = [Pi(\rho_{\mathrm{l}} - \rho_{\mathrm{v}})]^4 \tag{2.1}$$

Where σ is IFT, Pi the Parachor constant for component i, $\mathrm{M_l}$ and ρ_{l} and ρ_{v} are the molar densities of the liquid and vapor phases.

Weinz and Katz (1943) extended the above relationship to a multicomponent hydrocarbon systems, where this model is widely used in petroleum industry for its simplicity.

$$\sigma = \sum_{i=1}^{n} [Pi(x\frac{\rho_{\mathrm{l}}}{M_{\mathrm{l}}} - y\frac{\rho_{\mathrm{v}}}{M_{\mathrm{v}}})]^4 \tag{2.2}$$

The Parachor model has been shown to produce a good match with the experimental data, for pure compounds and binary mixtures, but perform poorly in multicomponent hydrocarbon (Danesh 1998). The Parachor model under-predicts at low IFT

conditions and over-predicts at high IFT values with the most accurate results around 1 mN/m for the particular case reported (Danesh 1998).

Few researchers have attempted to modify the Parachor model mentioned earlier by changing the scaling exponent. Hough and stegemeir (1961) proposed to change scaling exponent m to 3.67, Lee and Chein (1984) proposed change of m to 3.91 and based on modern physics it was shown that m should be 3.88 (Schechter and Guo 1998).

2.2.1.2 Mechanistic Parachor model

Ayirala and Rao (2006) , modified the Parachor model and called it a mechanistic Parachor model. The model introduces a ratio of diffusivities between the fluid phases raised to an exponent into original Parachor model to include the mass transfer effect.

Details of how to use mechanistic Parachor model is described in detail in (Ayirala 2005).

$$\sigma = (D_A B / D_B A)^n \sum_{i=1}^{n} [Pi(x \frac{\rho_{\mathrm{l}}}{M_{\mathrm{l}}} - y \frac{\rho_{\mathrm{v}}}{M_{\mathrm{v}}})]^4 \tag{2.3}$$

2.3 Vanishing Interface Technique Experiments

Rao(1997) proposed Vanishing Interface Technique (VIT) to determine minimum miscibility pressure. The technique is based on measuring interfacial tension between oil (simulating residual oil) and gas (simulating injected or equilibrated gas), using pendent drop or/and capillary tube method. The technique connects miscibility to zero interfacial tension, by measuring interfacial tension (IFT) as a function of pressure and extrapolating the plot/data to zero IFT to determine miscibility pressure. Rao, vali-

dated the technique by comparing the results from VIT with slim tube results for two different Canadian reservoir cases,Rainbow and Gillwood using ethane and propane as injection gases. The study showed that the MMP measured were close to the ones measured using slim tube.

Rao and Lee (2002, 2003) used VIT method to determine minimum miscibility pressure and gas composition for Canadian Tera Nova offshore field. they used three different gas compositions with Terra Nova crude oil. They reported MMP values of 62.9, 57.8 and 31.8 for 9.08- 9.49 %, 21.24- 21.65 % and 28.9- 29.8 % of C_2+ gas enrichment respectively. In addition they conducted injection gas optimization, where C_2+ was 32%. Rao and Lee (2003, utilized the experimental results and compared them to slim tube and raising bubble results.

Ayirala and Rao (2006) later measured interfacial tension for standard gas-oil system of known phase behavior characteristics (CO_2-nC_{10} and CO_2-C_1-nC_4-nC_{10}) at elevated pressure and temperature. They reported interfacial tensions for a binary (CO_2-nC_{10}) system at 100°F and a quaternary (CO_2-C_1-nC_4-nC_{10}) system at 160 °F as a function of pressures. Ayirala's experiments were based on exposing a first drop of oil to CO_2 (fresh or equilibrated) and measure the IFT. Despite that, the VIT MMPs were comparable to slim tube, which indicate the multi-contact effect did have a bigger effect on the MMP, suggesting also a need for detailed a VIT measurement of a complex systems (multi-component oil) to further validate the technique.

Sequeira and Rao (2006) extended the applicability of VIT to a real CO $_2$-live oil system using the pendent drop and capillary rise techniques. They measured gas-oil interfacial tension between CO $_2$ and crude oil from a depleted Louisiana oil field at a reservoir temperature of 238 °F. First, the stock tank oil from the depleted Louisiana oil field was recombined with the separator gas at 238 °F and used for the VIT experiments. They, investigated the effect of different gas-oil ratios (Molar: Rm= 8.346 and Rm =

2.33, and volumetric: Rv = 5.667 and Rv =0.818) on the fluid phase composition, densities and interfacial tension, and demonstrated convergence of data to the same zero interfacial tension pressure, therefore insensitivity of equilibrium MMP on the variation of the gas-oil ratio. In addition, they demonstrated the approach to critical mixture formation in VIT experiments.

Saini and Rao (2010) measured the CO_2-oil IFTs of two recombined oils from field in Mississippi and used VIT method to determine MMP. They reported VIT-MMP of 24.3- 24.4 MPa (3533- 3543 psia), which was 4% less than MMP calculated using tie-line method 25.4 MPa (3685 psia). All experiments were conducted at reservoir temperature of 289 °F. Two IFT measurement methods were used, the pendent drop and the capillary rise techniques. Saini also reported to use volumetric gas-oil ratio of 90- 10 % for the IFT measurements.

Awari (2013) measured interfacil tension of three different oils, Gullfaks C, Arab AH 50 and West Texas intermediate dead crud oil with CO_2 and N_2. They reported IFT measurements for pressures between 100-600 psi, all at temperatures of 22 °C, in addition they reported an extra set of measurement for Gullfaks C at temperature of 60 °C and pressure between 100- 300 psi. They concluded in their study the following:

1. CO_2 showed lower IFT, therefore it is better than N_2 for gas injection.
2. They were able to measure IFT as a function of pressure using different gases.
3. They assumed zero IFT pressure is first contact miscibility.
4. Zero IFT pressures for CO_2 runs were lower than the N_2 runs.

Ghorbani and co-workers (2014) measured interfacial tension as a function of pressures for an Iranian oil reservoir. They reported a VIT MMP of 6000 and a slim tube MMP of 2746. They reported a big deviation supporting the claims of Orr and co-workers (Orr

and Jessen 2007; Jessen and Orr 2008). In addition they tested another ten samples using VIT method, and reported that GOR does effect the MMP determined using VIT. In their study they also developed a correlation that can be used instead of running the VIT experiment.

2.4 Vanishing Interface Technique Modeling

Orr and Jessen (2007) performed phase equilibrium calculations using Peng Robinson equation of state and the Parochor model. They assessed standard binary (CO $_2$-C $_{10}$), tertiary (CO $_2$-C $_4$-C $_{10}$) and Quaternary systems (CO $_2$-C $_1$-C $_4$-C $_{10}$). They also assessed Zick′ fluid system. They considered two assumptions in their runs either constant or variable GOR. They compared the results obtained using their prediction approach with the tie-line MMP method and concluded that in some cases VIT could result in miscibility pressures that match tie-line, MMP. But someother VIT MMP could deviate substantially from the slim tube or calculated MMP. So they cautioned not to use the method alone. They attributed the deviation to a limitation in the experimental technique to simulate the critical composition that could be observed in porous media.

Ayirala and Rao (2007) compared VIT-MMP measurements with the MMP result using Phase behavior calculations. The calculations were based on Peng Robinson equation of state. They used data for Rainbow Keg River and Terra Nova cases (Rao and Lee 2002; Rao and Lee 2003). In their study compared the VIT MMPs with the MMP calculated using tuned and and un-tuned EOS. They even tested the sensitivity of different parameters. They found that the MMP calculated using untuned PR-EOS reasonably matched VIT MMPs.

Jessen and Orr (2008) analyzed the behavior of VIT approach using phase equilibrium calculations for 13 gas/oil systems. Measured densities and slim tube data were available for these systems, but not interfacial tension data. Consequently they simulated the IFT data using Parachor model, assuming single contact. The study resulted in either over estimation or underestimation of MMP and they attributed the difference to limitation in simulated VIT technique and clearly suggested that simulated VIT is not a reliable single source of information for multi-contact miscibility.

2.5 Gas Assisted Gravity Drainage (GAGD) Process Development

Rao et al (2004) introduced the concept of GAGD, which basically consist of injecting CO_2 through vertical wells at the top of the pay zone and recovering oil from the bottom using horizontal wells. They presented few preliminary lab results, visual and core floods, proving the GAGD concept and the resulting high recoveries.

Sharma (2005) investigated the effect of dimensionless parameters on GAGD performance by conducting number of displacement experiments in a Hele shaw type model. Mainly he studied the effect of Bond number, capillary number, the mobile water saturation and operating conditions. Bond and capillary numbers showed good correlation with GAGD recovery.

Kulkarni (2005) conducted experimental study where he injected gas in WAG, CGI and GAGD modes. He compared the performance of these different modes. He also investigated number of parameters with relation to GAGD. The following are some of the parameters he investigated: 1) gas injection rate, injection type (miscible or immiscible), injection mode (tertiary or secondary), homogeneous and heterogeneous (fractured against non-fractured core). In addition, he performed dimensionless analysis, extensive literature review. Through his work he managed to:

1. Prove the concept of GAGD.
2. Demonstrate high oil recoveries resulted from the floods.
3. Modify Li and Horne model to accurately predict GAGD recoveries.

Paidin (2006) conducted an experimental study, where he studied the effect of wettability and vertical fracture on GAGD performance. He used a physical model consisting of Hele Shaw model, glass beads or silicon sand. He varied injection condition, injection mode and type of gas. Paidin concluded that the oil wet porous medium improved and the vertical fractures improved the performance of GAGD.

Mahmoud (2006) used glass visual models filled with Ottawa Silica sand to investigate few GAGD configurations that will be applicable to field applications. He studied the effect of injection depth, injection rate, viscosity, fracture, wettability and other parameters. Here are some points based on Mahmoud′ study:

1. There are three possible mechanisms responsible for high oil recoveries: a) darcy displacement before gas break through. b) Gravity drainage after break through. c) Film drainage in gas invaded zones.

2. GAGD works with gravity domination and further gravity force overcomes any permeability heterogeneity, which leads to better sweep resulting in higher oil recovery.

3. Gas injection depth had no effect on GAGD ultimate recovery.

4. Naturally fractured system appeared to be good candidate of GAGD. Mahmoud recommended immiscible GAGD instead of miscible GAGD, just to maintain gravity force domination.

Paidin (2013) investigated different configuration of conventional GAGD process. He conducted few core flood experiments using cores from onshore Louisiana reservoir.

Then he performed a field scale numerical simulation to optimize the process. He also complemented his analysis with an economic evaluation. His major findings are the following:

1. GAGD application resulted in significant additional recovery as seen the lab experiment and results from the simulation investigation.

2. Proposed 2-single well variations to the conventional GAGD process.

2.6 Flue gas and N_2 injection

Shokoya (2005) investigated the effect of flu gas composition on oil recovery experimentally and numerically. He conducted core floods, where he used three different gases with the following composition:

- 100% N_2.
- 1 % C_1, 16% CO_2 and 83% N_2.
- 1 % C_1, 30% CO_2 and 69 % N_2.

He used two different recombined oils:

- Oil (A) with N_2 = 0.25 mol %, CO_1 = 0.34 mol % C_1 = 35.85 mol % and C_2+ = 63.56 mol%.

- Oil(B) with N_2 = 1.34 mol %, CO_1 = 0.12 mol % C_1 = 17.35 mol % and C_2+ = 81.19 mol%.

Two different reservoir temperatures were reported, 116 °C for oil A and 80.6 °C for oil B. His core flood procedure in brief, involved first saturating the core with brine (1% NaCl), determine pore volume and the porosity, then saturating the core with dead oil, then recombined oil for 1.5 PV. Finally displace the oil using one of the

gases at a rate of 8.55 cm^3/hr. All floods were performed in horizontal mode. Then he matched his calibrated his compositional simulation model with the experimental data. He reported the following:

- Oil recoveries at break through and 1 PV, see table 2.1.
- Oil recoveries of different CO_2 in gas mixture.
- It is crucial to calibrate a simulation model with the lab data before using it for prediction.

Rivera (2010) , evaluated the effect of flue gas injection of the Barrancabermeja refinery to recover oil in the B sand of the Llanito oil field, Colombia. They sampled the reservoir fluid and ran PVT analysis and performed few displacement tests. In their study they investigated few injection options. The following were B reservoir properties: K =240 mD, Swi =46%, porosity = 0.2 and reservoir pressure of 2350 at 145 °C. 2.2 gives summary of their recoveries.

Table 2.1: Shokoya(2005) coreflood oil recovery using flue gas

	Oil A		Oil B			
	(mole%)		(mole%)			
N_2	0.248		1.339			
CO_2	0.344		0.12			
C_1	35.848		17.347			
C_2	3.746		6.436			
C_3	2.162		5.889			
iC_{i4}	0.413		0.873			
nC_{n4}	0.461		1.78			
iC_{i5}	0.104		0.448			
nC_{n5}	0.98		2.503			
C_6	1.635		3.786			
C_7+	54.059		59.479			
	27.7 MPa		41.6 MPa		17.6 MPa	
Recovery	(BT)	(1PV)	(BT)	(1PV)	(BT)	(1PV)
N_2	0.26	0.33	0.43	0.51	-	-
Flue gas 1	0.29	0.38	-	-	0.31	0.45
Flue gas 2	0.31	0.409	-	-	0.37	0.50

Table 2.2: Rivera (2010) corefloods using flue gas

	RF (BT)	RF (1PV)	RF (Abdn)
Continuous gas injection (CGI) at injection rate = 1 cc/min	55.15	5	61.95
Continuous gas injection (CGI) at injection at pressure 4700 psi = 1 cc/min	18.71	20	23.64
Continuous gas injection (CGI) at injection at pressure 3600 psi = 1 cc/min	18.07	20	32.82
Slug gas inj 0.3 PV+ WF at 4700 = 1 cc/min	38.75	39.7	39.7
Slug gas inj 0.3 PV+ WF at 3600 = 1 cc/min	35.42	40	40
Water alternating Gas (WAG-1)	31.8	34.66	34.66
Water alternating Gas (WAG-2)	35.44	38.56	38.56

Chapter 3

Modeling Vanishing Interface Technique to Calculate Zero-IFT Pressure

This chapter models the effect of GOR on VIT technique. Two cases were considered here using three different gas- oil systems to cover a range of fluid (ternary to multicomponent systems), CO_2-nC_4-nC_{10}, CO_2-nC_1-nC_4-nC_{10} and crude oil systems. The first case is the effect of fixing gas-oil ratio (molar and volumetric) on zero-IFT pressure. Second case is the effect of changing GOR as opposed to fixing GOR during the experiments. All VIT experiments were simulated using an equation of state (EOS) for estimating fluid phase parameters, and the Parachor model for gas-oil IFT calculations. Also, a modification to a reported calculated approach was adapted to simulate the actual VIT experimental procedure. The first section, gives a description of VIT calculation procedure, followed by results of the analysis, discussion and summary sections.

3.1 VIT Simulation Using EOS

There are two versions of VIT experiments reported in the literature: 1) where VIT experiment is initiated by introducing a load of oil and gas phases in the optical cell and then IFT is measured at different pressures. In this version of VIT the pressure is increased by adding more gas resulting in GOR to change (Rao 1997; Saini and Rao 2010; Ayirala and Rao 2011). 2) The experiment is designed to run either on a constant volume or constant molar gas-oil ratio. For each pressure the optical cell is cleaned and charged with an accurate amount of gas and oil that generates constant

GOR and IFT is measured. In other words, the experiments follow a path defined by (p-x) phase envelop quality or molar fraction line. It is important to note that, Orr and Jessen (2007) VIT simulation assumed two different cases of variable composition and constant composition. The variable composition case assumed variation in composition due to increase in CO_2, which simulates the first VIT experimental procedure. The constant composition assumption was intended to reflect the second VIT experimental procedure. This assumption caused large error in zero-IFT pressures. This work to provides additional proof that such procedure does not represent VIT experiments and hence could not match the reported experimental behavior.

In order to generate a model that portrays fluid phase behavior and predict VIT experiments an approach used by Orr and Jessen was adopted (Orr and Jessen 2007). Then the assumption of constant composition was modified to accurately simulate VIT experiments to examine the effect of changing GOR on zero IFT pressure.

The modification used in this study is as follows: first calculate the quality lines or molar fraction lines representing fraction in the mixture. Then perform flash calculations in such a manner that GOR remains constant. Here it is refereed to the approach that uses quality lines as constant volume and the approach that uses molar fraction lines as constant molar. Table 3.1 shows the parameters used to describe the PR-EOS for three and four component gas-oil systems.

Peng-Robinson equation of state (Peng and Robinson 1976) and Schechter and Guo parachor model (Schechter and Guo 1998) were used. Table 3.1, shows the parameters used to describe the PR-EOS for three and four component gas-oil systems. A commercial simulator, WinProp (Winprop 2013) was used for all EOS calculations in this study. The following steps summarize a typical VIT simulation procedure:

1. Tune the equation of state (EOS) to match experimental values if available.

Table 3.1: Parameters used for phase equilibrium calculation

Component	T_c(K)	P_c(MPa)	ω	M_w
Carbon Dioxide (CO_2)	304.2	7.4	0.23	44.01
Methane (C_1)	16.6	4.6	0.01	16.04
n-Butane (C_4)	425.2	3.8	0.9	58.12
n-Decane (C_{10})	617.0	2.1	0.40	143

2. Input the gas and oil compositions.

3. Calculate phase envelop quality lines for the system concerned, representing the gas-oil ratios used.

4. Select feeds based on quality lines or molar fraction lines that will generate required fixed or variable GOR for flash calculation.

5. Perform flash calculations with mixed feed at fixed temperature and defined pressure steps.

6. Calculate equilibrium liquid and vapor densities and compositions using EOS.

7. Calculate IFT by substituting the compositions and densities in the parachor model below:

$$\sigma = \sum_{i=1}^{n} [Pi(x\frac{\rho_l}{M_l} - y\frac{\rho_v}{M_v})]^{3.88} \tag{3.1}$$

Where σ is the IFT, Pi the Parachor constant for component i, M_l and M_v the molecular weights of the liquid and vapor phases, ρ_l and ρ_v are the mass densities of the liquid and vapor phases and n is the number of components in the system.

8. Generate a plot of interfacial tension against pressure at a fixed temperature and extrapolate to zero IFT.

9. Repeat Steps 3-7 for different gas oil ratios (molar or volumetric).

3.2 Results

This section presents the results of the analysis performed using the methodology mentioned in section 3.1.

3.2.1 Effect of Fixing GOR on Zero-IFT Pressure

First, a system consisting of oil (made up of 40 mol% normal butane (C_4) and 60 mol% normal decane(C_{10})) and CO_2 gas at 71.1 °C was considered. Four gas-oil mixtures of the CO_2-nC_4-nC_{10} system, 20-80%, 50-50%, 80-20% and 95-5%, were chosen to evaluate the GOR effect on the zero-IFT pressure. The EOS phase compositions for (CO_2-C_4-C_{10}) were compared to the composition reported in (Metcalfe and Yaborough 1979), Figure 3.1 shows a ternary diagram comparing measured composition and EOS calculated composition at 71.1 °C (160°F) and at 8.62 MPa (1249.9 Psia). It is clear from the ternary diagram that the phase compositions predicted by EOS match the ones from Metcalfe and Yarborough, assuring the robustness of the EOS model used.

Next, VIT experiments were simulated assuming constant volumetric GOR. Equilibrium density and composition were calculated using PR-EOS and IFT using Parachor equation for different pressures. Figure 3.2 and 3.3 show the calculated IFTs for (CO_2-C_4-C_{10}), for four different volumetric gas-oil mixtures, 20-80 %, 50-50%, 80-20 % and 95-5 %. The IFTs decline as pressure increases for all GOR cases, matching VIT experimental behavior and proving that there is no early termination at bubble point or dew point as simulated by Orr and Jessen (2007, 2008). A regression equation was

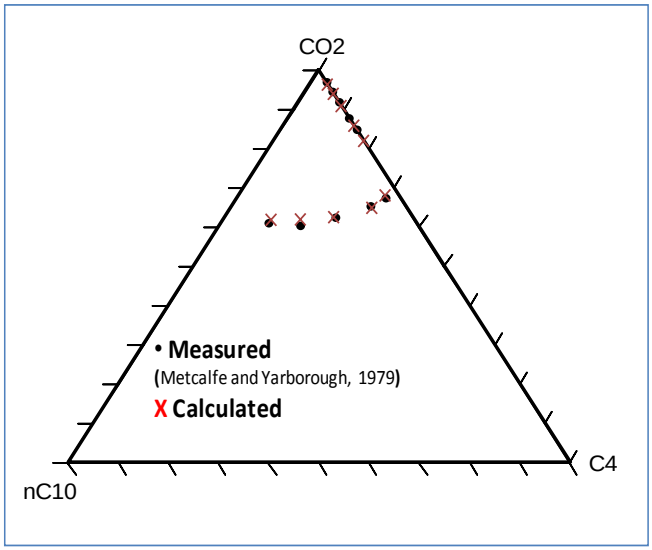

Figure 3.1: Comparison of calculated and reported phase compositions for the CO_2-nC_4-nC_{10} system at 71.1 °C (160 °F) and at 8.62 MPa (1249.9 Psia).

obtained and extrapolation of regression equation to zero IFT gives zero-IFT pressures of 11.4 MPa, 11.38 MPa, 11.34 MPa and 11.45 MPa respectively for 20-80 %, 50-50 % and 80-20%, 95-5% volumetric gas-oil ratios.

Similar behavior can be observed using constant molar GOR. Figure 3.4 and 3.5 show calculated IFTs for (CO_2-C_4-C_{10}), for different molar gas-oil ratios, 20-80 %, 50-50 %, 80-20 % and 95-5 %. The IFTs decline as pressure increases for all GOR cases. A regression equation obtained and extrapolation of regression equation to zero-IFT gives zero-IFT pressures of 11.44 MPa, 11.4 MPa, 11.45 MPa and 11.5 MPa respectively for 20-80 %, 50-50 % and 80-20 %, 95-5 % molar gas-oil mixtures. The deviation is almost negligible compared to constant composition approach from reference (Jessen and Orr 2008). These zero-IFT pressures from constant gas-oil ratios are also quite close to those obtained using constant volume ratios.

Figures 3.6 presents the pressure composition (P-x) phase diagram for (CO_2-C_4-C_{10}) system generated using PR-EOS. The dotted lines present the paths for GOR

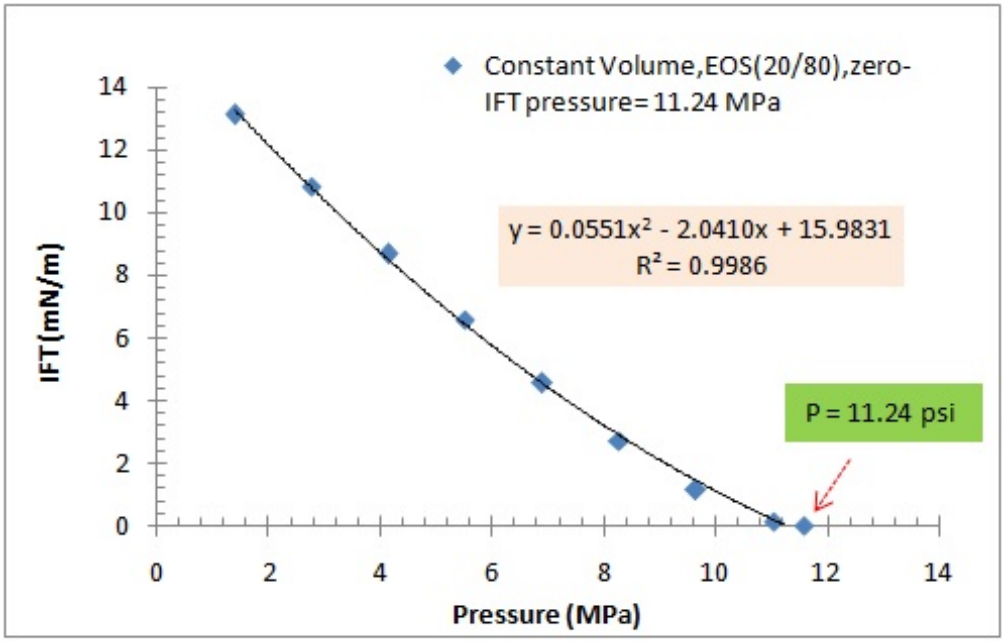

(a) Volumetric gas-oil mixtures 20-80%

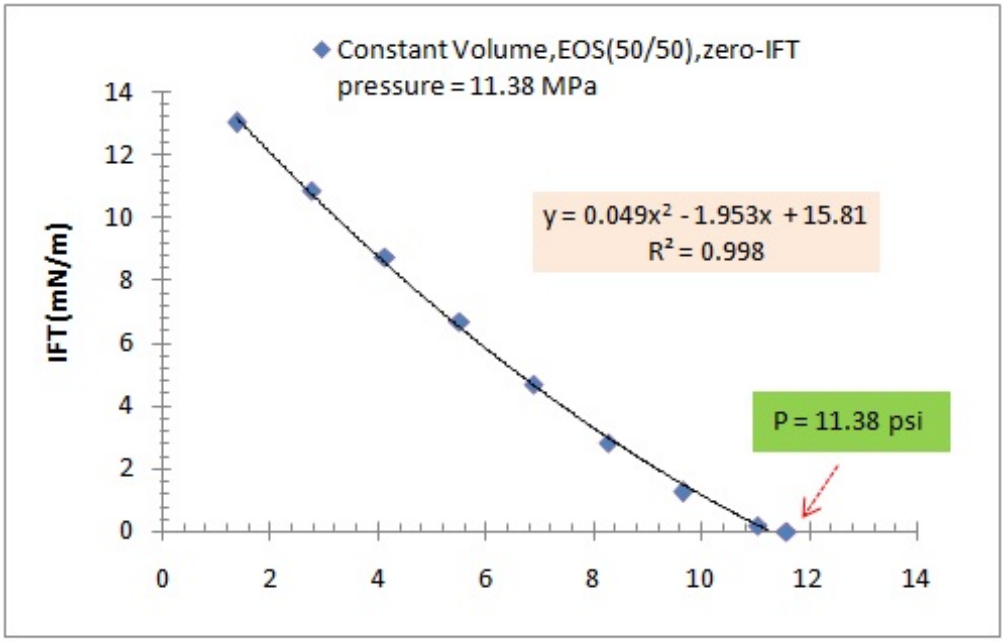

(b) Volumetric gas-oil mixtures 50-50%

Figure 3.2: Calculated IFTs for (CO_2-C_4-C_{10}), for four different volumetric gas-oil mixtures, 20-80% and 50-50% 71.1 °C.

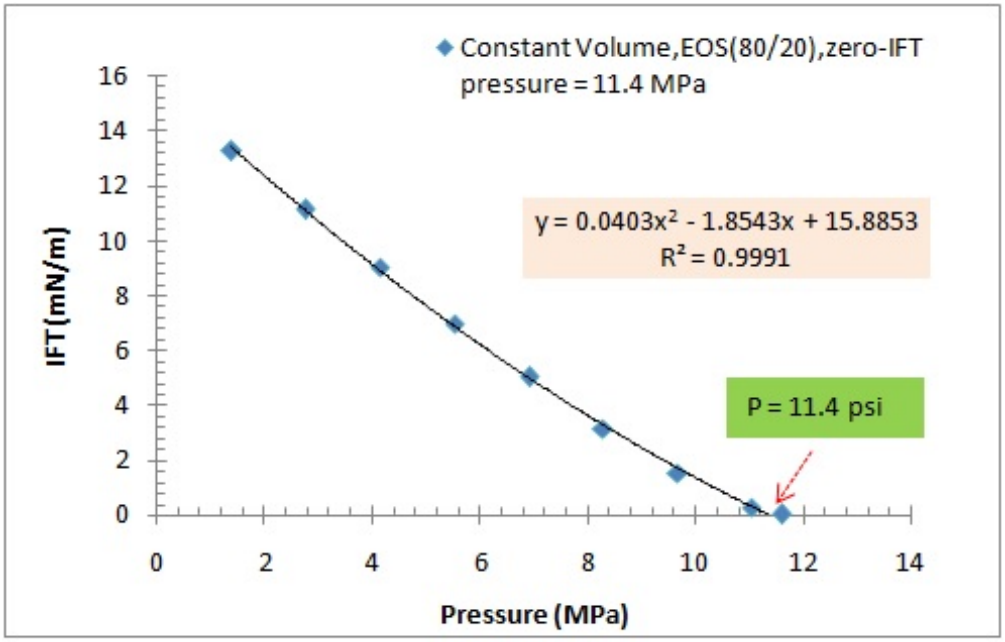

(a) Volumetric gas-oil mixtures 80-20%

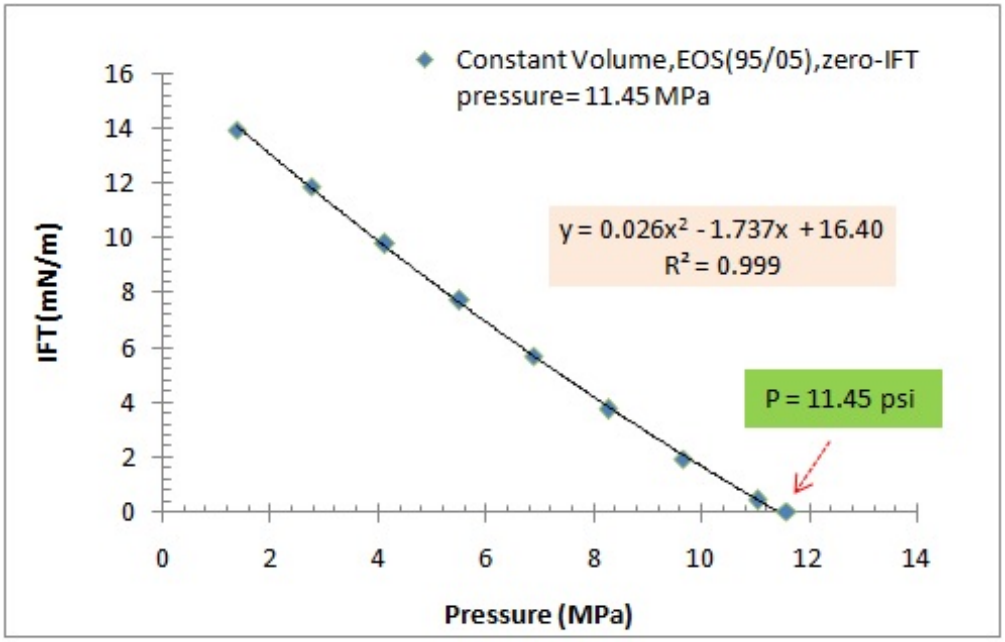

(b) Volumetric gas-oil mixtures 95-5%

Figure 3.3: Calculated IFTs for (CO_2-C_4-C_{10}), for four different volumetric gas-oil mixtures, 80-20% and 95-5% at 71.1 °C.

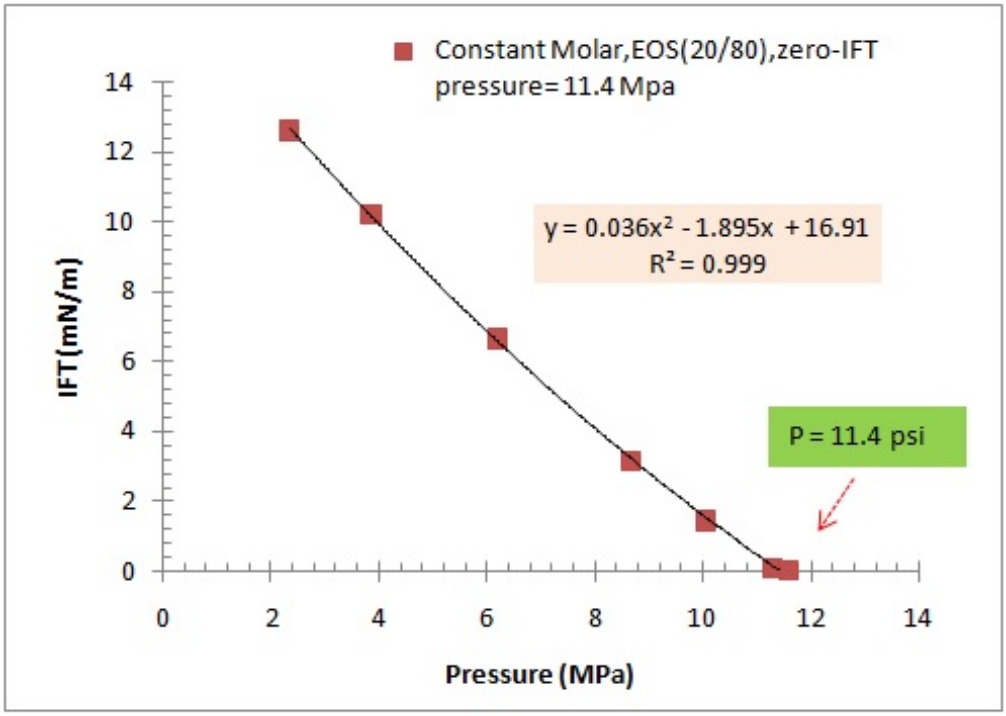

(a) Molar gas-oil mixtures 20-80%

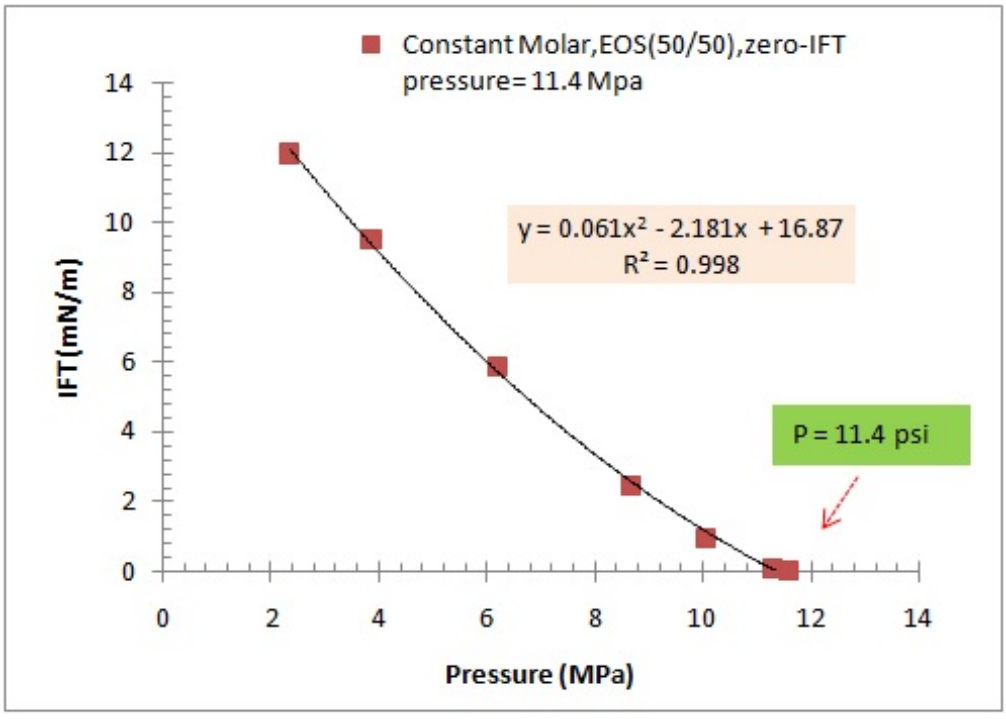

(b) Molar gas-oil mixtures 50-50%

Figure 3.4: Calculated IFTs for (CO_2-C_4-C_{10}), for different molar gas-oil mixtures, 20-80% and 50-50% 71.1 °C.

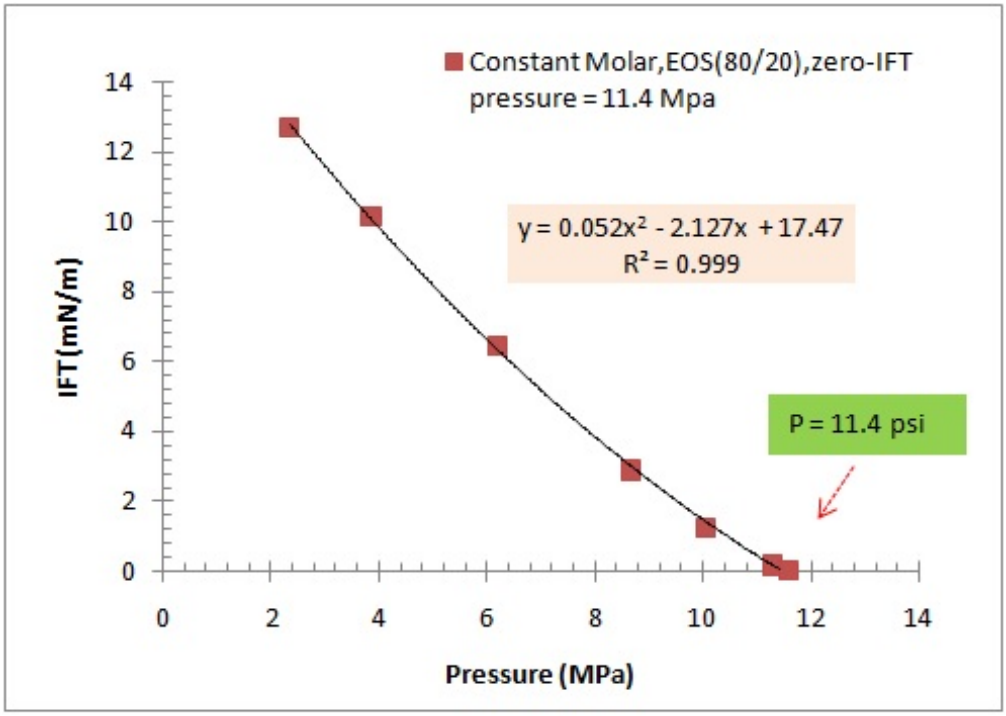

(a) Molar gas-oil mixtures 80-20%

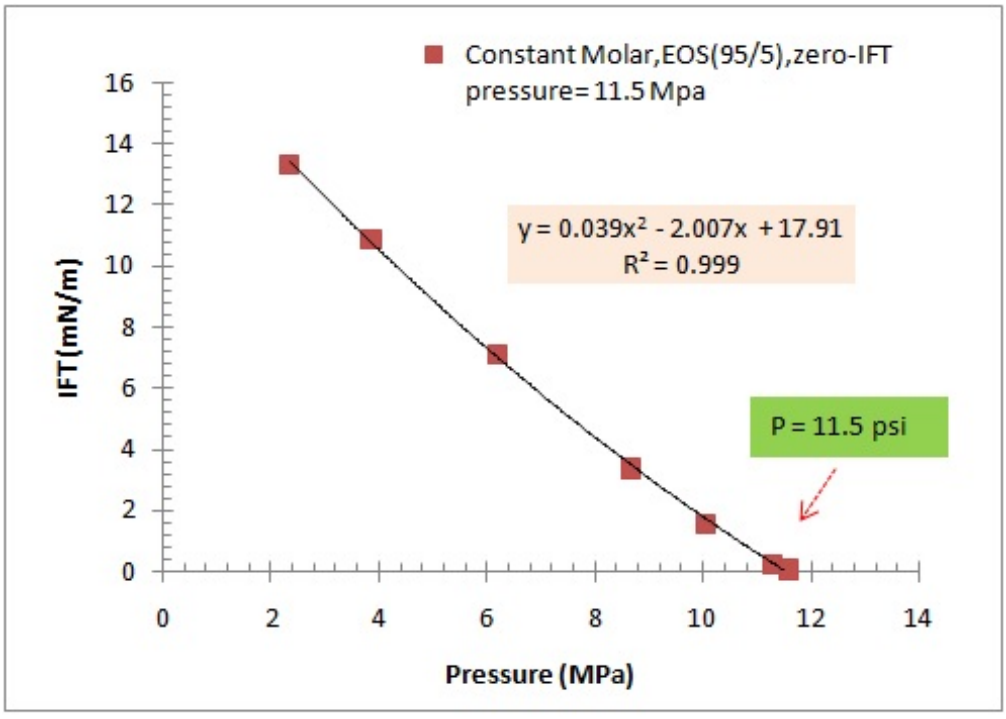

(b) Molar gas-oil mixtures 95-5%

Figure 3.5: Calculated IFTs for (CO_2-C_4-C_{10}), for different molar gas-oil mixtures, 80-20% and 95-5% at 71.1 °C.

20-80 %, 50-50 %, 80-20% and 95-5 %, that was followed in order to achieve the results presented earlier. All the paths, or the quality lines, remain in two phase region and converge towards a single point, the critical point of the system. This validates the reported experiments (Sequeira, Ayirala, and Rao 2008; Ayirala and Rao 2011) and proves: 1) measurement of IFTs beyond their bubble or dew point is possible and 2) several GOR paths lead to the same zero-IFT pressure.

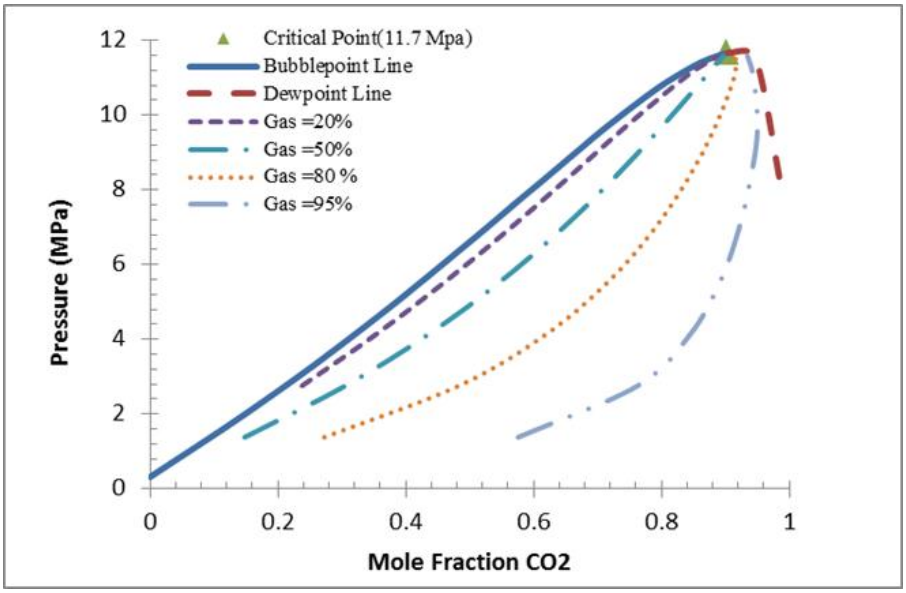

Figure 3.6: Pressure-composition phase diagram for mixtures of a) CO_2-C_4-C_{10} at 71.1 °C (160 °F) for a constant volumetric GOR approach.

Figure 3.7 compares calculated IFTs for (CO_2-C_4-C_{10}) system using Orr and Jessen (Orr and Jessen 2007) constant composition approach, for three different gas-oil mixtures, shown by the dashed lines, 20-80 %, 50-50 %, and 95-5 %, with the 20-80% GOR calculated using volume gas-oil mixtures in this study(solid line) and available experimental IFT data (Nagarajan, Gasem, and Robinson 1990). Note that constant composition approach results in termination of IFTs of 20-80 %, 50-50 % and 95-5

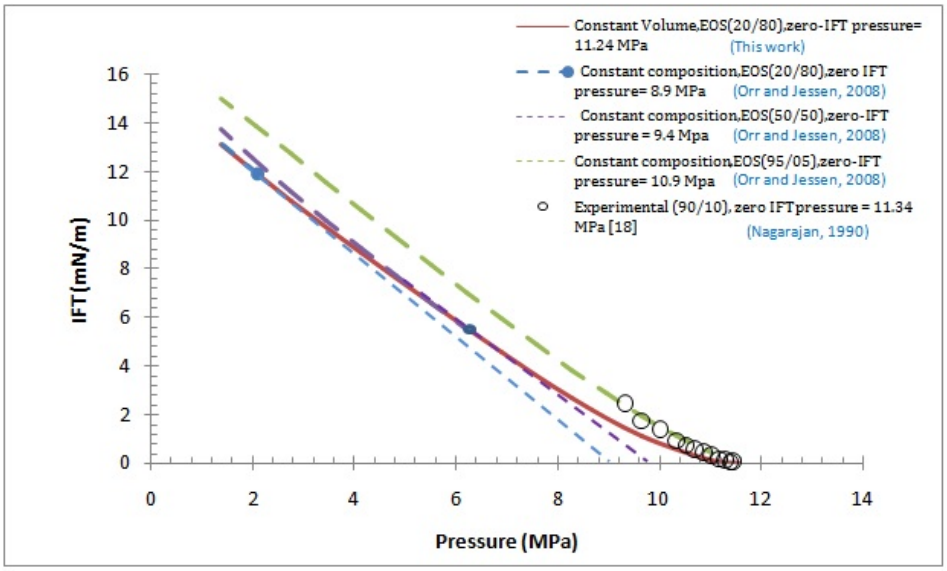

Figure 3.7: Comparison of calculated IFT using Orr and Jessen constant composition gas oil mixture approach with this study assuming constant volumetric gas-oil ratio, for CO_2-C_4-C_{10} at 71.1 °C (160°F).

% molar gas-oil mixtures at their respective bubble-point and dew point pressures, namely, 2.6 MPa and 6.5 MPa and 10.8 MPa when the corresponding gas-oil IFTs are 11.9, 5.5, and 0.4 mN/m. Also, extrapolating these data (dashed lines) to zero-IFT pressure as done by Orr and Jessen (2007) will result in large errors, due to extrapolation from large gas-oil IFT values. The VIT technique relies on being able to measure low IFT values and then extrapolating the measured IFT data to zero IFT. Any attempt to simulate VIT should also focus on low IFT regions necessitated by gas-oil miscibility requirements.

Similar approach was followed with the quaternary system to check if similar conclusion applies to a different system. So the system used consisted of carbon dioxide (CO_2), methane (C_1), normal butane (C_4) and normal decane (nC_{10}). The analysis performed on this system was based on an oil composition scenario of (24.57% C_1, 29.77% nC_4 and 45.66% nC_{10}) for two different gas-oil ratios mixtures, 20-80 % and 80-20 %.

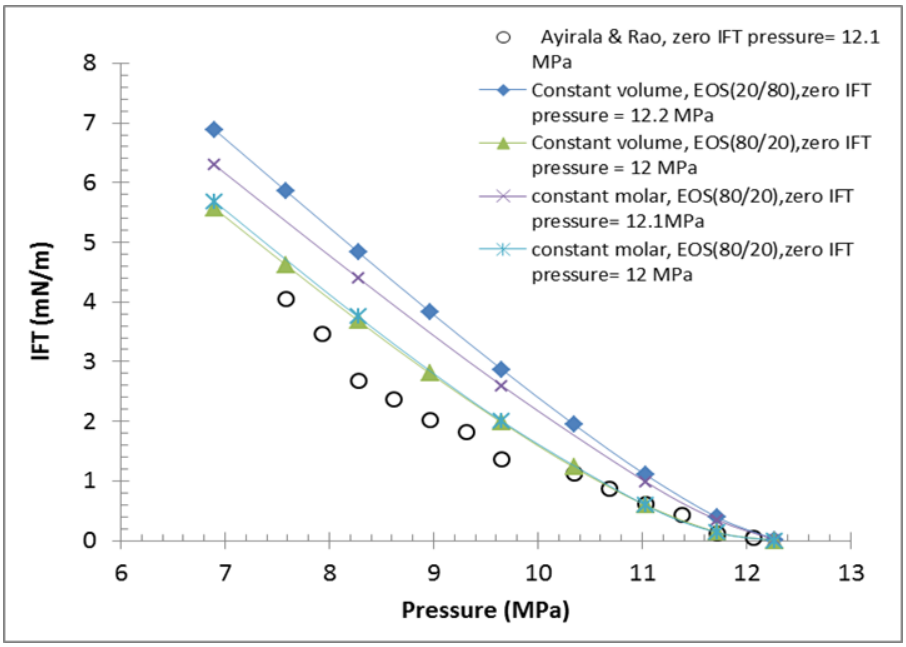

Figure 3.8: Calculated IFTs assuming constant gas-oil molar ratio and constant volume ratio.

Figure 3.8 compares the approach of calculating IFT assuming different volumetric and molar gas-oil ratios. The calculated IFTs do not entirely match the measured values; but they converge to a single zero-IFT pressure matching experimental behavior (Ayirala and Rao 2011). Both approaches result in zero-IFT pressure of 12-12.2 MPa. This matches well with reported experimental zero-IFT pressure for this fluid system (Ayirala and Rao 2006).

Next a multicomponent system, CO_2-live multicomponent reservoir crude oil, was considered. This system was reported by Sequeira (2006). Table 3.2 gives the composition of the oil and the EOS model properties of the components. Sequeira reported experimental zero-IFT pressure of 42.6 MPa and 42.9 MPa for two constant molar gas-oil ratios of 0.893-0.107 (Rm= 8.346) and 0.7-.3 (Rm = 2.33) at 114.4 °C. Similarly, he reported zero-IFT pressure of 42.3 MPa and 42.5 MPa for two constant volumetric gas-

oil ratios 0.85-0.15 (Rv = 5.667) and 0.45-0.55 (Rv =0.818) at 114.4 °C. Using equation of state the densities and compositions were calculated and compared against reported values, and then flash calculations were performed. IFTs were calculated at different pressures and different GORs. Figure **??** compares the approach of calculating IFT for Sequeiras and two different molar gas-oil mixture ratios (GOR = 0.893-0.107 and 0.7-0.3). Both approaches result in zero-IFT pressure of 42- 44 MPa, which matches well with the reported values of 42.3- 42.8 MPa from Sequeia.et.al for this fluid system. It is clear from the graphs that at pressures less than 35 MPa, the experimental IFT at different GORs, show a spread compared to the calculated ones, but they all converge to almost the same zero-IFT pressure, this can also be seen from the comparison made in Figure **??**.

3.2.2 Effect of Varying GOR on Zero IFT Pressure

The effect of varying GOR during VIT experiment on zero-IFT pressure was evaluated. A hypothetical case was considered, where GOR was assumed to change between 20-80% and 80-20% for the mixture of CO_2-C_1-C_4-C_{10} during VIT measurement and using EOS and Parchor model to calculate the IFTs as a function of pressure. Figure 3.10a and b present calculated (P-x) phase diagram for mixtures of CO_2-C_1-C_4-C_{10} at 71.1 °C for a variable gas-oil ratio. The dashed lines present volume quality lines (20-80 % and 80-20%) and circles present the change in GOR with pressure during a hypothetical VIT experiment, so in terms of VIT experiment we relax the condition of fixing GOR. From P-x diagram, the symbols converge to a single point, critical point, which also can be observed from calculated IFT values. A regression equation was obtained and extrapolation of regression equation to zero-IFT gives a zero IFT pressure of 12.1 MPa, which matched reasonably the values calculated using constant volume approach

mentioned earlier. So it is clear that this case also converges to a particular zero-IFT pressure, where it also matches with the values obtained using a fixed GOR option.

3.3 Discussion

The analysis performed on the ternary, quaternary and a multi-component systems, shows that irrespective of the compositional path adopted in the calculation procedure (constant volumetric or molar gas-oil ratio), single zero- IFT pressure is obtained which also agrees with the zero-IFT miscibility pressures reported from VIT experiments. This analysis also shows that straight-line extrapolation of relatively high gas-oil IFTs calculated at bubble point pressures, as done by Orr and Jessen could differ markedly from the measured miscibility pressures.

The main difference between the approaches used in this chapter and the constant composition approach reported by Orr is that the calculation in this paper follows fixed paths, either volume quality line path or molar fraction line path that guarantees a convergence to a single zero-IFT pressure, critical point.

Based on the analysis here, it is obvious that zero-IFT pressure corresponds to the critical pressure of the system, and VIT can be used to determine it via fixed or variable GOR options.

3.4 Summary

The flowing can be summarized based on the analysis in this chapter:

1. The effect of GOR on zero-IFT pressure was examined here to understand its impact on VIT behavior.

Table 3.2: Composition of oil and gas and properties of the component used to model CO_2-live Oil system.

Component	Composition		Properties and EOS Paramters			
	oil(%)	gas(%)	M_w	T_c(K)	P_c(MPa)	ω
CO_2	0.006	100	44.0	304.2	7.38	0.23
N_2	0.011	0	28.0	126.2	3.40	0.04
C_1	23.141	0	16.0	190.6	4.60	0.01
C_3	0.085	0	44.1	369.8	4.25	0.15
iC_4	0.148	0	58.1	408.1	3.65	0.18
nC_4	0.444	0	58.1	425.2	3.80	0.19
iC_5	0.943	0	72.2	460.4	3.39	0.23
nC_5	0.908	0	72.2	469.6	3.38	0.25
C_6	2.835	0	86.0	507.5	3.29	0.28
C_7+	71.479	0	2.18	732.6	1.72	0.59

2. VIT behavior of ternary, quaternary and multicomponent gas-oil systems were examined using PR-EOS and Parachor model.
3. VIT technique can be simulated by calculating densities and compositions using PR-EOS and IFTs using Parachor model.
4. The resulting zero-IFT pressures based on the analysis matched the critical pressures of the gas-oil system used, suggesting the robustness of the VIT technique in determining minimum miscibility pressures.
5. Adopting proper gas-oil IFT calculation procedure that reflects actual VIT experimental procedures, made it possible to obtain reliable prediction of gas-oil zero IFT pressure that agrees closely with VIT technique and other independent experimental IFT measurements.
6. Constant volumetric, molar gas-oil ratios or variable gas-oil ratios result in similar zero-IFT pressures of the gas-oil system which also agrees with the miscibility pressures from VIT experiments.
7. All analysis in this chapter and prior reported experiments (Ayirala and Rao 2006; Sequeira 2006) suggest zero-IFT pressure is independent of GOR.

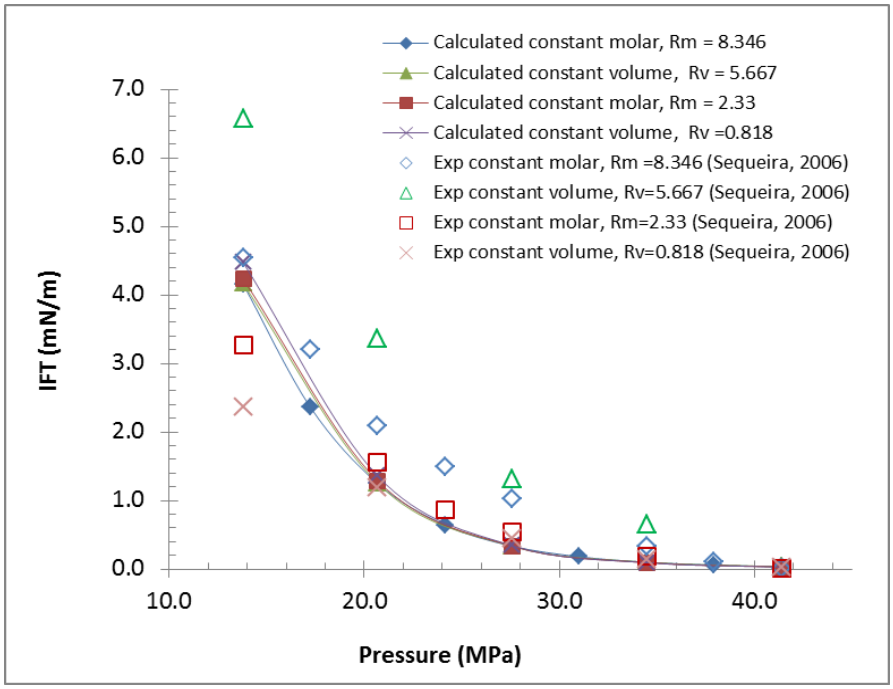

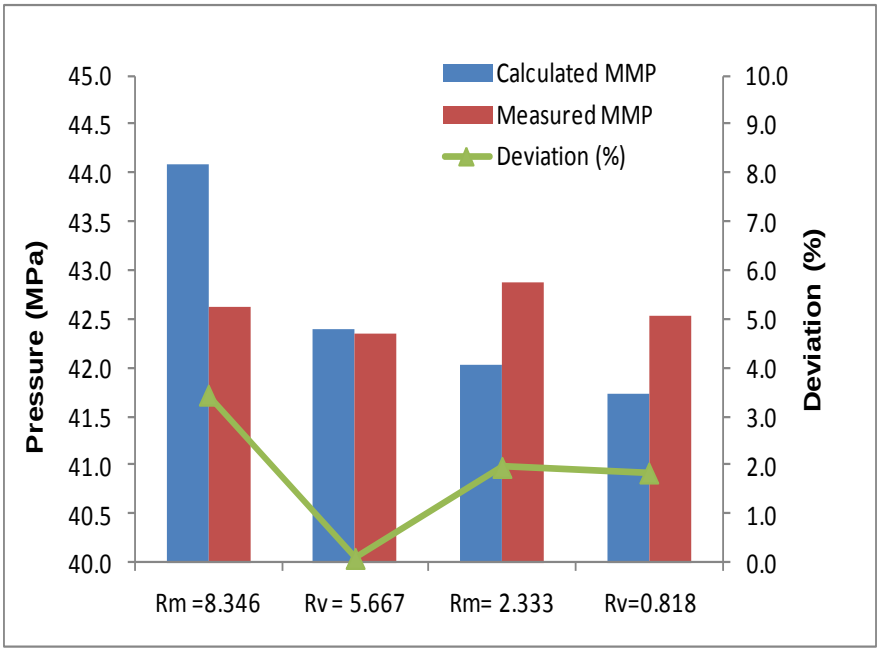

Figure 3.9: Calculated IFTs assuming constant gas-oil molar ratio and constant volume ratio, CO_2-live Oil system, Sequeira's system, at 114.4 °F. b) Comparison between calculated and Sequeiraś experimental IFT's

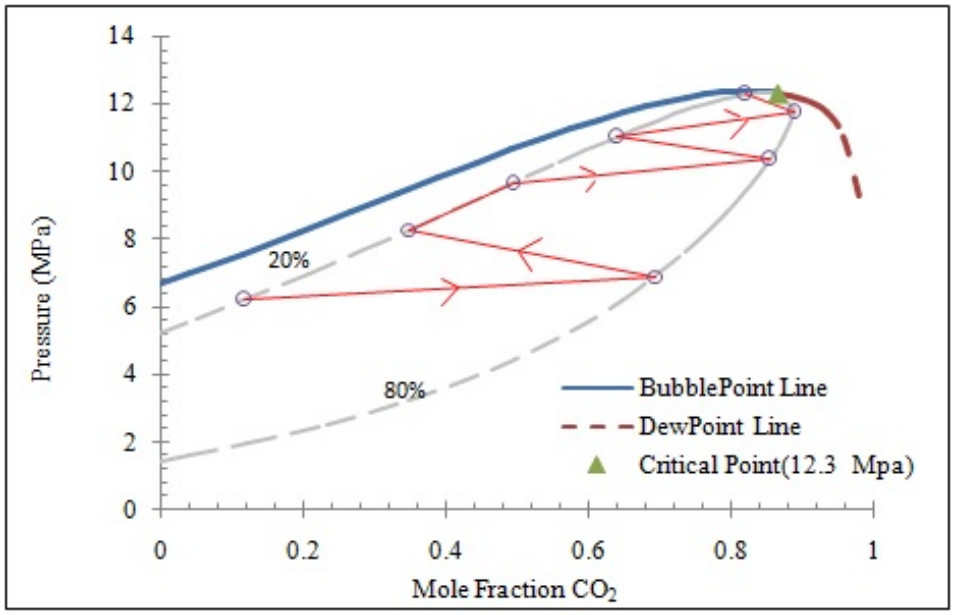

(a) Pressure-composition phase diagram for mixtures of CO_2-C_1-nC_4-nC_{10}

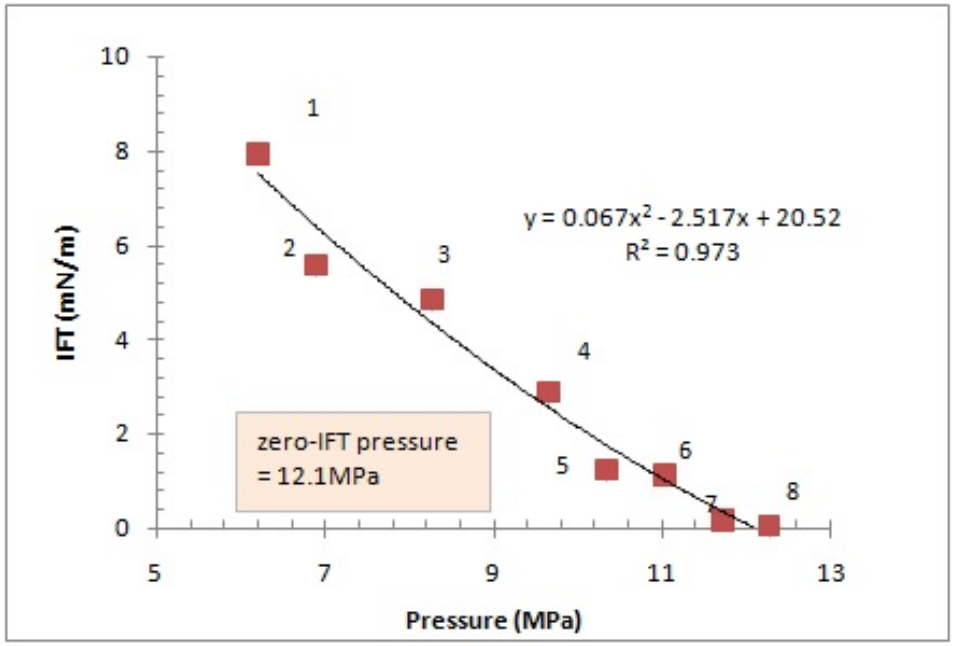

(b) Calculated IFTs for (CO_2-C_1-nC_4-nC_{10}), for variable gas-oil ratio.

Figure 3.10: a) Pressure-composition phase diagram for mixtures of CO_2-C_1-nC_4-nC_{10} at 71.1 °C, for a variable gas-oil ratio. b) Calculated IFTs for (CO_2-C_1-nC_4-nC_{10}), for coressponding gas-oil ratios as in a).

Chapter 4

Interfacial Tension Method for Near Miscibility Pressure Determination

This chapter presents a simple method for estimating near-miscibility pressures that is based on a simple gas-oil interfacial tension calculation procedure. The method assumes near miscibility conditions at low interfacial tensions and relies only on using a cubic equation-of-state (EOS) for compositional calculations and the Parachor model for interfacial tension calculations. This method enables rapid calculation of NMPs for multiple component gas-oil systems. The first section describes the procedure of how to calculate interfacial tension using PR-EOS and the Parachor model, then illustration of the method using Zick fluid, explained in section 4.2) along with some sensitivity results before presenting several examples of using this IFT-based method to estimate near miscibility pressure (NMP) and its comparison to slimtube technique.

4.1 NMP Determination Using IFT Based Method

This section describes the basic steps in estimating MMP using the IFT based method. The method depends on flash calculation using Peng- Robinson EOS (Peng and Robinson 1976) for compositional calculations and (Schechter and Guo 1998) Parachor model for interfacial tension calculations. All EOS simulations were conducted using commercial software (Winprop 2013). The following steps summarize the procedure for estimating near miscibility pressure with this IFT-based method

1. Set EOS parameters including reservoir temperature and starting pressure and fluid composition.

2. Input the original compositions of gas and oil. The heavy component should all be lumped into C_7+.

3. Mix the gas and oil at desired gas-oil ratio and flash the mixture at fixed temperature and defined pressures.

4. Calculate equilibrium liquid and vapor densities and compositions using PR-EOS.

5. Calculate IFT by substituting the compositions and densities in the Parachor model shown below:

$$\sigma = \sum_{i=1}^{n} [Pi(x\frac{\rho_{\mathrm{l}}}{M_{\mathrm{l}}} - y\frac{\rho_{\mathrm{v}}}{M_{\mathrm{v}}})]^{3.88} \tag{4.1}$$

   Where σ is the IFT, Pi the Parachor for component i, M_{l} and M_{v} the molecular weights of the liquid and vapor phases, ρ_{l} and ρ_{v} are the mass densities of the liquid and vapor phases and n is the number of components in the system.

6. Generate a plot of interfacial tension against pressure at a fixed temperature.

7. Determine the pressure at desired low IFT cutoff. This pressure is assumed to be the estimated MMP using IFT-based method.

The IFT-based method proposed here to calculate near miscibility pressure is expected to be applicable to any multi-component gas-oil system.

4.2 Zick's Slim Tube study

Zick (1986) used three different systems (A, B and C)in his evaluation of condensing/vaporizing Mechanism. Table 4.1 shows Zick fluid systems (Reservoir Oil A, B and

Solvent A and B). Zick ran few slim tube experiments to measure MMP and characterize miscibility mechanism. He used 60 ft and 2 inch slim tube packed with sand (Zick 1986). In this section the IFT-based method was tuned using Zick fluid system (Zick 1986) that was reported to be :

1. Oil A is assumed to be depleted from 21.4 MPa to 20.7 MPa
2. Solvent A is mixed with 20 mol% methane to result in Solvent A2.

Table 4.2 shows composition, EOS and Parachor model properties used at 185°F.

Table 4.1: Zick fluids (Zick 1986).

	mole fraction			
Component	Reservoir fluid A	Solvent A	Reservoir fluid B	Solvent B
CO_2	0.0699	0.2218	0.0063	0.0004
C_1	0.4146	0.2349	0.4015	0.5694
C_2	0.0540	0.2350	0.0514	0.1302
C_3	0.0360	0.2745	0.0325	0.1430
C_4	0.0245	0.2745	0.0280	0.0816
C_5	0.0173	-	0.0206	0.0460
C_6 -C_7	0.0411	-	0.0400	0.0194
C_8 -C_{10}	0.0781	-	0.0849	-
C_{11}-C_{14}	0.0716	-	0.0927	-
C_{15}-C_{119}	0.0635	-	0.0811	-
C_{20}-C_{29}	0.0586	-	0.0666	-
C_{30}+	0.0708	-	0.0944	-
C_7+ Molecular weight	275		-	

Here the PR-EOS was characterized using Whitson method, charaterise C_{7+} as follows (Whitson and Brule 2000):

1. Use Twu or Lee-Kesler critical correlation for acentric factors, Tc and Pc.

2. Use Soreide correlation for specific gravity.

3. Use Chueh-Prausnitz equation for C_1 through C $_{7+}$ pairs.

Next use density and composition of solvent-oil system at desired pressures and fixed reservoir temperature with the Parachor model to calculate interfacial tension. This procedure of flash calculation for phase composition and IFT calculation was repeated at varying pressures.

Table 4.2: Composition, EOS and Parachor model parameters used for Zick fluid system at 185°F (Ahmadi and Johns 2011).

Component	Composition		EOS Properties			Binary Interaction parameter
	mole fraction					
	Oil	Gas	T_c(K)	P_c(MPa)	ω	CO_2
CO_2	0.0656	0.1775	87.79	1069.443	0.228	-
C_1	0.3711	0.3878	-116.59	666.018	0.008	0.105
C_2	0.0538	0.188	90.05	707.094	0.098	0.13
C_3	0.0373	0.2196	205.97	614.673	0.152	0.125
C_4	0.0261	0.0271	305.69	550.125	0.193	0.12
C_5	0.0187	-	385.61	488.511	0.251	0.115
C_6	0.0218	-	453.65	429.831	0.296	0.115
C_7+	0.4056	-	939.02	247.56	0.661	0.115

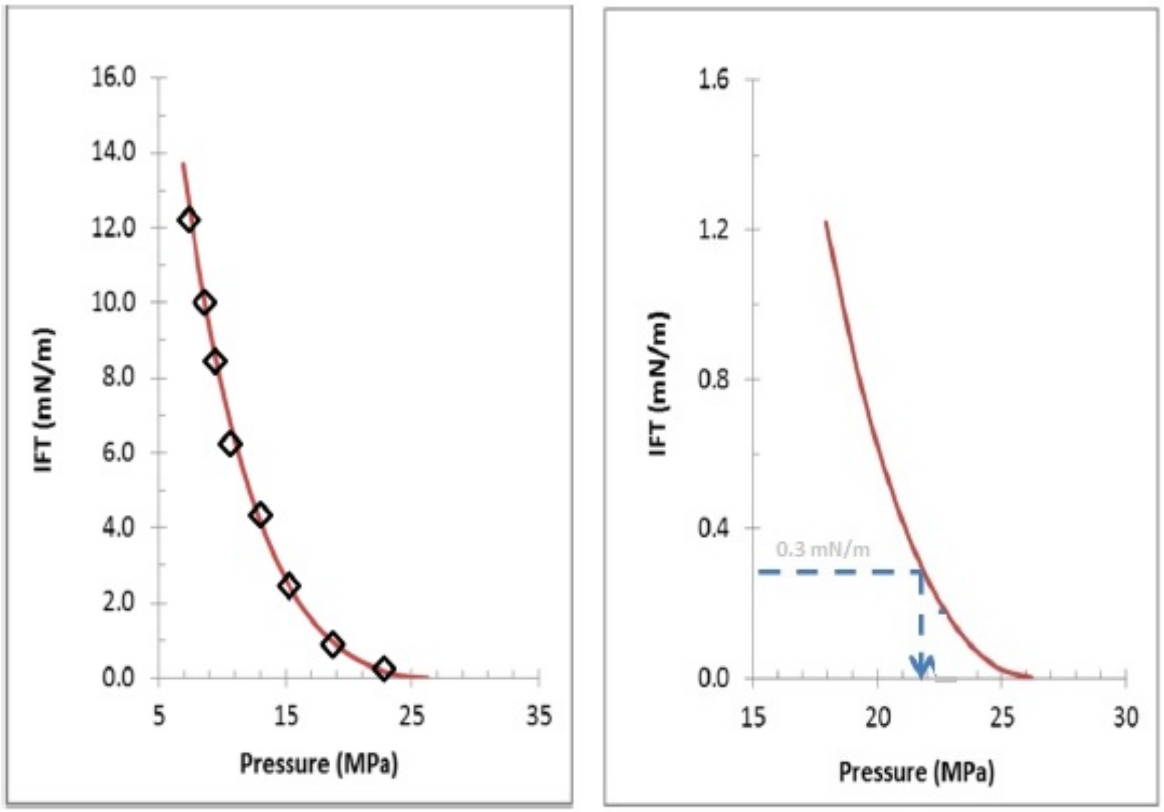

Figure 4.1: Shows the calculated IFTs for Zick fluid at 185° F: a) IFT vs. pressure for Zick fluid system. b)IFT vs. pressure for Zick fluid system for IFT less than 1.2 mN/m, showing also the NMP at 0.2 mN/m.

Next, the calculated IFTs were plotted against pressure, as shown in Figure 4.1. The left plot shows the IFT from 14 to zero mN/m and the plot on the right zooms in IFT range between 1.2 to zero mN/m. At Zick MMP of 21.6 MPa (for the concerning system) IFT was identified (0.3 mN/m) and defined to be the IFT cutoff that results in Zicks MMP.

4.2.1 Sensitivity Analysis

The IFT-based method uses PR-EOS and reported Parachor model. It also depends on estimated parameters that go along with EOS and Parachor models. Therefore,

here we evaluate the implication of different parameters used in EOS. The parameters evaluated in the analysis are:

1. IFT that corresponds to NMP, where the following values were used (0, 0.001, 0.01, 0.1, 0.2, 0.3) mN/m.

2. The critical pressure, P_c, of the heaviest component in the characterized heptane-plus fraction which was varied within ± 5 %.

3. The critical temperature, T_c, of the heaviest component in the characterized heptane plus fraction which was varied within ± 5%.

4. Molecular weight, M_w, of the heaviest component in the characterized heptane plus fraction which was varied within ±n the characterized heptane plus fraction which was varied within, ± 2%, ± 5% and ± 10%.

Table 4.3 shows the summary of parameter sensitivity. The comparisons between different parameters lead to the following observations:

- The deviation resulting from the variation in the IFT cut offs were reasonably low, less than 5%, for values above 0.2 mN/m and when 11- 23% for values less than 0.2 mN/m.

- Variation in Pc showed maximum deviation up to 9% and minimum of 1% in NMP.

- Variation in Tc showed maximum deviation up to 14% and minimum of 5% in NMP.

- M_w seems to have no influence on calculated MMP for Zicks fluid system.

- Variation in Parachor constant, showed a maximum deviation in MMP of 8% and a minimum deviation of 0.5%.

Therefore, based on the analysis, it is clear that most prominent parameter on the proposed method is the IFT cutoff. The errors in the other parameters can be minimized further, by tuning the EOS to match PVT data.

Table 4.3: Effect of different parameters on Near Miscible pressure (NMP) using Zick's fluid system

Method	NMP	Deviation(%)
Zick slim tube	21.6	
Cutoff IFT= 0	26.5	22.7
Cutoff IFT= 0.1	24.0	11.1
Cutoff IFT= 0.2	22.6	4.6
Cutoff IFT= 0.3	21.7	0.5
Pc +5%	23.6	9.3
Pc -5%	21.3	1.4
Tc +5%	24.6	13.9
Tc -5%	20.5	5.1
M_w +5%	22.5	4.2
M_w -5%	22.5	4.2
Parachor constant(C_7+) +2%	22.6	4.6
Parachor constant(C_7+) +5%	22.8	5.6
Parachor constant(C_7+) +10%	23.3	7.9
Parachor constant(C_7+) -2%	22.1	2.3
Parachor constant(C_7+) -5%	22.0	1.9
Parachor constant(C_7+) -10%	21.7	0.5

4.3 More Examples

This section describes more examples using IFT based technique. It also investigates the influence of commonly available characterization method for the heavy fraction of the reservoir fluid and evaluates the influence of tuning EOS using different PVT experiments on the proposed method.

4.3.1 Fluid Database

A published database (13 reservoir oils, each with one or few injection gases) was considered (Jaubert, Avaullee, and Souvay 2002). The data base includes detailed compositional data, standard PVT experiments, swelling tests and slim tube MMPs. The database provided a detailed compositional analysis (up to C_{20} +), it also includes molecular weight and specific gravity for each cut (C_7 to C_{20} +). In this section, individual Jaubert fluids are referred as JF1 to JF12. Table 4.4 summarizes the 12 oil-gas systems used in this study in terms of densities and injection gas compositions. The densities of the fluid varied between 939 to 951 kg/m3 and the molecular weight between 460 to 560 g / mol. This method was designed for hydrocarbon injection gas-oil systems, Table 4.4 lists some of the properties of 12 reservoir fluids and 12 different gas mixtures.

4.3.2 Characterization and Tuning Approach

EOS models were developed using characterization method suggested by Whitson et al. (1989) using PR-EOS. The fluids were characterized using nine components. Then these models were subsequently tuned to match available experimental data (CCE, CVD and swelling test), where densities, saturation pressures and relative volume were matched and compared to experimental data. The tuning approach was restricted to

Table 4.4: Jaubert reservoir fluids and injection gases.

	Oil density	M_w (C_{20}+)	Injection gas (mol)					Slim- tube MMP
Fluid	kg/m3	g/mol	H_2S %	N_2 %	CO_2 %	C_1 %	C_2+ %	MPa
1	951.2	560	-	0.48	4.96	58.05	36.51	22.1
2	949.3	530	-	0.48	4.96	58.05	36.51	23.5
3	925.3	474	-	0.49	1.82	81.39	16.30	37.6
4	905.0	418	-	0.41	1.65	81.71	16.23	37.9
5	956.0	450	-	-	-	88.00	12.00	36.6
6	937.7	442	0.25	0.42	2.85	75.55	20.93	32.3
7	914.6	455	-	-	4.35	81.14	14.51	29.6
8	914.6	455	-	-	4.35	81.14	14.51	26.3
9	881.1	411	2.35	0.27	4.35	73.09	19.94	35.9
10	917.1	434	2.72	0.22	4.43	66.10	26.53	28.7
11	927.0	450	-	0.47	2.25	85.34	11.94	33.5
12	939.0	460	3.81	0.20	7.57	64.90	23.52	32.7

only change pseudo components paramters (Pc, tc, acentric factor, ect). Three different stages of tuning were exercised to evaluate the effect on the prediction of NMP.

1. Base prediction based on the default characterization.

2. Prediction after regression of CCE and DDE and swelling test

3. Prediction after regression of CCE, DDE, swelling test and ST-MMP.

For regression using CCE and swelling test data, critical temperature (T_c), critical pressure (P_c) and molecular weight (M_w) for C_7+ and, the acentric factor were used as the tuning parameters to match the density and relative volumes of the experiments. Different weight factors, mostly less than 5, were used in this study.

4.3.3 Results

Two examples from the fluids are covered in this section using the IFT based method to estimate MMP. First example covers Jaubert fluid system 1 (JF1). JF1 is a 34.8 API fluid, where the injected gas contains 4.96 mole % of CO_2, 58.05 % methane and 36.5 C_2+ . The EOS for this fluid was tuned to match the PVT experiments including swelling test. Figure 4.2a shows the calculated IFT as a function of pressure for JF-1. The ST-MMP reported for this oil-gas system is 22.1 MPa at 215.06°F and the IFT based method predicts NMP to be 22.2 MPa at IFT = 0.3 mN/m. This is a deviation of less than 0.5%.

Second example considers Jaubert fluid system 12 (JF12). This fluid is a 37.4 API fluid. The fluid contains hydrogen sulfide and Nitrogen in both the oil and the gas injected. The EOS for this fluid was tuned to match the PVT experiments including swelling test and slim tube experiment. Figure 4.2c shows the results for JF12 system. The slim tube MMP reported for this oil-gas system is 32.7 MPa at 219.92°F and the

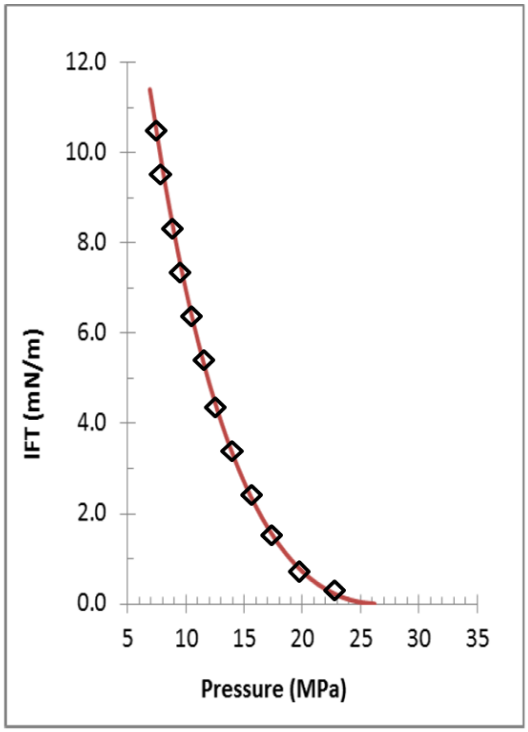

(a)

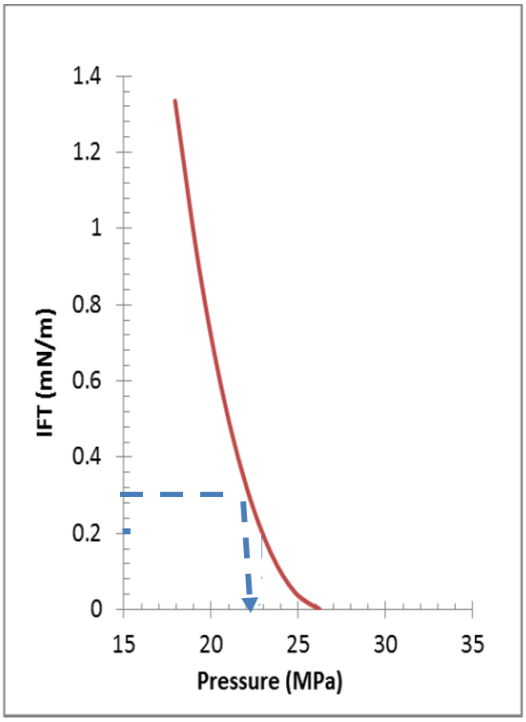

(b)

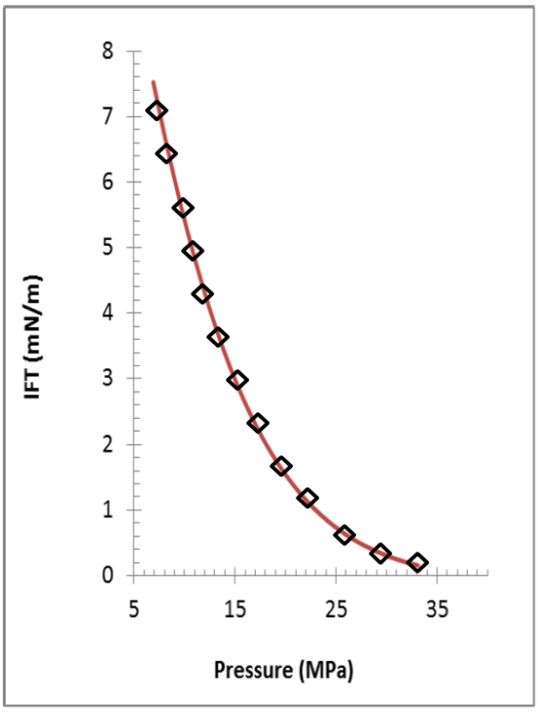

(c)

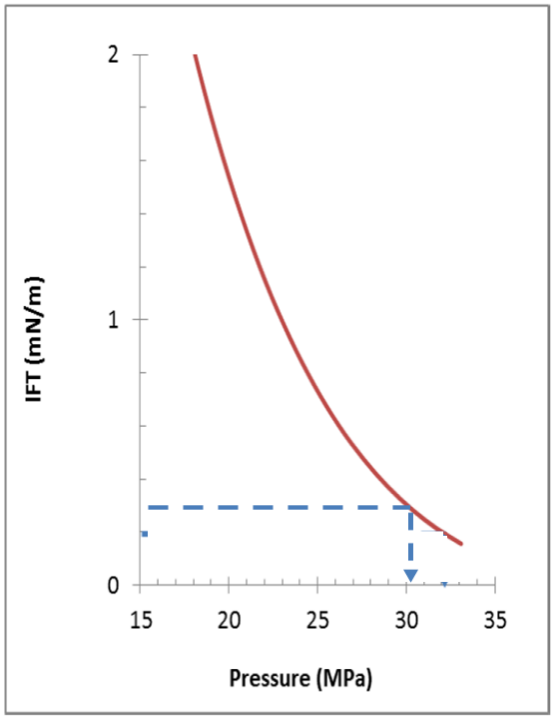

(d)

Figure 4.2: Calculated IFTs for JF1 and JF2: a) IFT vs. pressure for JF1 system. b)IFT vs. pressure for JF1 system for IFT less than 1.2 mN/m. c) IFT vs. pressure for JF12 system. d)IFT vs.pressure for JF12 system for IFT less than 1.2 mN/m

IFT based method predicts NMP to be 30.3 MPa at IFT of 0.3 mN/m. This also is a deviation of less than 7%. The rest of the examples of NMP estimation also matched reported MMP from slim tube. The highest deviation was observed to be around 7%. The estimates were based on minimum deviation from the actual MMP value after tuning EOS.

The rest of the samples MMP estimation also matched reported NMP from slim tube. The highest deviation was observed to be around 6%, see table 4.5. These estimates were based on minimum deviation from the actual MMP value after tuning EOS.

4.4 Discussion

Previous work in the area of miscibility pressure and interfacial tension underlines the importance of the relation between IFT and miscibility pressure. A lot or work was done through VIT technique to establish the link between IFT and miscibility pressure through experiments or computationally. However, this paper presents a different approach that in it uses PR-EOS, a Parachor model, set of assumptions to estimate MMP and a cut off criteria to match slim tube experiments. In this section we summarize the results from the 12 system of Jaubert et al. (2002)

In this section we summarize the results from the 12 system of Jaubert et al. (2002). Figure 4.3 compares the MMP estimates from the IFT based method to the measurement slim tube MMP. The MMP estimates obtained from the IFT based method using a cutoff that was determined by matching Zick MMP, agree remarkably well with slim tube measurements. This also proves that slimtube yields NMP (low IFT)and not necessary the MMP (IFT=0).

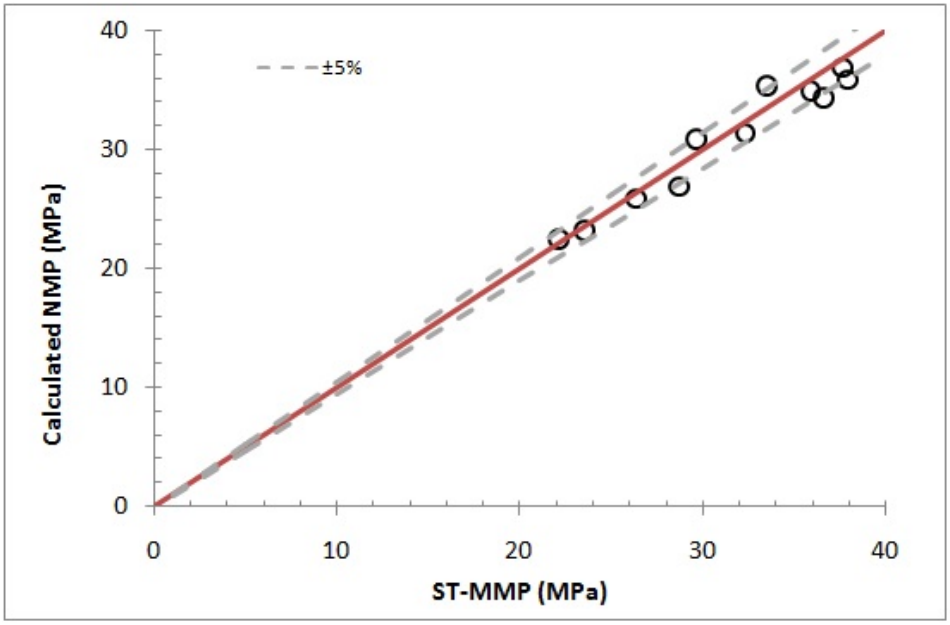

Figure 4.3: Comparison of MMP values estimated from MMP-IFT based method with the values from experimental slim tube experiments for 12 multicomponent systems reported by Jaubert(Jaubert, Avaullee, and Souvay 2002)

.

With the results shown earlier, the technique seems to give reliable results, when gas and oil are both made up of multiple components. The method presented here can be used for initial estimates of MMPs in multi-component gas-oil systems.

4.5 Summary

An IFT-based calculation procedure is presented here to estimate a reasonable NMP in multicomponent gas-oil systems. Based on the analysis and results presented in this paper the following can be summarized:

1. An IFT based approach was proposed here to estimate NMP of gas-oil systems. The method involves calculating densities and composition using and equation of state and calculating interfacial tension using a Parachor model. The method

is simple, robust and faster than the conventional slim tube simulation or the actual slim tube experiment.

2. A sensitivity analsyis was performed on Zicks system to asses the influence of, Pc, Tc, IFT cutoff, Mw and Parachor constant on the IFT based method to estimate NMP. The analysis showed that the most prominent parameter on the proposed method is the IFT cutoff.

3. 12 reservoir fluid systems of varying compositions were tested using the proposed method and the estimated MMPs agreed with slim tube MMPs within about 7%.

4. The agreement of IFT-based NMP estimate to ST-MMPs indicate that the slim tube actually yields near miscibility pressure (at gas-oil IFT of 0.3 mN/m)rather than true miscibility pressure (MMP) which occurs at zero IFT pressure.

Table 4.5: Summary of deviation of the calculated NMP using the IFT based method (at IFT = 0.3 mN/m

System (JF)	Experimental Slim tube MMP MPa	NMP-IFT based method MPa	difference %
1	22.1	22.62	0.5
2	23.5	23.3	0.9
3	37.6	37.0	1.6
4	37.9	36.0	5.0
5	36.6	34.5	5.7
6	32.3	31.5	2.5
7	29.6	31.0	4.7
8	26.3	26.0	1.1
9	35.9	35.0	2.5
10	28.7	27.0	5.9
11	33.5	35.5	6.0
12	32.7	30.0	8

Chapter 5

Experimental Material, Apparatus and Procedures

To evaluate the effect of different injection gas types (CO_2, N_2 and flue gas) on GAGD performance, miscibility pressure was measured first for different gas-nC_{10} cases. Then their effect on GAGD performance was evaluated trough displacement experiments.

The chapter describes the apparatus and procedures used to measure miscibility pressure, via vanishing interfacial technique (VIT). The method is based on measuring IFT for gas-oil system at different pressures and extrapolate IFT values to zero IFT pressure, for more details see section 2.3.1. Four different gases were used for VIT experiments:1) CO_2 (100 mole %), 2) CO_2 (85 mole%)- N_2 (15 mole%), 3) CO_2(15 mole%)- N_2 (85 mole%) and 4) N_2 (100 mole%) were used as injection gas from 200 to up to 2000 psi and at 100 ^oF.

Next, Parachor model was to used predict the interfacial tension for different gas mixture-oil system that contains N_2 in injected gas.

Finally, the chapter describes the apparatus and procedures used to perform vertical corefloods, to asses the performance of GAGD using different gases. Three gas type was used for corefloods: CO_2 (100 mole %), CO_2 (85 mole%) -N_2 (15 mole %) and N_2 (100 mole%) were used as injection gas from 200 to up to 2000 psi and at 100 ^oF.

In summary, Chapter 5 presents a description of material and equipment used, followed by experimental procedure in measuring density and interfacial tension, determining VIT-MMP, GAGD corefloods and VIT experiment modeling procedures.

5.1 Experimental Material

To meet the experimental objectives of this research the following material were used: Berea sandstone cores purchased from Cleveland Quarries. The core used were one foot in length and 2 inches in diameter and had a permeability ranging from 50-200 mD and porosity of 15-20%. Fluids used for flooding experiments were: 1) nC_{10} purchased from Fisher scientific. 2) Carbon dioxide CO_2 and Nitrogen N_2 were from Accurate gas products. 3) Deionized water from Water Quality Laboratory at Louisiana State University (LSU). Cleaning fluids used to clean the core apparatus and flow lines were toluene, acetone from Fisher scientific and deionized water.

5.2 Experimental Apparatus

5.2.1 Interfacial Tension and Measurement Apparatus

Interfacial tension experiments in this study were performed using high pressure high temperature HPHT IFT optical cell. Figure 5.1 shows IFT experimental setup for HPHT experimental rig. The set up consists of high pressure high temperature cell, connected to fluid supply vessels and gauges. In a addition a recording and processing system. A detailed descriptions of different component of the IFT cell system is described bellow:

- HPHT optical cell, that can handle up to 400 °F and 20000 psi. The cell consists of stainless steel structure, side caps, side glass to allow visibility and vertical arm fixed on the top of the cell and to injection needle, see Figure 5.2.
- A transfer vessels used to store oil, that can handle pressures up to 3000 psi, see Figure 5.3.

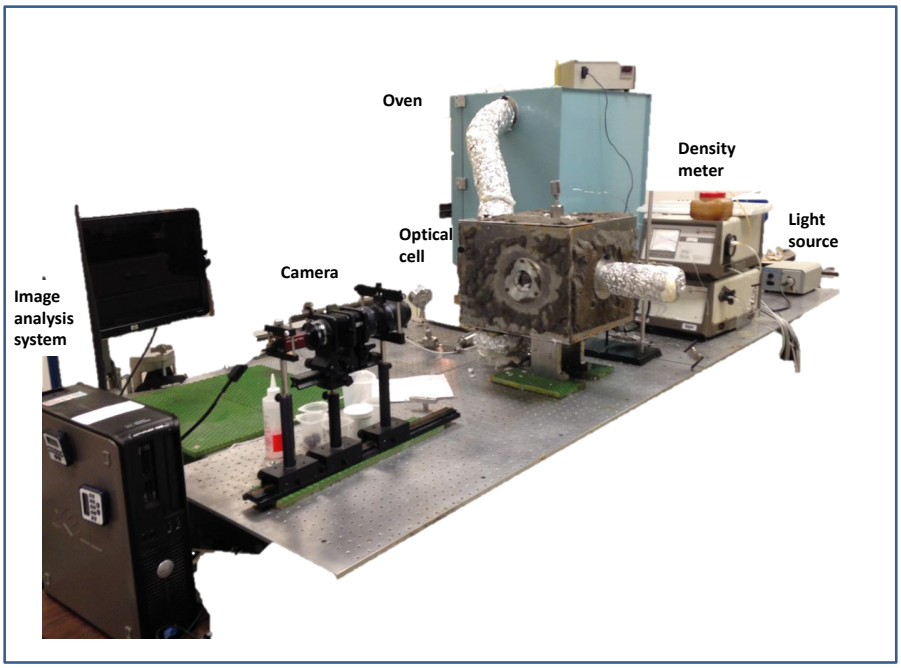

Figure 5.1: IFT experimental setup used for HPHT pendent drop IFT measurement. The system consists of one optical cell, oil transfer vessel, ruska pump, density meter, camera, image analysis system, pressures and temperature gauge.

- A Ruska positive displacement pump that is used to store and pump injection gas, see Figure 5.4. This pump was used inject and compress gas.
- Anton Paar Density meter (DMA HP and DMA 4500) to measure densities of liquid and gas during the experiment, see Figure 5.5.
- Pressure and temperature gauges, used to monitor and read values.
- A light source and a digital camera with a lens that is used to capture images of oil drop. The camera is fixed on adjustable stands to allow moving it for better images, see Figure 5.6.
- Liquid and gas sampling outlet. These outlets were connected to the density meters.

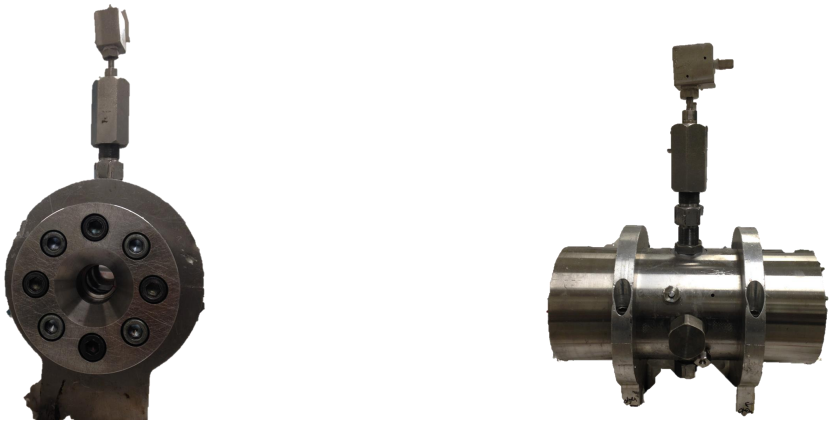

(a) View1 (b) View2

Figure 5.2: HPHT Optical cell

- A heating oven, used to heat the system to a desired temperature, see Figure 5.1.

Figure 5.3: Transfer Vessel

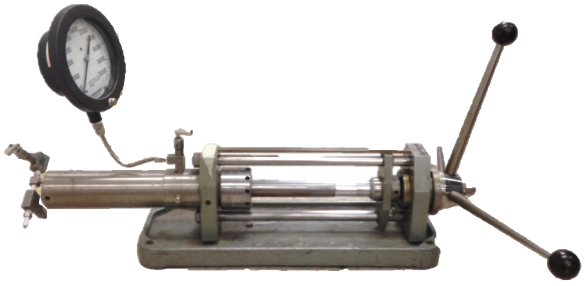

Figure 5.4: A Ruska positive displacement pump

Figure 5.5: Anton Paar Density meter (DMA HP and DMA 4500)

Figure 5.6: Digital camera

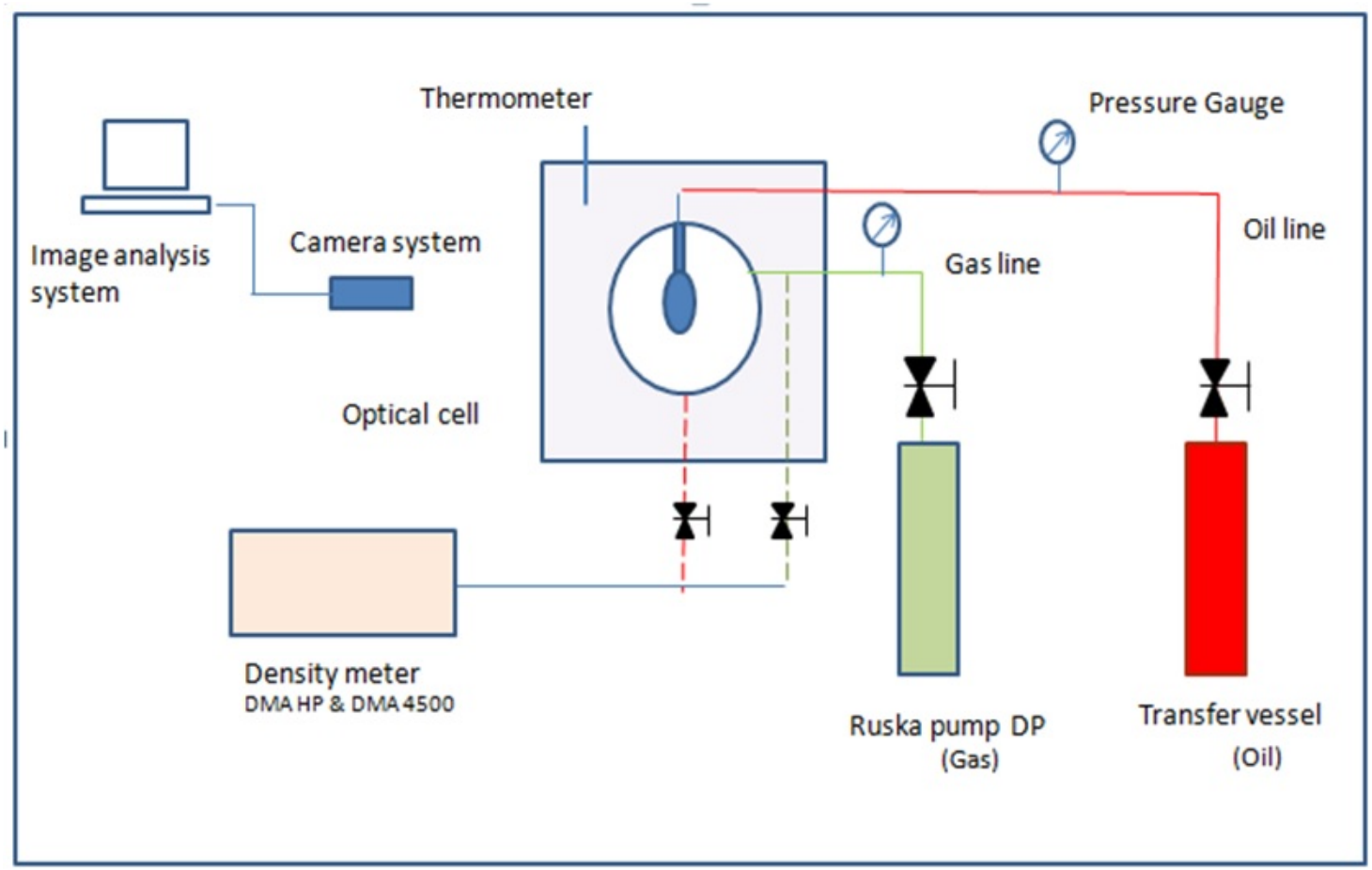

Figure 5.7: Schematic of the experimental setup used for HPHT pendent drop IFT measurement. The system consists of one optical cell, oil transfer vessel, Ruska pump, density meter, camera, image analysis system, pressures and temperature gauge.

5.2.2 Coreflood System

Figure 5.12 shows coreflood apparatus setup. The setup was assembled to achieve the research objectives mentioned in section 1.2. The system consist of core holder, injection system, production system and measuring/monitoring system. A detailed descriptions of different component of the coreflood system is described bellow:

- Hassler-type coreholder: The coreholder was manufactured by Phoenix instruments. The core holder accommodates a 1 ft long core with a diameter of 2 inches. The core holder can sustain pressures as high as 5000 psi and temperatures up to 400 °F. The core is put inside a viton core sleeve. A heating tape was used with glass wool insulation material to maintain a constant working temperature of 100 °F, see Figure 5.8.

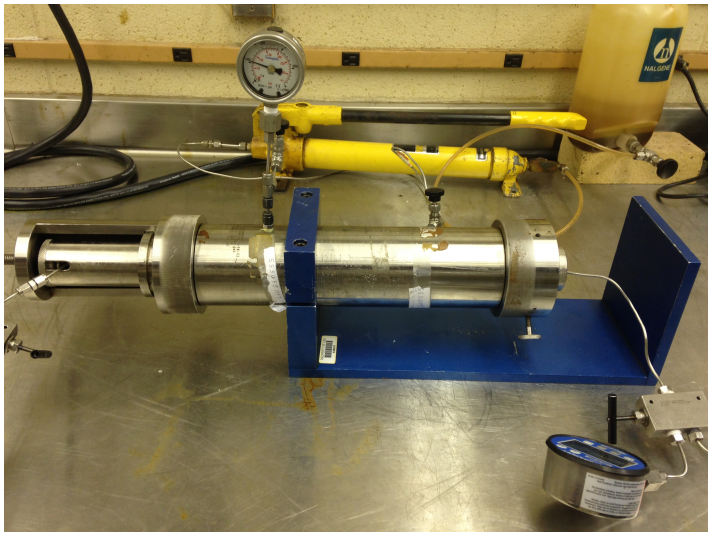

Figure 5.8: Hassler-type coreholder

- Pressure and temperatures gauges: they waere used to monitor inflow pressure, outflow pressure and confining pressure. The pressure gauges can handle pressure

upto 10000 psi. All pressure gauges were manufactured by Ashcroft. The digital pressure gauges had a maximum pressure rating of 10000 psi, Figure 5.9.

Figure 5.9: Pressure Gauge

- A constant rate syringe pump: It was used to pump fluids into the cores (oil, water, and gas).
- Hydraulic oil pump: was connected to core holder and was used to provide the necessary confining pressure to the core within the core holder.
- 100 and 250 cc burette : was used to collect and measure produced fluids (oil and water).
- Gasemeter or wet gas meter: used to collect and measure gas volumes. Manufacturer: GCA Precision Scientific.
- Back pressure regulator: to provide the necessary pressure against the flow of water, oil and gas.
- Flow lines: different sizes of flow lines were used to construct the flowing network to allow the flooding to core with respected fluids.

- Floating piston transfer vessels : 3 transfer vessels are used, for the oil, gas and water. These transfer vessel are connected to a pump from one side and to the core from the other side.

Figure 5.10: 1ft Berea sandstone

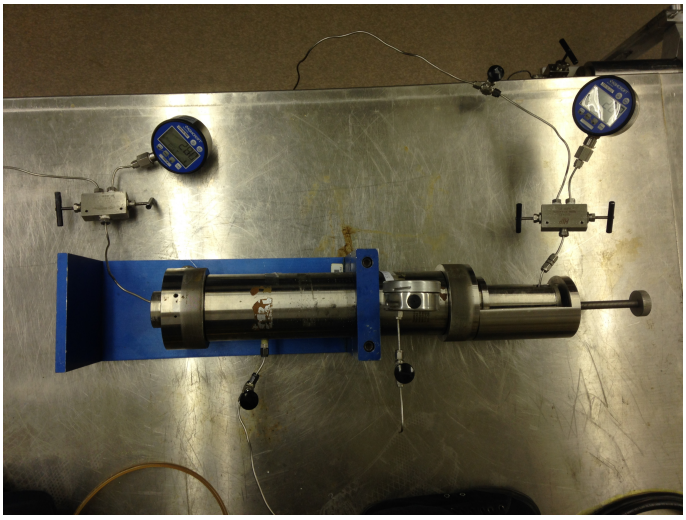

Figure 5.11: Top view core flood system

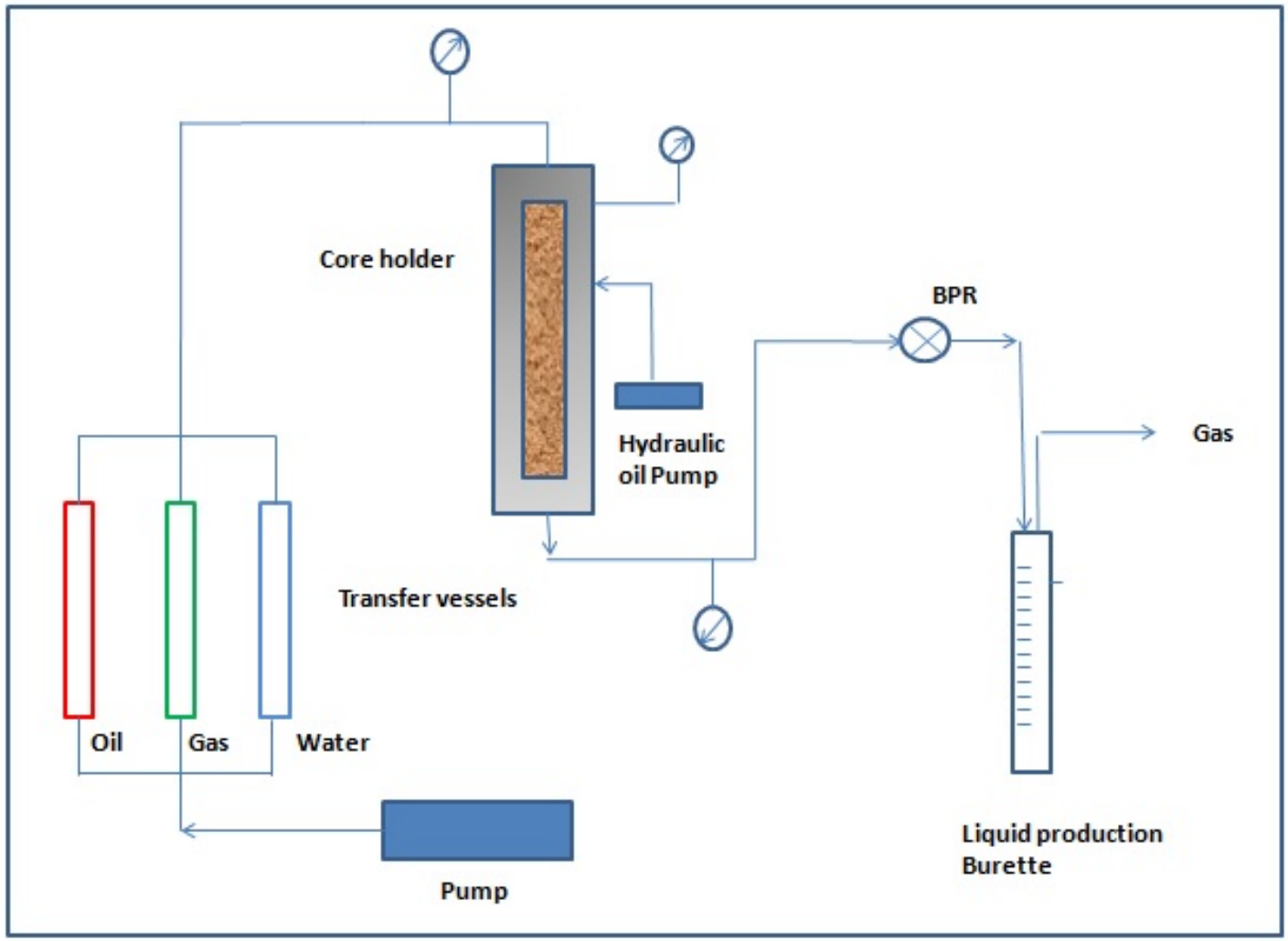

Figure 5.12: Schematic of the experimental setup used for HPHT core floods. The setup mainly consists of core holder, flow lines, gauges, transfer vessels, burette and pumps

5.3 Experimental Procedures

This section gives a detailed description of the experimental procedures followed in this research for:

1. Interfacial tension measurements, and measuring miscibility pressure, via VIT method.

2. DIsplacment test via vertical high pressure corefloods.

5.3.1 Interfacial Tension and Miscibility Pressure Measurements (VIT)

The following sections provide detailed descriptions of the procedures and methods used in the laboratory while carrying out cleaning, density calibration, density measurement and IFT measurement.

5.3.1.1 Cleaning Procedures

IFT is a delicate parameter to measure and is sensitive to any contamination. So cleaning always preceded any measurement. A typical cleaning sequence is as follows: all lines (gas and oil) are flushed with toluene to remove any traces of hydrocarbon that is remaining. Then the lines are flushed with acetone to remove any remaining toluene. Finally the lines are rinsed with deionized water and dried using air or N_2. Similar process is followed with the cleaning the optical cells, injection needles, valves, glasses and transfer vessels (Ayirala and Rao 2011) .

5.3.1.2 Density Calibration

All density measurements in this chapter were performed at high pressures and high temperatures using Anton Paar Scientific densitometer DMA HP and DMA 4500. The measurement accuracy is typically 0.001 g/cc.

Initially the density meters was calibrated by measuring the period of oscillation of two standard fluids and determine two coefficients A and B that can be plugged with the period on oscillation of unknown sample into the following equation to calculate the density (Sequeira ; Sequeira, Ayirala, and Rao 2008).

$$P = AxP^2 - B \tag{5.1}$$

The density meter was calibrated using water and nitrogen at defined pressures and temperatures. Then the calibration was tested by measuring a sample of Nitrogen and comparing it to values reported by the National Institute of Standards and Technology website(NIST). After every density calibration and measurement is completed the external density cell is cleaned with toluene and acetone and dried with either air or nitrogen, similar approch to what was reported by (Sequeira).

5.3.1.3 IFT Measurement

The following steps were followed in conducting IFT measurements in this study at elevated temperatures and pressures.

- Prepare the fluids (oil and gas), by loading the gas and oil in the ruska pump and transfer vessel respectively. First the vessels are cleaned to prevent any contamination. Then vessels are filled with oil using a funnel. Next, gas is loaded by connecting the vessel to a gas cylinder and adjusting the regulator to get the

required pressure. Cautious must be practiced when vessels are loaded with either gas or oil.

- Heat up the IFT cell to desired temperature, 100 °F. This is achieved by setting the temperature of the oven connected to the system to concerned temperature and left for 1-2 hours.
- Evacuate the optical cell using a vacuum pump to remove any traces of dust. This is accomplished by connecting the top or the bottom of the IFT cell to a vacuum pump and vacuuming for 1hr.
- Introduce the gas and oil into the cell in calculated amount to attain desired gas-oil ratio (molar or volumetric) using either hand pump or other method.
- Allow fluids to reach equilibrium then introduce a drop of oil at the tip of capillary tube at the top of the optical cell.
- Capture the images of the pendent drop of oil using the camera using drop shape analysis (ADSA)software program.
- Repeat the last step for another 5-7 pendent oil drops.
- Open the valve at the top of the cell this allows the gas to flow through the line connected to Anton Paar densitometer. This is done to measure gas density. The density are measured at high pressures high .
- Similarly collect oil from the oil outlet (bottom of the cell) and and measure oil density using the Anton Paar densitometer.
- Process the captured images and use the measured densities to calculate the interfacial tension using the ADSA calculation procedures (Rotenberg, Boruvka, and Neumann 1983).

- Drain and clean the cell and flow lines with toluene and acetone and dry them with air or nitrogen.

5.3.1.4 Digitization Apparatus and IFT Determination

Initially the camera, optical cell and the light sources are aligned in such that a drop image can be captured clearly by the camera. The images are then saved on a computer hard drive. Axisymmetric Drop Shape Analysis (ADSA) software is used to process the images and determine the IFT. The program uses an objective function to minimizes the error between the observed drop and a theoretical Laplacean representation of the shape of the interface between two phases. The interfacial tension values are then calculated in a series of iteration loops until the calculation converges to a final value, for details refer to (Rotenberg, Boruvka, and Neumann 1983).

5.3.2 GAGD Corefloods

To investigate the effect of gas mixtures, especially flue gas, on GAGD performance, the following setup as shown in Figure 5.12, was used to run GAGD displacement experiments. All experiments were performed at 100° F and at three different pressures, 500, 1000 and 2000 psi. Three different gas mixtures were used, CO_2, N_2 and flu gas. The following steps were followed to prepare the cores, saturate it with oil, water flood and gas flood the cores (Kulkarni 2005; Paidin 2013).

5.3.2.1 Pore Volume Determination

This step is to determine pore volume and subsequently determine the porosity of the core. That is done by vacuuming the core and then injecting brine (5% NaCl) into the core at rate of 1-2 cc/m. Then pore volume and the porosity were calculated by dividing amount of brine imbibed by total bulk volume of the core.

5.3.2.2 Absolute Permeability Determination

Next is to determine absolute permeability of the core. This was achieved by flooding the core with brine at three different rates (1, 2 and 3 cc/m). Then Darcy equation was used to calculate the permeability, by plotting flow rates against pressures and determining the permeability from the slope of the plot.

5.3.2.3 nDecane (nC_{10})-Flood

Next after determining permeability, the core is saturated with n-decane (nC10), by injecting n-decane (nC10) at a rate of 1 cc/m for 2-4 pore volumes. Later the oil was pumped at three different injection rates to allow to determine oil relative permeability using flow rate vs pressure plot. Pressure (down stream and upstream), oil volume, water volume and time are recorded. By the end of this run, connate water saturation and relative permeability end points are determined. Finally the oil is left to age for 24 hrs, this allows the oil to reside in the core.

5.3.2.4 Secondary Brine-Flood

Here the core is flooded using brine, by injecting in a horizontal mode for 2 PV at 1 cc/m or less if the core had low permeability. Later the oil was pumped at three different injection rates, to determine Krw. All pressure (down stream and upstream), oil volume, water volume and time are recorded. By the end of this run, recovery efficiency and relative permeability end points are determined. Finally the system,core holder, is switched to a vertical configuration (see Figure 5.13) and is left to age for 24 hrs, this allows the oil to reside in the core.

Figure 5.13: Core holder situated vertically for GAGD experiments

5.3.2.5 Miscible and Immiscible GAGD Flood

Finally the core is flooded with gas (CO_2, N_2 or flue gas), by injecting vertically from the top, for 2 PV at 0.167 cc/m at defined pressures depending on immiscible or miscible pressures. Later the gas was pumped at two different injection rates. Pressures (down stream and upstream), oil volume, water volume and time are recorded. By the end of this run, recovery efficiency and relative permeability end points are determined.

5.4 Parachor Model for Gas-Oil Systems Using N_2 and Flue Gas

To model VIT experiments, Peng-Robinson Equation of state (Peng and Robinson 1976), Parachor model with two different exponent (3.88 and 4) were used. A commercial simulator WinProp (Winprop 2013) was used to generate the phase compositions, phase densities. EOS was tuned to match experimental data, mainly density data. Then

the Parachor model was used predict the interfacial tension for different gas mixture-oil system. Data was plotted as IFT against pressure at a fixed temperature and IFT is extrapolated to zero IFT to determine MMP of the system studied here.

5.5 Experimental Design

The goal here was to assess the effect of different gas type (CO_2, N_2 and flue gas) on the recovery in GAGD in miscible and immiscible mode. Therefore miscibility pressure was determined for four different gas mixtures with C_{10}: CO_2 (100 mole%), CO_2(85 mole%)- N_2(15 mole %), CO_2(15 mole%)- N_2(85 mole%) and N_2 (100 mole%). Then the floods were conducted at three different pressures low pressure 500 psi, medium pressure 1000 psi and high pressure 2000 psi. The temperature was kept constant at 100 $_o$F to be consisted with the IFT data. Three different set of core flood experiments were conducted, different injection gas mixture was used for each set. CO_2 was used for set-1 and N_2 for set-3 and a 15-85 % mixture of CO_2 and N_2 was used for Set-2.

Table 5.1: List of GAGD coreflood experiments

Set	System	pressure (psi)
Set-1	CO_2/nC_{10}	500
		1000
		2000
Set-2	CO_2- N_2 (85-15%)/nC_{10}	500
		1000
		2000
Set-3	N_2/nC_{10}	500
		1000
		2000

Chapter 6
Experimental Results and Discussion

This chapter presents results of IFT measurements, VIT measurements, VIT modeling and the GAGD corefloods. The chapter is divided into two main sections: 1) miscibility pressure determination through IFT measurement and 2) GAGD coreflood, displacement results. First, the IFT measurement using pendent drop method to determine miscibility pressure is presented, where four different gas- nC_{10} cases are considered. The first case used 100% CO_2 for gas. The second case used gas that contained 15% N_2 and 85% CO_2. The third case used gas that contained 85% N_2 and 15% CO_2. The fourth case used 100% N_2 for gas. All measurements were performed at pressures from 200 to 2000 psi and at 100 °F. Then the results were used to assess the performance of Parachor model in predicting gas-oil IFT.

Following miscibility pressure determination, three sets of GAGD coreflood results, total of nine experiments, are presented. All corefloods were performed on 1ft long Berea core, saturated initially with 5 % NaCl brine. A typical experiment involved setting core initial conditions by flooding it with nC_{10}. Then waterflooding it to simulate a secondary recovery process. Both the nC_{10} and waterflood were performed by injecting the fluids horizontally from right to left. Then the core assembly was setup vertically follwoed by injecting gas into the core from the top. Three different corefloods were conducted for each of the gas composition, at 500 psi, 1000 psi and 2000 psi giving a total of eight immiscible displacement experiments and one miscible displacement experiment.

6.1 Miscibility Pressure Measurements and Calculations

6.1.1 Density Calibration

Initially, the density meter, Anton Paar densitometer DMA HP was calibrated using N_2 and de-ionized water, covering pressures from 200- 2000 psi at fixed temperature of 100°F.

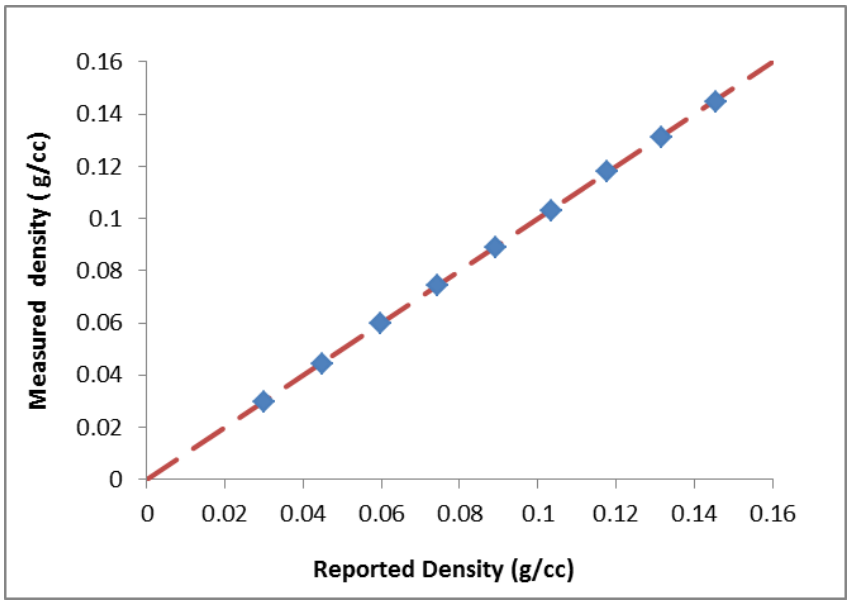

Figure 6.1: Comparison between the measured density (this study) and density reported by NIST for N_2 at different pressures 200-2000 psi.

Then, densities of N_2 were acquired covering the range of 200-2000 psi at 100 °F. Subsequently the densities were compared to reported densities from NIST, to assess the accuracy of the densitometer. Figure 6.1 compares the measured N_2 densities with the reported values from NIST. A good match between the reported and measured densities observed from the straight line with unity slope indicating a good calibration

of density meter used. This supported the usage of the densitometer to measure the densities of the unknown samples.

6.1.2 Density and Interfacial Tension Measurements

Measurement of gas-oil IFT and densities of the equilibrated fluid phases were performed at various pressures from 200 to 1000-2000 psi at constant gas-oil volume ratio of 80-20 % at 100 °F. This particular system GOR was selected due availability of some reported VIT data (Ayirala 2005) that aids in calibrating and validating initial data.

Four sets of density and IFT measurements were conducted, as shown in table 6.1. The first set, used 100 % CO_2 gas. The second set used gas comprising of 85 % CO_2 and 15 % N_2. The third set used gas comprising of 15 % CO_2 and 85 % N_2. The fourth case used 100 % N_2. This was done to investigate the effect of different gas types, specifically flue gas on IFT and MMP.

The densities of the equilibrated fluid phases at different pressures were measured as per procedure described in section 5.31, using DMA HP densitometer.

Table 6.1: List of gas composition for VIT and corefloods.

CO_2/n-Decane
N_2-CO_2 (15-85%/nC_{10})
N_2-CO_2 (85-15%)/nC_{10}
N_2/nC_{10}

6.1.2.1 Density measurement of CO_2-nC_{10} system at 100 °F

Gas-oil densities of the equilibrated fluid phases were performed at pressure from 200 to 1000 psi at constant gas-oil volume ratio of 20% nC_{10} and 80 % CO_2 at 100 °F.

This case aimed in calibrating the technique used to insure the right VIT procedure is followed.

Figure 6.3 is a plot of equilbrated fluid phase densities as a function of pressures for CO_2-nC_{10} system at 100 °F. The graph shows gas phase density increases significantly while there is a slight increase of liquid density with pressure. The difference in densities between the two phases is decreasing with increasing pressure supporting the notion of approaching miscibility condition. This observation matches what was reported previously (Ayirala 2005).

6.1.2.2 Density measurement of nC_{10} against Gas-2 (15 % N_2+ 85 % CO_2) system at 100 °F

Figure 6.6 is a plot of equilbrated fluid phase densities as a function of pressures for C_{10} against Gas-2 (15 % N_2+ 85 % CO_2) system at 100 °F. The graph shows a similar trend to what was seen the previous system of CO_2-nC_{10}. The gas phase density increases while there is a slight increase of liquid density with pressure. Also, the difference in densities between the two phases is decreasing with increasing pressure indicating miscibility pressure is being approached.

6.1.2.3 Density measurement of nC_{10} against Gas-3 (85 % N_2+ 15 % CO_2) system at 100 °F

Figure 6.9 is a plot of equilbrated fluid phase densities as a function of pressures for nC_{10} against Gas-3 (85 % N_2+ 15 % CO_2) system at 100 °F. The graph shows gas phase density increases while there is a slight increase of liquid density with pressure. The difference in densities between the two phases is decreasing with increasing pressure, but in less rate than the previous two cases.

6.1.2.4 Density measurement of N_2- nC_{10} system at 100 °F

Figure 6.12 is a plot of equilbrated fluid phase densities as a function of pressures for N_2- nC_{10} system at 100 °F. The graph shows similar trend to the ones seen in other cases.

6.1.2.5 IFT measurement of CO_2-nC_{10} system at 100 °F

Gas-oil IFT of the equilibrated fluid phases were performed at pressures from 200 to 1000 psi at constant gas-oil volume ratio of 20 % nC_{10} and 80 % CO_2 at 100 °F. This case aimed in calibrating the technique used to insure the right VIT procedure is followed. Table 6.2, summarizes the densities and IFT measurements for CO_2-nC_{10} system at 100 °F. IFT were measured from 0 to 1000 psi. It was challenging to measure IFT at pressures above 1000 PSI, due to un-equilibrium nature of drop of nC_{10} at conditions above 1000 psi. This also agrees with Ayirala (2005) results.

Table 6.2: Summary of fluid densities and CO_2-nC_{10} IFT measurements at 100 °F

Pressure	Gas density	Liquid density	Density difference	IFT
psi	g/cc	g/cc	g/cc	mN/m
200	0.028	0.714	0.686	18.998
400	0.035	0.745	0.711	15.552
600	0.085	0.746	0.662	11.790
800	0.189	0.732	0.543	7.912
1000	0.219	0.774	0.555	3.967

Figure 6.2 shows images of nC_{10} drops surrounded by CO_2 at different pressures at 200- 1000 psi and fixed temperature of 100 °F. At 200 psi there was a good equilibrium

pendent shape of nC_{10} but as pressure increased the size of the drop decreased and at pressures beyond 1000 psi the drop was not stable.

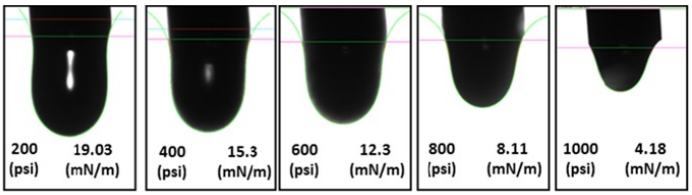

Figure 6.2: Images of nC_{10} drops surrounded by CO_2 at different pressures at 200- 1000 psi and fixed temperature of 100 °F.

Figure 6.4 shows the measured IFT of the CO_2-nC_{10} system at 100 °F at different pressures. It is clear that IFT is decreasing with increasing pressure, which matches what was reported for such a system (Ayirala and Rao 2011). Also from the figure NMP (Pressure at 0.3 mN/m)was determined to be 1198.7 psi.

A liner eqaution was fitted for the IFT data for the CO_2-nC_{10} system. The linear regression equation is shown in Figure 6.4. The coefficient of determination was 0.998, indicating a good fit. The extrapolation of the regression equation to zero IFT results in a VIT-MMP of 1215 psi. This value matches the VIT-MMP reported of 1150 psi and slim tube MMP 1250 psi (Ayirala and Rao 2011).

6.1.2.6 IFT measurement of nC_{10} against Gas-2 (15 % N_2+ 85 % CO_2) system at 100 °F

Gas-oil IFT measurement were performed at various pressures from 200 to 1200 psi at constant gas-oil volume ratio of 80 % gas (85 % CO_2-15 % N_2) and 20 % nC_{10} to determine the minimum miscibility pressure for the system. Table 6.3, summarizes the IFT and densities results. IFT were measured from 0 to 1200 psi.

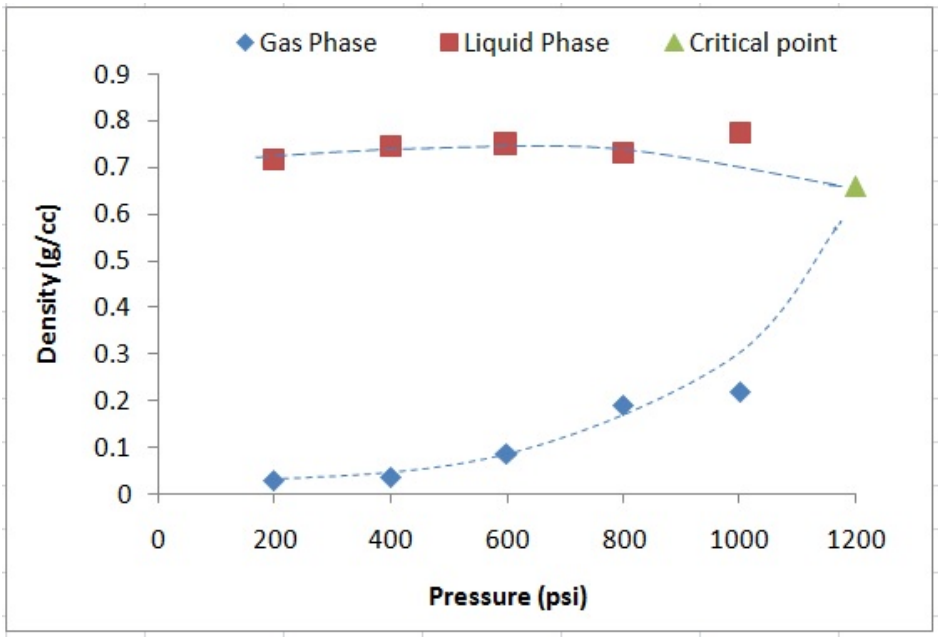

Figure 6.3: Equilibrated Gas and liquid phase densities for CO_2- nC_{10} system at 100 °F

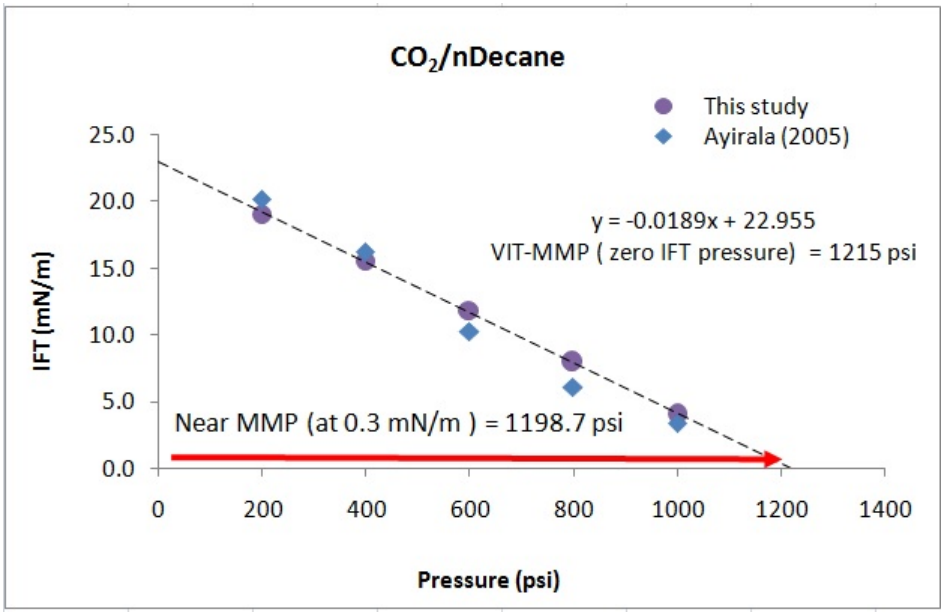

Figure 6.4: Equilibrium gas-oil IFT for CO $\%_2$-nC_{10} system at 100°F. VIT- MMP = 1215 psi, near MMP =1199 psi and Ayirala's VIT MMP = 1215 psi

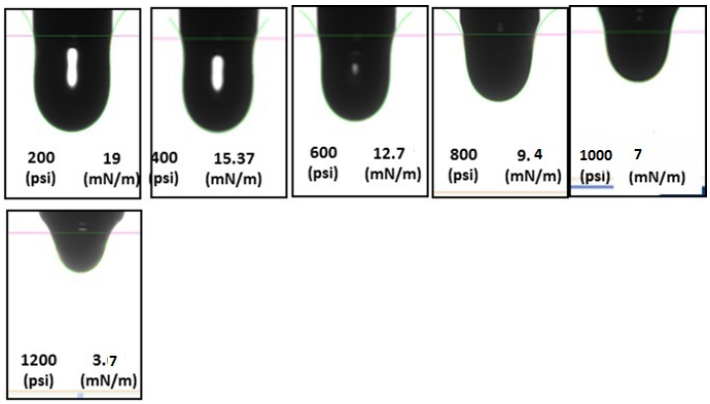

Figure 6.5: Images of nC_{10} drops surrounded by CO_2(85 mole %) -N_2(15 mole %) at different pressures (200-1200 psi)at 100 °F.

Figure 6.7, shows the measured interfacil tension of the CO_2(85 mole %) -N_2(15 mole %)-nC_{10} system at 100 °F at different pressures. It is clear that the interfacial tension is also decreasing with increasing pressure, which matches the previous system.

A linear equation was used to fit IFT and pressure for the CO_2 (85 mole %) -N_2 (15 mole %)- nC_{10} system. The linear regression equation is shown in Figure 6.7. The coefficient of determination value of 0.9983 indicates a good fit. The extrapolation of the regression equation to zero IFT results in a VIT MMP of 1465 psi. Also from the figure NMP (Pressure at 0.3 mN/m) was determined to be 1444.6 psi.

Figure 6.5 shows images of nC_{10} drops surrounded by CO_2(85 mole %) -N_2(15 mole %) at different pressures (200-1200 psi)at 100 °F. similar to previous case (CO_2-nC_{10} case) the pendent drop was more profound at low pressures and decreased in volume at higher pressures. The current system allowed to acquire a drop at equilibrium at pressure of 1200 psi, then the drop was in un-equilibrium state after that.

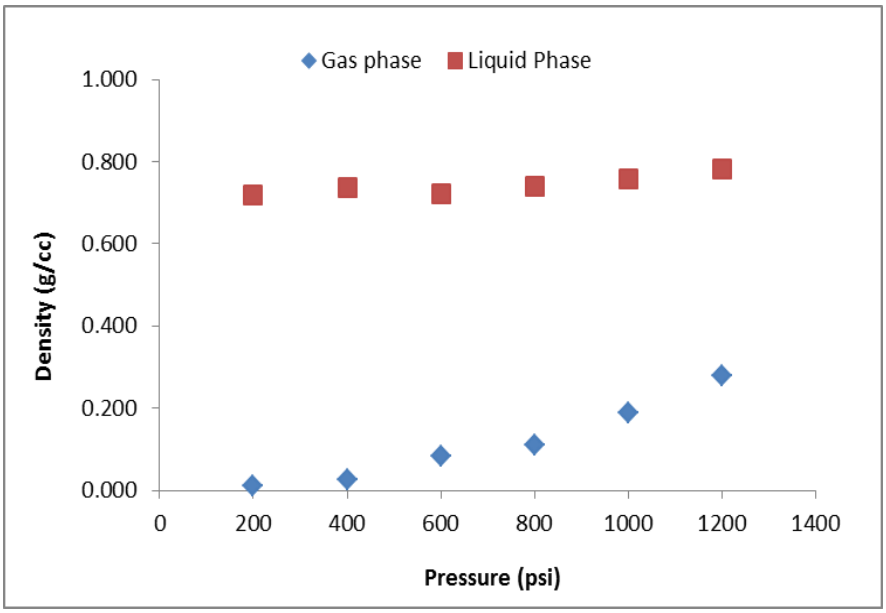

Figure 6.6: Equilibrated gas (CO_2(85 mole %) -N_2(15 mole %)) and liquid phase (nC_{10}) densities at 100 °F

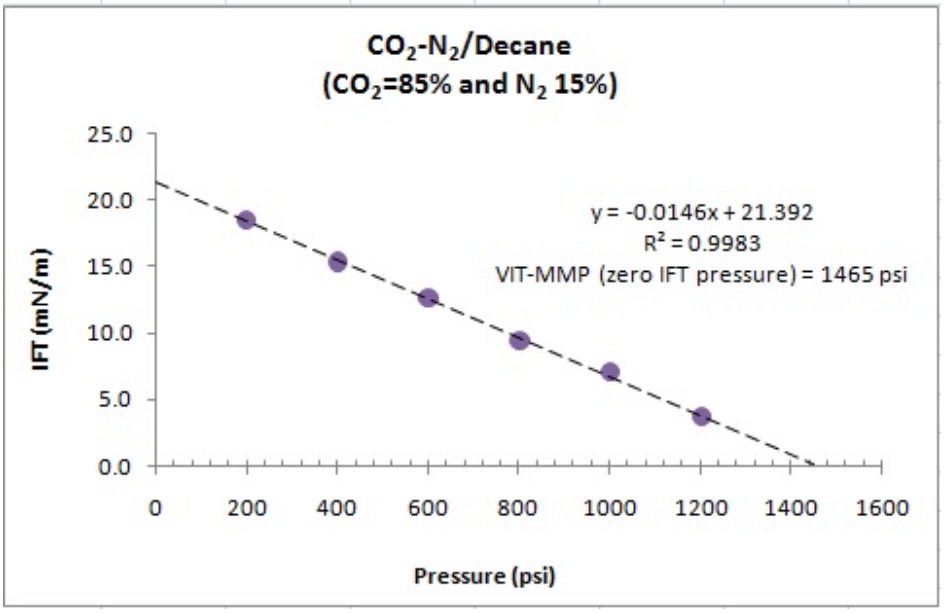

Figure 6.7: Equilibrium gas-oil IFT for CO_2(85 mole %) -N_2(15 mole) - nC_{10} system at 100 °F. VIT-MMP = 1465 psi

Table 6.3: Summary of fluid densities and IFT for CO_2(85 mole %) -N_2(15 mole %)-nC_{10} system at 100 °F

Pressure	Gas density	Liquid density	Density difference	IFT
psi	g/cc	g/cc	g/cc	mN/m
200	0.010	0.719	0.710	18.557
400	0.024	0.738	0.714	15.400
600	0.081	0.721	0.639	12.700
800	0.110	0.740	0.630	9.383
1000	0.189	0.758	0.569	7.093
1200	0.278	0.782	0.504	3.698

6.1.2.7 IFT measurement of nC_{10} against Gas-3 (85 % N_2+ 15 % CO_2) system at 100 °F

Gas-oil IFT measurement were performed at various pressures from 200 to 2000 psi at constant gas-oil volume ratio of 80 % (15 % CO_2 and 85 % N_2) and 20 % nC_{10} and. Table 6.4, summarizes the IFT and densities measurements for CO_2- N_2- nC_{10} system at 100 °F. It can be seen from table 6.4 and Figure 6.16.

Figure 6.8 shows images of nC_{10} drops in CO_2-N_2 at different pressures (200-2000 psi) at 100 °F. IFT were aqured at pressures up 2000 psi. The oil drop images were clear. This is attributed to the fact the IFT of this system is higher compared to the other systems.

Figure 6.10, shows the measured IFT of the CO_2(15 mole %) -N_2(85 mole %)-nC_{10} system at 100 °F at different pressures. It is clear that the interfacial tension is also decreasing with increasing pressure.

A linear equation fit IFT measured for the CO_2(15 mole %) -N_2(85 mole %)- nC_{10} system. The equation is shown in Figure 6.10. The coefficient of determination value

Table 6.4: Summary of fluid densities and IFT for CO_2(15 mole %) -N_2(85 mole %)-nC_{10} system at 100°F

Pressure	Gas density	Liquid density	Density difference	IFT
psi	g/cc	g/cc	g/cc	mN/m
200	0.023	0.715	0.692	19.876
400	0.028	0.717	0.690	18.733
600	0.067	0.709	0.642	17.017
800	0.110	0.709	0.599	15.480
1000	0.099	0.689	0.590	14.668
1200	0.130	0.730	0.600	14.858
1400	0.169	0.738	0.568	13.385
1600	0.178	0.723	0.545	13.103
1800	0.160	0.740	0.580	12.944
2000	0.152	0.724	0.572	12.240

of 0.94 indicates a good fit. the extrapolation of the regression equation to zero IFT results in a VIT MMP of 4556 psi.

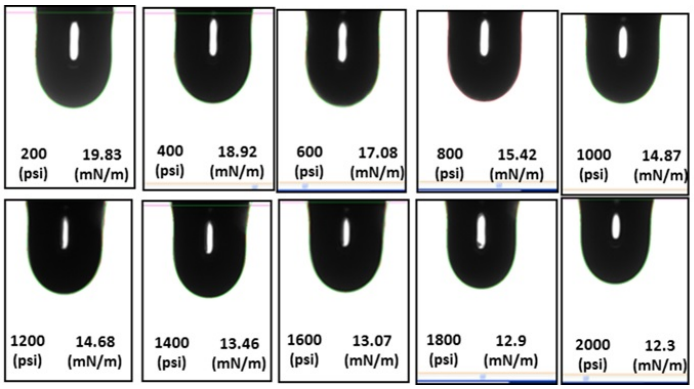

Figure 6.8: Images of nC_{10} drops in CO_2-N_2 at different pressures (200-2000 psi) at 100 °F.

6.1.2.8 IFT measurement of N_2- nC_{10} system at 100 °F

Gas-oil IFT measurement were performed at various pressures from 200 to 2000 psi at constant gas-oil volume ratio of 20 % nC_{10} and 80 % N_2. Table 6.5, summarizes the IFT and densities measurements for CO_2-nC_{10} system at 100 °F.

Figure 6.11 shows images of nC_{10} drops in CO_2-N_2 at different pressures (200-2000 psi) at 100 °F. IFT were acquired at pressures up 2000 psi. The oil drop images were clear, in equilibrium this is attributed to the fact the IFT of this system is higher compared to the other systems.

Figure 6.13 shows the measured IFT of N_2-nC_{10} at 100 °F at different pressures. It is clear that the interfacial tension is also decreasing with increasing pressure.

A good correlation was obtained for IFT and pressure for the N_2-nC_{10} system. The regression equation is shown in Figure 6.13. The coefficient of determination value of 0.95 indicates a good fit. The extrapolation of the regression equation to zero IFT results in a VIT -MMP of 4687 psi.

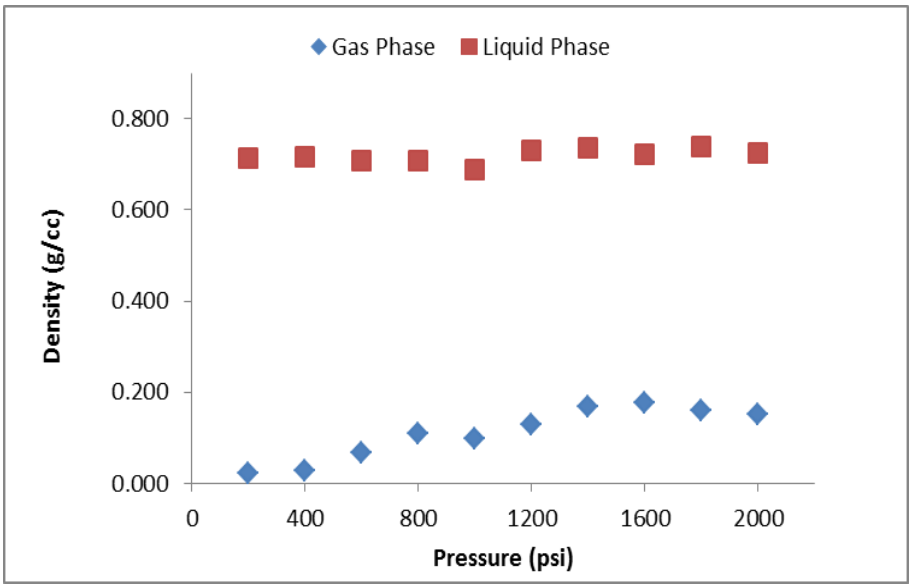

Figure 6.9: Equilibrated gas (CO_2(15 mole %) -N_2(85 mole %)) and liquid phase (nC_{10}) densities at 100 °F

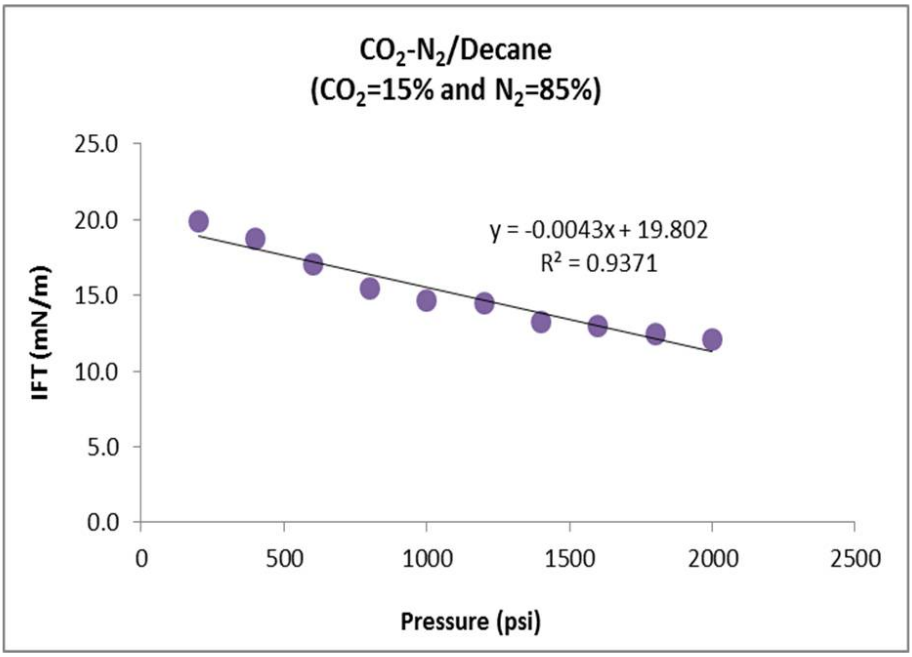

Figure 6.10: Equilibrium gas-oil IFT for for CO_2(15 mole %) -N_2(85 mole %)-nC_{10} system at 100 °F. VIT-MMP = 4556 psi

Table 6.5: Summary of fluid densities and IFT N_2-nC_{10} measurements at 100°F

Pressure	Gas density	Liquid density	Density difference	IFT
psi	g/cc	g/cc	mN/m	
200	0.014	0.733	0.719	21.356
400	0.025	0.720	0.695	18.877
600	0.052	0.711	0.658	18.133
800	0.078	0.721	0.643	17.633
1000	0.077	0.725	0.649	16.737
1200	0.153	0.741	0.588	14.899
1400	0.169	0.788	0.619	14.457
1600	0.192	0.724	0.531	13.767
1800	0.166	0.744	0.578	13.690
2000	0.170	0.703	0.533	12.651

6.1.3 Interfacial Tension Modeling

6.1.3.1 IFT prediction

In order to asses the performance of the Parachor model in predicting IFT of systems that contain N_2, a similar approach as in chapter 3 was used with tuning EOS to match measured data. Then effect of the Parachor exponent and the Parachor constant for the heavy component were evaluated.

$$\sigma = \sum_{i=1}^{n} [Pi(x\frac{\rho_{\mathrm{l}}}{M_{\mathrm{l}}} - y\frac{\rho_{\mathrm{v}}}{M_{\mathrm{v}}})]^{3.88} \tag{6.1}$$

Where σ is the IFT, Pi the Parachor constant for component i, M_{l} and M_{v} the molecular weights of the liquid and vapor phases, ρ_{l} and ρ_{v} are the mass densities of the liquid and vapor phases and n is the number of components in the system. PR-EOS

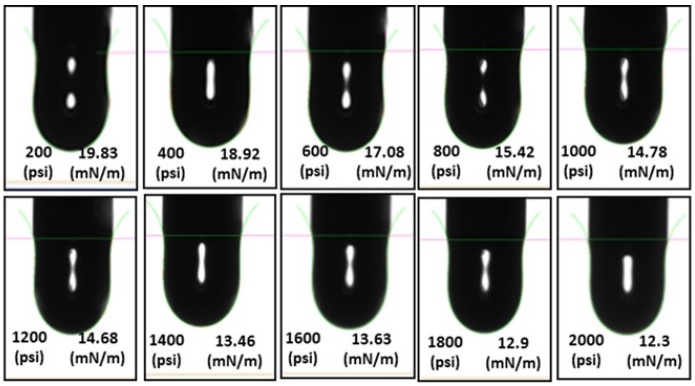

Figure 6.11: Images of nC_{10} drops surrounded by N_2 at different pressures (200-2000 psi) at 100 °F.

was tuned to predict the densities measured in the lab, then Parachor model was used to predict gas-oil IFT.

The systems mentioned earlier are used here, see below:

- System 1: CO_2 (100 mole %).
- System 2: CO_2(85 mole %)- N_2(15 mole %).
- System 3: CO_2(15 mole %)- N_2(85 mole %).
- System 4: N_2 (100 mole %).

Figure 6.14 shows the comparison between measured and calculated density difference between gas and liquid phase densities. The x-axis presents the measured density difference values and the y-axis shows the calculated ones using PR EOS.

Figure 6.15 shows the calculated IFT using the Parachor model with two different exponents (3.88 and 4). The exponent value of 3.88 Parachor model performed better than n =4 for all four cases.

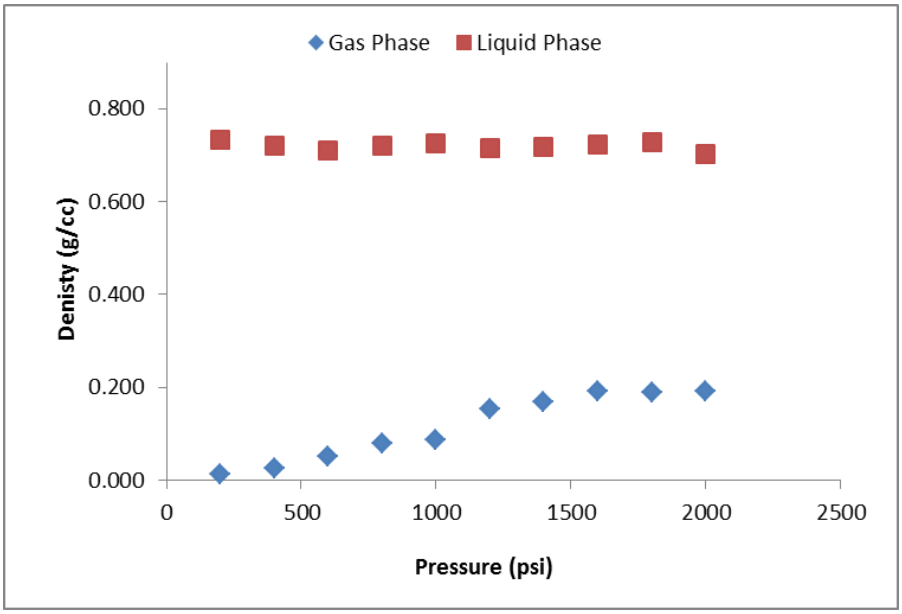

Figure 6.12: Equilibrated gas and liquid phase densities for N_2-nC_{10} at 100 °F

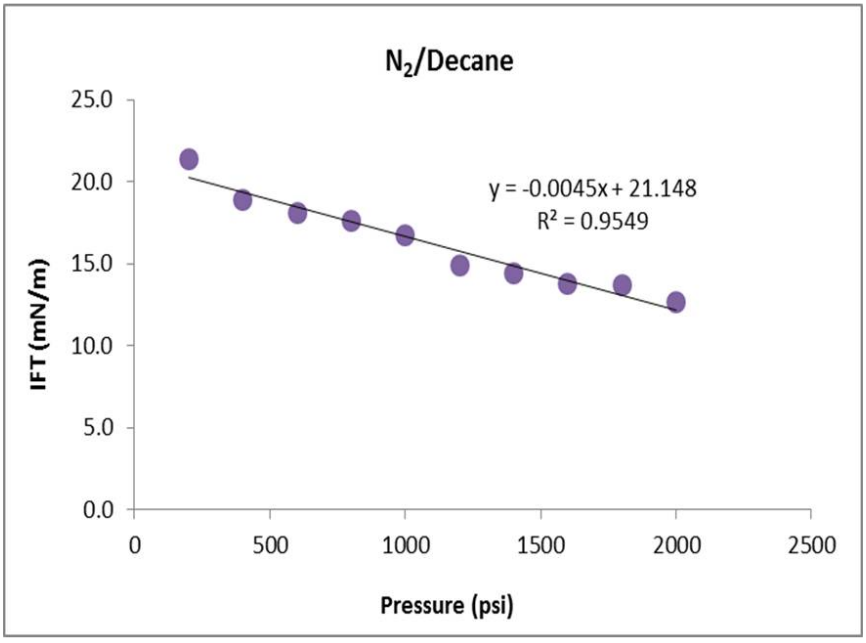

Figure 6.13: Equilibrium gas-oil IFT for for N_2-ndecane system at 100 °F. VIT-MMP = 4687 psi

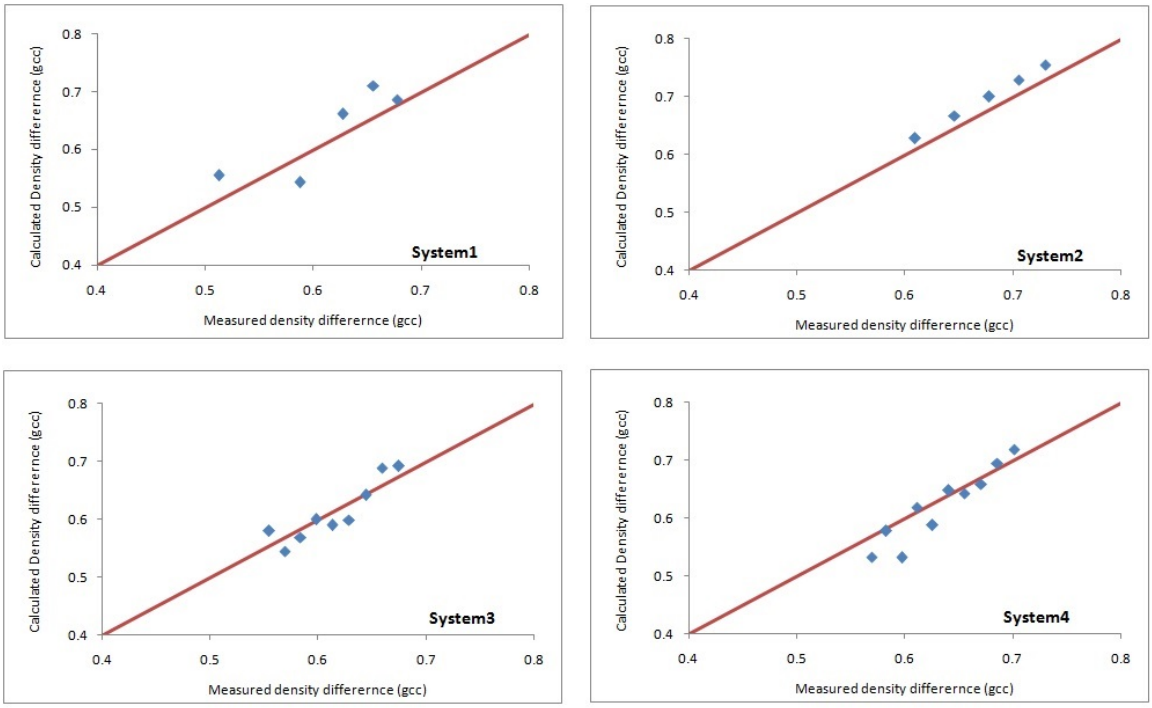

Figure 6.14: Comparison between measured and calculated and gas-oil density difference using PR-EOS for system-1 (top left), system-2 (top right), system-3 (bottom left) and system-4 (bottom right. The x- axis presents the measured density difference values and the y- axis shows the calculated ones using PR-EOS. System 1) CO2-nC10, System 2) CO_2-N_2-nC_{10}, System 3)CO_2-N_2-nC_{10} and System 4)N_2-nC_{10}.

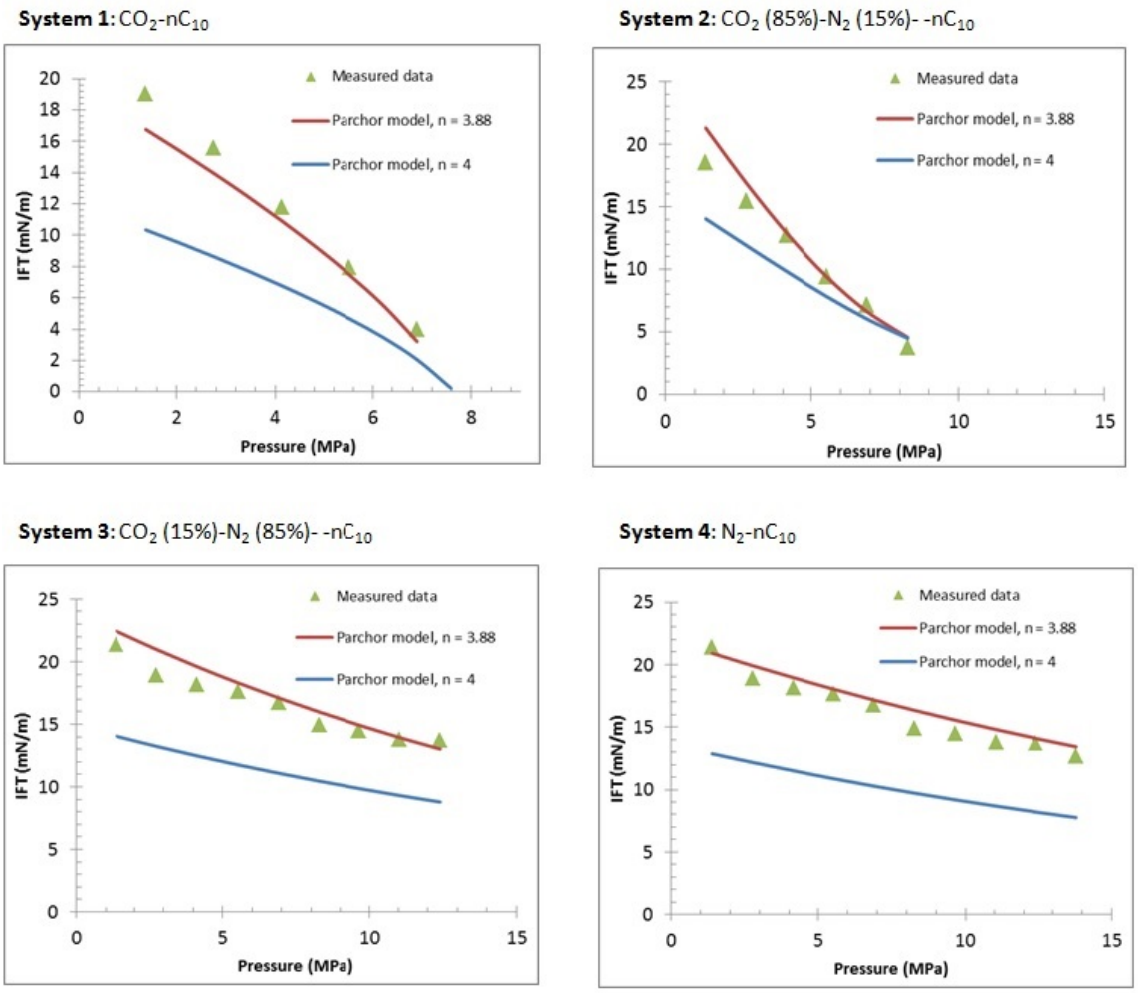

Figure 6.15: Comparison between measured and calculated interfacial tension for system-1 (top left), system-2 (top right), system-3 (bottom left) and system-4 (bottom right), the x-axis presents the measured IFT values and the y-axis shows the calculated ones using Parachor model. System 1) CO2-nC10, System 2) CO_2-N_2-nC_{10}, System 3)CO_2-N_2-nC_{10} and System 4)N_2-nC_{10}.

6.1.3.2 Comparison between measured VIT-MMP and calculated VIT-MMP

Table 6.6 compares MMP measured and calculated using IFT method. It is clear that the EOS-IFT method can predict the experiment, provided the EOS was tuned to match experimental data. The approach used to predict IFT and MMP is clearly reasonable, since it resulted in minor differences.

Table 6.6: measured vs calculated gas -nC_{10} miscibility pressure

System	Measured VIT MMP	Predicted VIT MMP	Difference
	MPa	MPa	%
System-1	8.4	8.5	1.2
System-2	10.1	9.7	4.0
System-3	31.4	27.3	13.1
System-4	32.3	35.7	10.5

6.1.4 Discussion

Figure 6.16, shows the comparison between the four gas mixtures data on IFT as a function of pressure. The following can be observed:

1. The more CO_2 content in the gas mixture the lower the interfacial tension at particular pressure. For example at 800 psi the IFT for case1(injection gas contains 100 % CO_2), case 2 (injection gas contains 15 % N_2 and 85 % CO_2), case 3 (injection gas contains 85 % N_2 and 15 % CO_2)and case 4 (injection gas contains 100 % N_2)are 7.912, 9.38, 15.48 and 17.63 mN/m respectively.

2. Increase N_2 concentration in gas mixture elevates MMP, this can be observed in MMP values of case1, case 2, case 3 and case 4 being 1250 psi, 1465 psi, 4556 psi, 4687 psi respectively.

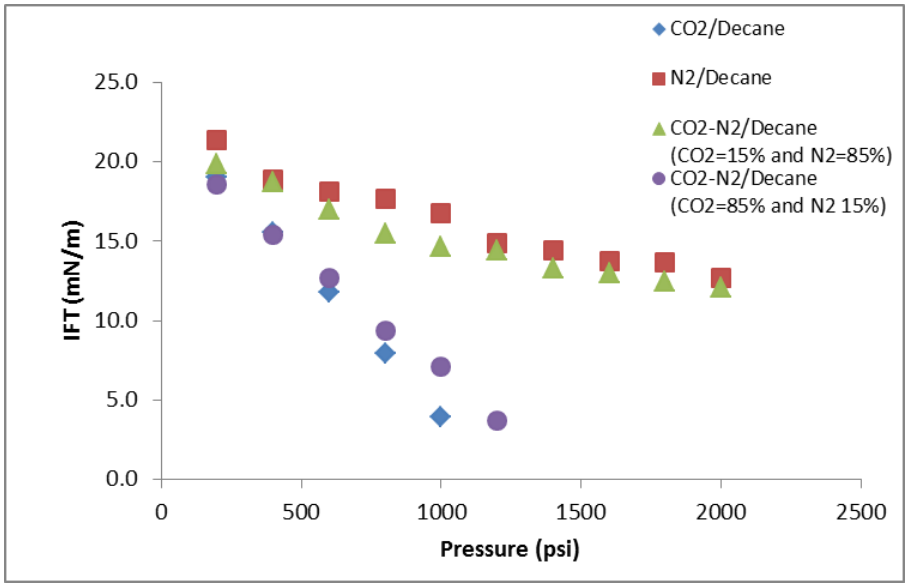

Figure 6.16: IFT Vs. Pressure for four different systems:1) CO2-nC10, 2) CO_2-N_2-nC_{10}, 3)CO_2-N_2-nC_{10} and 4)N_2-nC_{10} at 100 °F.

A calculation method adopted from chapter 3 (EOS and Parachor model) was used here to asses if it can predict IFT and VIT MMP for systems that contain Nitrogen gas.

Previous studies reported that the Parachor model did not predict well the IFT of N_2-oil systems (Schechter and Guo 1998). Therefore here we assessed IFT prediction for N_2- nC_{10} and N_2-CO_2-nC_{10} systems using the Parachor model. After tuning EOS and obtaining a good density match, the Parachor model with the exponent value of 3.88 matched all experimental data quite well. Although we agree with the others that the Parachor value is not a constant in cases involving nitrogen and can be improved

via tuning EOS. Therefore this work suggests tuning the EOS to match experimental data, density and composition then use Parachor model with exponent 3.88 to get a better match with measured IFT.

Comparing the calculated VIT-MMP it was observed that the more N_2 in the system the more deviation between the measured and collated VIT MMP. For system 3 and 4 the difference was more than 10 % due to high percentage of nitrogen in the systems. Again, the prediction can be improved further by acquiring more data to tune EOS to improve the prediction capability of the method.

6.1.5 Summary

This section has presented an experimental measurement of gas-oil interfacial tension as a function of pressure and the resulting miscibility pressures for four different gas mixtures-oil systems (CO_2-nC10, N_2-nC10, (15 %) CO_2- (85 %) N_2-nC10 and (85 %) CO_2- (15 %) N_2- nC10). IFT prediction using the Parachor model was also evaluated. The following can be summarized based on the results:

1. VIT technique, based on measuring IFT at varying pressures to determine miscibility pressure was successfully used to asses the miscibility of different gas mixtures with nC_{10}.
2. Minimum miscibility pressure (MMP) for the nC_{10} with CO_2 and N_2 as injection gases were determined using VIT technique. The MMP of N_2 -nC_{10} system of 4687 psi was significantly higher than the CO_2- nC_{10} system of 1215 psi at 100 ^oF.
3. Minimum miscibility pressure MMP for the nC_{10} with mixtures of CO_2 and N_2 as injection gases were determined using VIT technique. The MMP of CO_2 (15

%)- N_2(85 %)- nC_{10} system and CO_2 (85 %)- N_2(15 %)- nC_{10} system at 100 °F were, 4556 psi and 4687 psi respectively.

4. The Parachor model was successfully used to predict IFTs of the system used in this study.
5. The calculated VIT MMP were close to the measured values, supporting the usage of calculation technique especially if experimental data to tune EOS are available.
6. It was proved again that VIT method was fast and reliable to measure miscibility pressures for gas-oil system for gas injection EOR project.

6.2 Gas Assisted Gravity Drainage (GAGD) Corefloods

The last section presented fluid-fluid interaction results, where gas-oil interfacial tension was measured for different gas-oil system at high pressures and temperature. The results, and specifically MMP (zero IFT pressure) were considered in GAGD corefloods in this section.

Three sets of GAGD coreflood results are presented in this section. Each set is using a different injection gas, CO_2, N_2 and flue gas. For each set, three different pressures were tested, 500, 1000 and 2000 psi. These set of conditions were picked to allow comparison with previous work using GAGD (Kulkarni 2005). The following parameters and procedures were held constant for all the floods presented in this chapter:

1. Core temperature of 100 °F.
2. Overburden pressure of 500 psi more than core pressure.
3. Injection rates for nC_{10}, water and gas (1, 2 and 3 cc/min).

4. Brine of 5 % NaCl.

5. Core dimensions (1 ft long and 2 inches diameter).

6. Experimental setup and procedures (described in Chapter-5).

The GAGD corefloods described in this section include the nC_{10} and waterfloods secondary flood results for completeness. The three sets examine the effect of gas type on GAGD performance.

This section covers the results of corefloods using CO_2 in immiscible, near miscible (lower IFT compared to the immiscible case) and miscible conditions (above zero IFT pressure), followed by N_2 and flue gasflood results all in immiscible condition. Finally the results are discussed and then main findings are summarized at the end.

6.2.1 CO_2- Assisted Gravity Drainage Floods

Three different gas corefloods were conducted on GAGD mode and using CO_2:

1. Immiscible run at 500 psi.

2. Low IFT run at 1000 psi (IFT-MMP = 1215 psi).

3. Totally miscible run at 2000 psi.

6.2.1.1 Immiscible CO_2 Injection at 500 psi and 100°F

Figure 6.17 summarizes CO_2 assisted gravity drainage displacement experiment (core initialization, waterflood and GAGD flood) on 1-ft Berea core at 500 psi. First the core was flooded with nC_{10} until irreducible water saturation was achieved. Figure 6.17a, shows the amount of water recovered and nC_{10} produced during drainage cycle

(oil flood). Connate water saturation (Swc) and initail oil saturation (Soi) were determined to be 0.49 and 0.51 respectively. The pressure drop across the core during nC_{10} displacement is illustrated in Figure 6.17b.

Next the core was waterflooded at 1 cc/min for 2 PV, 2 cc/min for 1P V and 3cc/min for 1 PV. Figure 6.17c, shows the amount of oil recovered and water injected in the core during waterflood, secondary recovery, as a function of pore volume injected. Initially the oil cumulative production increased at steep slope, then less slope at around 0.17 PVI and plateaued at around 0.7 PVI. Figure 6.17d, shows the pressure drop during water displacement. Total oil produced at the end of waterflood was 0.28 PV, yielding recovery of 54 % of original oil in place (OIIP).

Finally CO_2 was continuously injected at 500 psi on gravity mode, tertiary recovery. Figure 6.17e shows a tertiary CO_2: Pure CO_2 vertical immiscible injection and pressure drop across the core during the CO_2-assisted gravity drainage. Oil produced at the end of 2 PVI was around 8 cc (0.07 PV), around 35 % recovery of the remaining oil in place (ROIP). The pressure difference peaked in early stage until breakthrough and then decreased to 4 psi by the end of the flood, see Figure 6.17f.

6.2.1.2 Low IFT CO_2 Injection at 1000 psi and 100°F

Figure 6.18 summarizes CO_2 gravity assisted drainage displacement experiment on 1-ft Berea core at 1000 psi. Connate water saturation (Swc) and initail oil saturation (Soi) were determined to be 0.46 and 0.54 respectively. Figure 6.18a, shows the water recovered and oil injected in the core during nC_{10} injection as a function of pore volume injected. The pressure gauges recorded a drop to 7 psi at 2 PVI, see Figure 6.18b

Figure 6.18c shows the oil recovered and water injected in the core during waterflood as a function of pore volume injected. Water breakthrough occurred at 0.3 PVI.

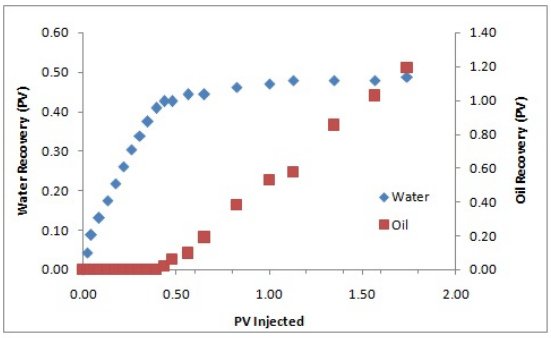

(a) Oilflood, cumulative oil and water production

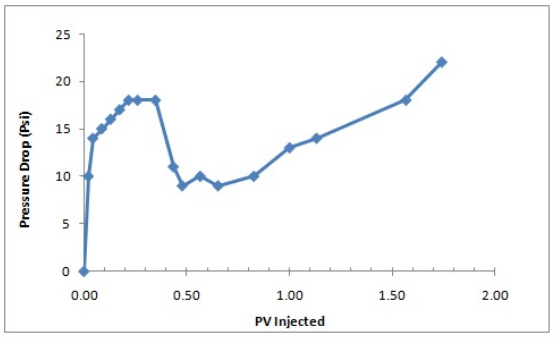

(b) Oilflood pressure drop

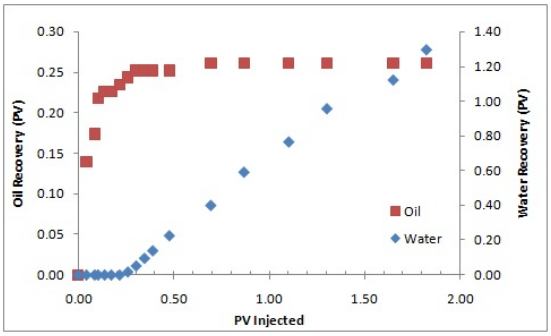

(c) Waterflood, cumulative oil and water production

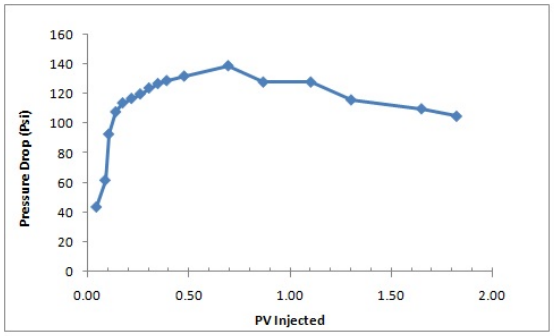

(d) Waterflood pressure drop

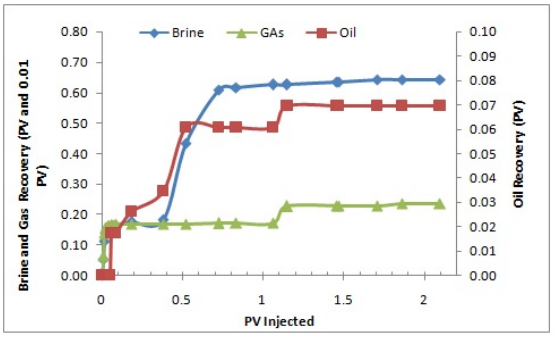

(e) Gasflood, cumulative liquid and gas production

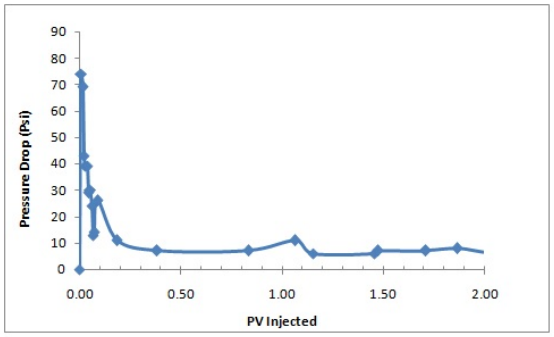

(f) Gasflood pressure drop

Figure 6.17: Immiscible CO_2 flood: 1-ft Berea core, using nC_{10} for oil and using CO_2 for gas injection. Brine has 5 % NaCl concentration. Core pressure is 500 psi and 100°F. a) Drainage Cycle: oilflood with nC_{10}. b) Imbibition Cycle: waterflood with brine. c) Tertiary CO_2 flood: pure CO_2 continuous vertical immiscible injection.

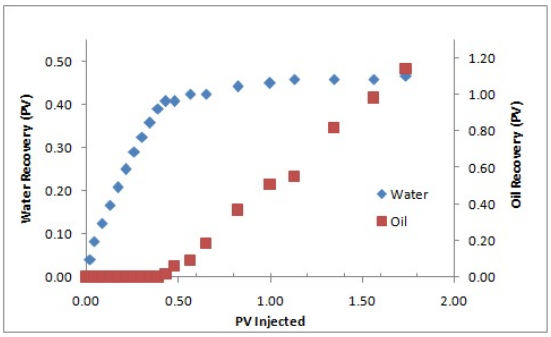

(a) Oil flood, cumulative oil and water production

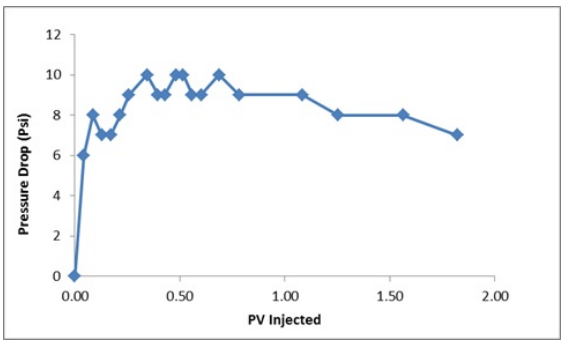

(b) Oil flood pressure drop

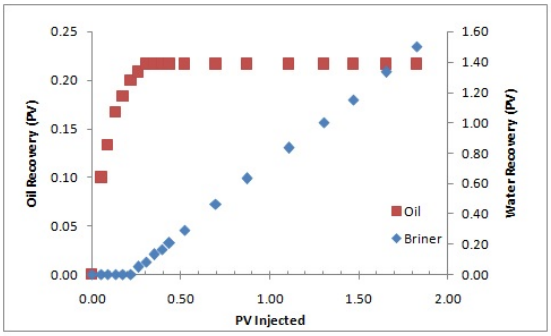

(c) waterflood, cumulative oil and water production

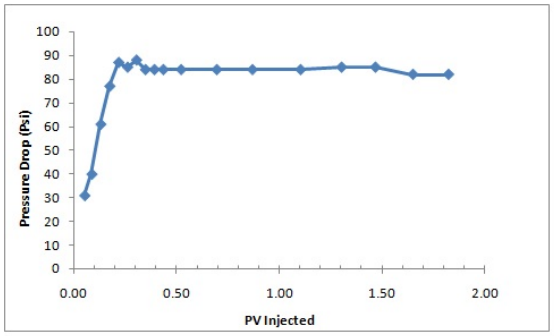

(d) waterflood pressure drop

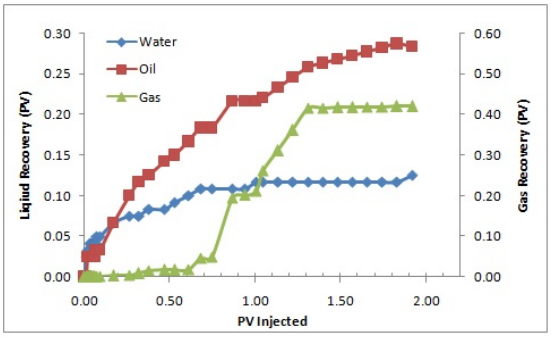

(e) gasflood, cumulative liquid and gas production

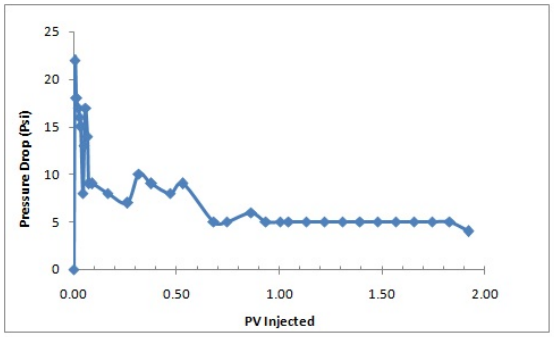

(f) gasflood pressure drop

Figure 6.18: Low IFT CO_2 flood: 1-ft Berea core, using nC_{10} for oil and using CO_2 for gas injection. Brine has 5 % NaCl concentration. Core pressure is 1000 psi and 100°F. a) Drainage Cycle: oilflood with nC_{10}. b) Imbibition Cycle: waterflood with brine. c) Tertiary CO_2 flood: Pure CO_2 continuous vertical near miscible injection.

Figure 6.18d, shows the pressure drop during water displacement. The pressure drop leveled around 85 psi after breakthrough.

Figure 6.18e shows a tertiary CO_2 flood results: pure CO_2 vertical low IFT flood and pressure drop during the CO_2-assisted gravity drainage. Total oil produced at the end of 2 PVI was around 34 cc (0.29 PV) resulting in a recovery of 94 % of remaining oil in place (ROIP). As for the pressure drop, it peaked at around 20 psi then then decreased after breakthrough to 4-5 psi at the end of the flood, see Figure 6.18f.

6.2.1.3 Miscible CO_2 Injection at 2000 psi and 100°F

Figure 6.19 summarizes CO_2 assisted gravity drainage displacement experiment (core initialization, waterflood and gasflood) on 1-ft Berea core at 2000 psi. Figure 6.19a, shows the water recovered and oil injected in the core during nC_{10} injection as a function of pore volume injected. Connate water saturation (Swc) and initail oil saturation (Soi) were determined to be 0.46 and 0.54 respectively. Figure 6.19b shows the pressure drop during nC_{10} displacement. The pressure drop leveled at around 20 psi at 2 PVI.

Figure 6.19c shows the oil recovered and water injected in the core during waterflood as a function of pore volume injected. Water breakthrough occurred at 0.24 PVI. Figure 6.19d, shows the pressure drop during water displacement. The pressure was around 67 psi at 2 PVI.

Figure 6.19e shows a tertiary CO_2 flood: Pure CO_2 vertical miscible injection and pressure drop during the CO_2-assisted gravity drainage. Initially only oil was produced. Then gas and water followed at 0.2 and 0.4 PVI respectively. Total oil produced at the end of 2 PVI was around 21 cc (0.21 PV) yielding around 100 % recovery of remaining oil in place (ROIP). The pressure drop recorded was 19 psi at the end of the flood, see Figure 6.19f.

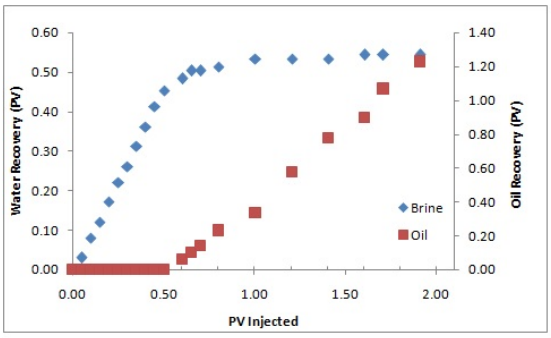

(a) Oilflood, cumulative oil and water production

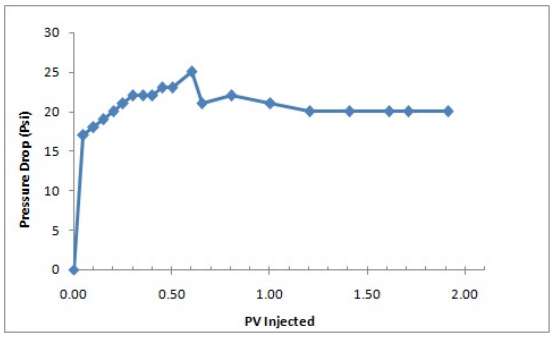

(b) Oil flood pressure drop

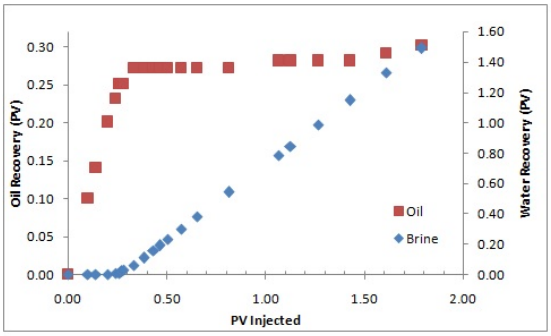

(c) waterflood, cumulative oil and water production

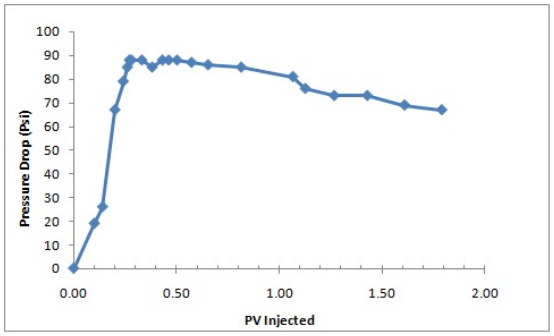

(d) waterflood pressure drop

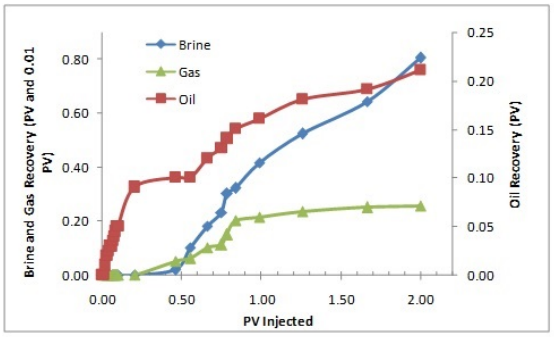

(e) gasflood, cumulative liquid and gas production

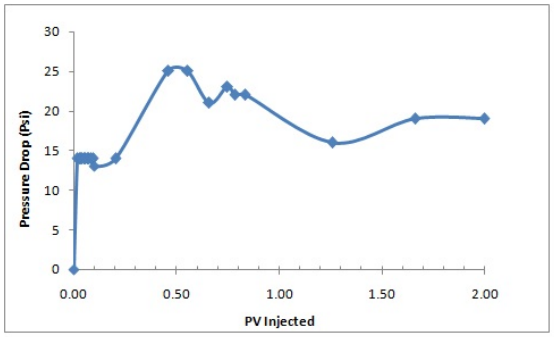

(f) gasflood pressure drop

Figure 6.19: Miscible CO_2 flood: 1-ft Berea core, using nC_{10} for oil and using CO_2 for gas injection. Brine has 5 % NaCl concentration. Core pressure is 2000 psi and 100°F . a) Drainage Cycle: oilflood with nC_{10}. b) Imbibition Cycle: waterflood with brine . c) Tertiary CO_2 flood: pure CO_2 continuous vertical miscible injection.

6.2.2 N_2 Assisted Gravity Floods

Three different gas coreflood cases were conducted using N_2. All gas floods were conducted on GAGD mode and all runs were immiscible at 500 psi 1000 and 2000 psi.

6.2.2.1 Immiscible Vertical N_2 Injection at 500 psi and 100°F

Figure 6.20 summarizes N_2 gravity assisted drainage displacement experiment (core initialization, waterflood and gasflood) on 1-ft Berea core at 500 psi. Prior to injecting N_2, the core was flooded with nC_{10} to set connate water saturation. Figure 6.20a, shows the amount of water recovered as oil was injected in the core during nC_{10} injection. The connate water saturation for this run was 0.31. The pressure drop across the core during nC_{10} displacement is illustrated in Figure 6.20b.

Next the core was subjected to waterflood at 1 cc/min for 2 PVI. Figure 6.20c shows the amount of oil recovered and water injected in the core during waterflood, secondary recovery, as a function of pore volume injected. Initially the oil cumulative production increased linearly then plateaued at around 0.24 PVI. Figure 6.20d shows the pressure drop during water displacement. Total produced oil at the end of waterflood was 0.28 cc (0.24 PV), yielding 38 % of original oil in place (OIIP).

N_2 was continuously injected at 500 psi on gravity mode, tertiary recovery mode. Figure 6.20e, shows a tertiary N_2 flood: Pure N_2 vertical immiscible injection and pressure drop during the N_2-Assistd gravity drainage. Total oil produced at the end of 2 PVI was around 16 cc giving around 30 % recovery of remaining oil in place (ROIP). As for the pressure drop, see Figure 6.20f

6.2.2.2 Immiscible Vertical N_2 Injection at 1000 psi and 100°F

Figure 6.21 summarizes N_2 gravity assisted drainage displacement experiment on 1-ft Berea core at 1000 psi. Similarly the core was initially saturated with nC_{10}. Figure

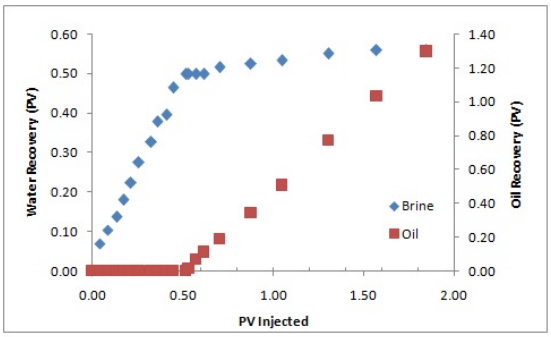

(a) Oil flood, cumulative oil and water production

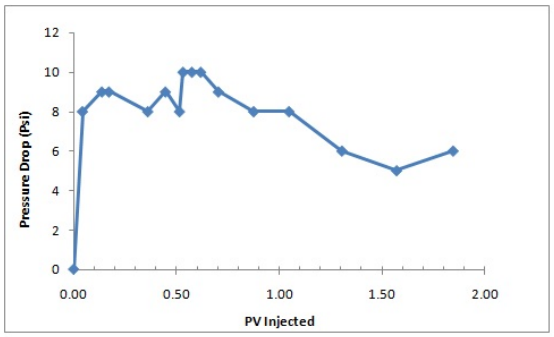

(b) Oil flood pressure drop

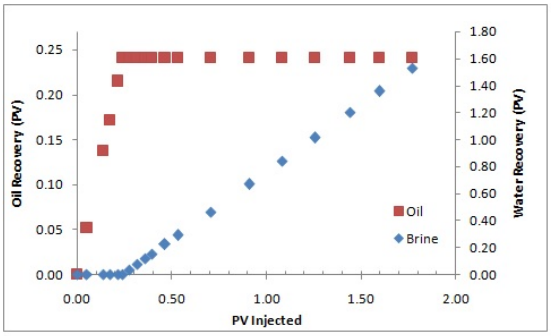

(c) waterflood, cumulative oil and water production

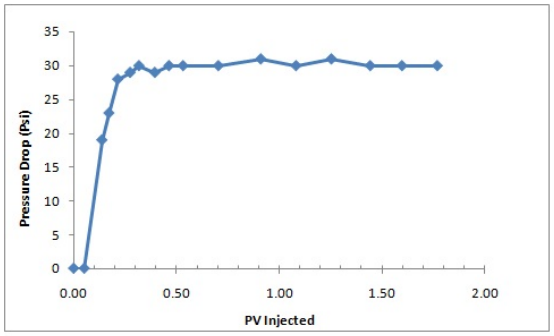

(d) waterflood pressure drop

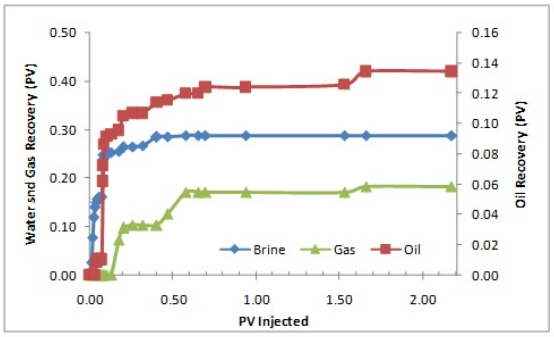

(e) gasflood, cumulative liquid and gas production

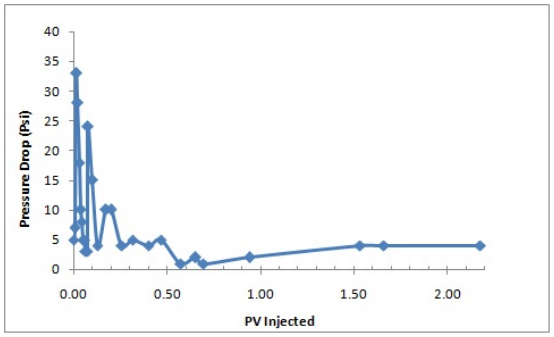

(f) gasflood pressure drop

Figure 6.20: Immiscible N_2 flood: 1-ft Berea core, using nC_{10} for oil and using N_2 for gas injection. Brine has 5 % Nacl concentration. Core pressure is 500 psi and 100°F. a) Drainage Cycle: oilflood with nC_{10}. b) Imbibition Cycle: waterflood with brine . c) Tertiary N_2 flood: Pure N_2 continuous vertical immiscible injection.

6.21a shows the amount of water recovered as oil was injected in the core during nC_{10} injection. By the end of nC_{10} flood the connate water saturation was 0.38. The pressure drop across the core during nC_{10} displacement, see Figure 6.21b.

Next the core was subjected to waterflood at 1 cc/min for 2 PVI. Figure 6.21c shows the amount of oil recovered and water injected in the core during waterflood, secondary recovery, as a function of pore volume injected. Initially the oil cumulative production increased linearly then plateaued at around 0.3 PVI. Figure 6.21d, shows the Pressure drop during water displacement. Total produced oil at the end of waterflood was 0.33 PV, yielding 53 % of original oil in place (OIIP).

N_2 was continuously injected at 1000 Psi in a core on gravity mode. Figure 6.21e, shows a tertiary N_2 flood: Pure N_2 vertical immiscible injection and pressure drop during the N_2-Assistd gravity drainage. Total oil produced at the end of 2 PVI was around 11.8 cc (0.1 PV) giving around 31 % recovery of remaining oil in place (ROIP). As for the pressure drop, see Figure 6.21f.

6.2.2.3 Immiscible Vertical N_2 Injection at 2000 psi and 100°F

Figure 6.22 summarizes N_2 gravity assisted drainage displacement experiment (core initialization, waterflood and gasflood) on 1-ft Berea Core at 500 psi. Prior injecting flue gas, the core was subjected to nC_{10} flood to set connate water saturation. Figure 6.22a, shows the amount of water recovered as oil was injected in the core during nC_{10} injection. By the end of nC_{10} flood the connate water saturation was 0.42. The pressure drop across the core during nC_{10} displacement is illustrated in Figure 6.22b.

Next the core was ed at 1 cc/min for 2 PV. Figure 6.22c shows the amount of oil recovered and water injected in the core during waterflood, secondary recovery, as a function of pore volume injected. Initially the oil cumulative production increased linearly then plateaued at around 0.2 PVI. Figure 6.22d, shows the Pressure drop

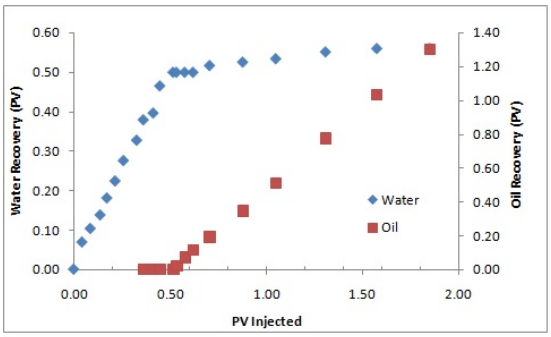

(a) Oil flood, cumulative oil and water production

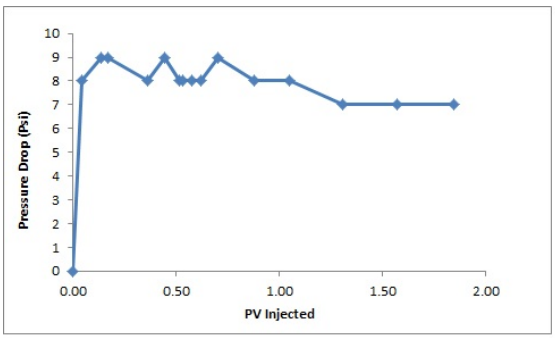

(b) Oil flood pressure drop

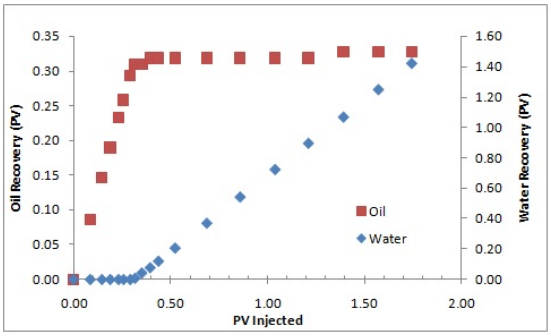

(c) Waterflood, cumulative oil and water production

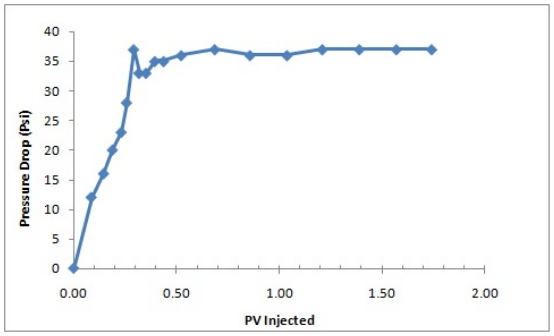

(d) Waterflood pressure drop

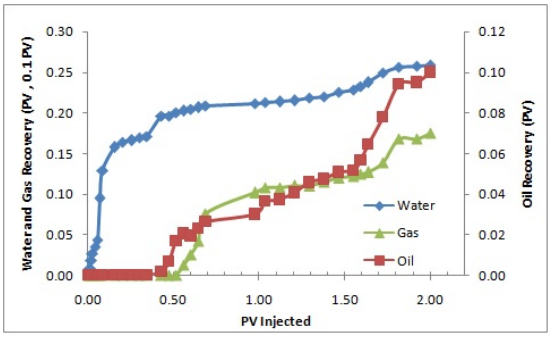

(e) Gasflood, cumulative liquid and gas production

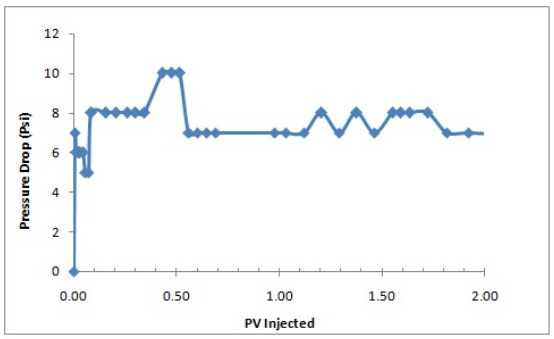

(f) Gasflood pressure drop

Figure 6.21: Immiscible N_2 flood: 1-ft Berea core, using nC_{10} for oil and using N_2 for gas injection. Brine has 5 % Nacl concentration. Core pressure is 1000 psi and 100°F . a) Drainage Cycle: oilflood with nC_{10}. b) Imbibition Cycle: waterflood with brine. c) Tertiary N_2 flood: Pure N_2 continuous vertical immiscible injection.

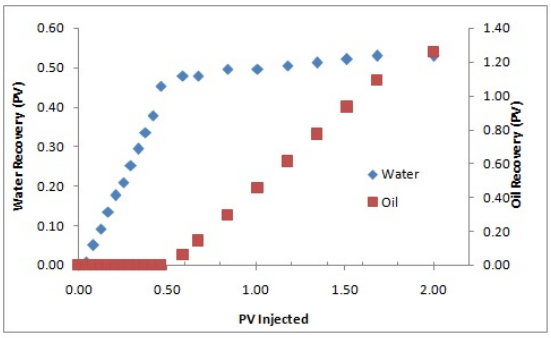

(a) Oilflood, cumulative oil and water production

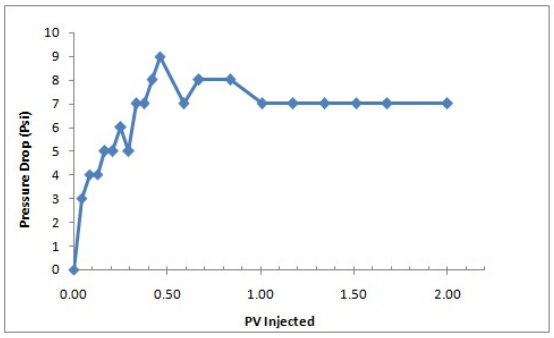

(b) Oilflood pressure drop

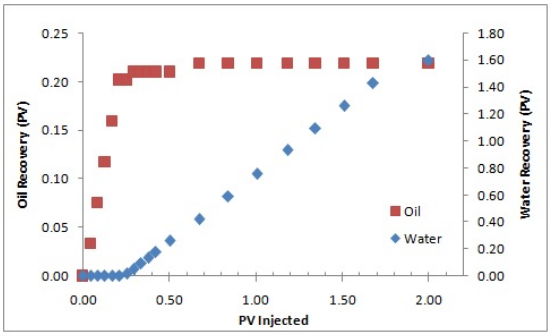

(c) Waterflood, cumulative oil and water production

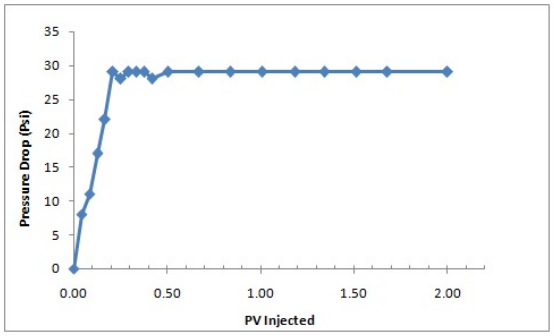

(d) Waterflood pressure drop

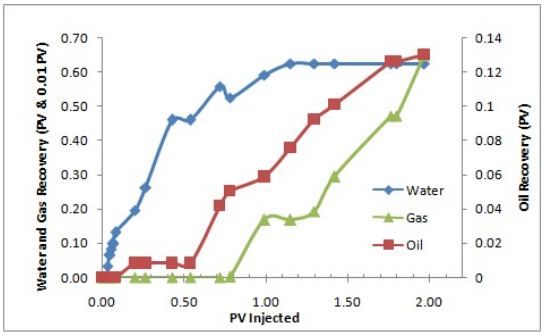

(e) Gasflood, cumulative liquid and gas production

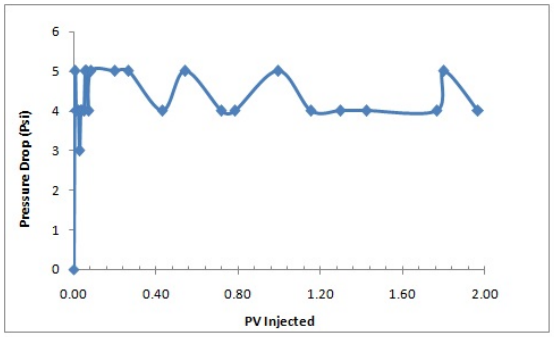

(f) Gasflood pressure drop

Figure 6.22: Immiscible N_2 flood: 1-ft Berea core, using nC_{10} for oil and using N_2 for gas injection. Brine has 5 % Nacl concentration. Core pressure is 2000 psi and 100°F. a) Drainage Cycle: Oilflood with nC_{10}. b) Imbibition Cycle: waterflood with brine. c) Tertiary N_2 flood: Pure N_2 continuous vertical immiscible injection.

during water displacement. Total produced oil at the end of waterflood was 26 cc (0.22 PV), presenting 38 % of original oil in place (OIIP).

N_2 was continuously injected at 2000 in a core on gravity mode, tertiary recovery mode. Figure 6.22eshows a tertiary N_2 flood: Pure N_2 vertical immiscible injection and pressure drop during the N_2-Assistd gravity drainage. Total oil produced at the end of 2PV was around (15.5 cc) giving around 36 % recovery of remaining oil in place (ROIP). As for the pressure drop, see Figure 6.22f.

6.2.3 Flue Gas Assisted Gravity Drainage Experiments

Three different gas coreflood sets were conducted using flue gas. All gas floods were conducted on GAGD mode and all runs were immiscible at 500 psi 1000 and 2000 psi.

6.2.3.1 Immiscible Flue Gas Injection at 500 psi and 100°F

Figure 6.23 summarizes flue gas gravity assisted drainage displacement experiment (core initialization, waterflood and gasflood) on 1-ft Berea Core at 500 psi. Similar to the earlier coreflood sets, the core was nC_{10} flooded. Figure 6.23a shows the amount of water recovered as oil was injected. The connate water saturation was 0.6.

Figure 6.23c shows the amount of oil recovered and water injected in the core during waterflood, secondary recovery, as a function of pore volume injected. Total oil produced at the end of waterflood was 28 cc (0.26 PV), yielding 68 % of original oil in place (OIIP). The pressure drop across the core was xx at the end of the flood, see Figure 6.23d.

Flue gas was continuously injected at 500 psi in a core on gravity mode, tertiary recovery mode. Figure 6.22e shows a tertiary flue flood: flue gas vertical immiscible injection and pressure drop during the flue gas-assisted gravity drainage. Total oil

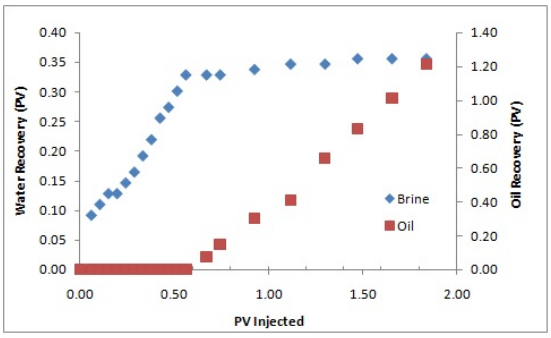

(a) Oilflood, cumulative oil and water production

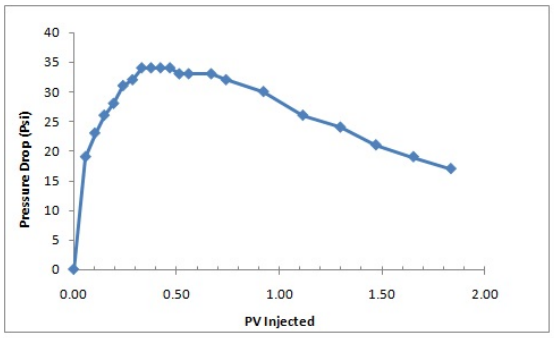

(b) Oilflood pressure drop

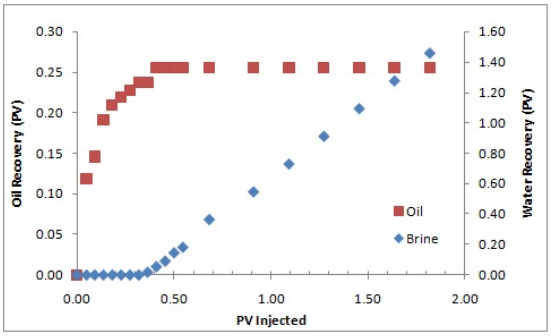

(c) Waterflood, cumulative oil and water production

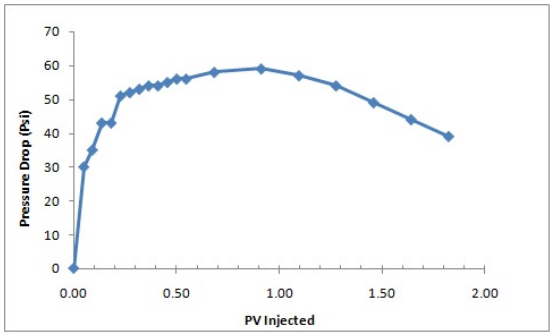

(d) Waterflood pressure drop

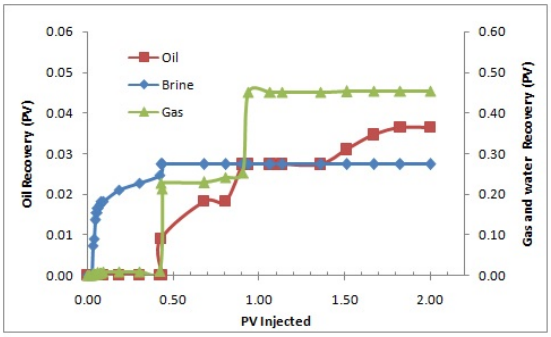

(e) Gasflood, cumulative liquid and gas production

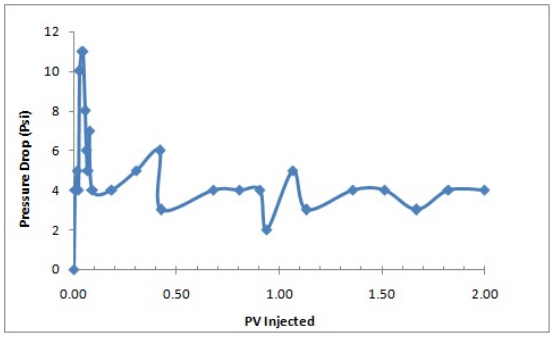

(f) Gasflood pressure drop

Figure 6.23: Immiscible flue gasflood: 1-ft Berea core, using nC_{10} for oil and using flue gas for gas injection. Brine has 5 % NaCl concentration. Core pressure is 500 psi and 100°F . a) Drainage Cycle: Oilflood with nC_{10}. b) Imbibition Cycle: waterflood with brine . c) Tertiary flue gasflood: flue gas continuous vertical immiscible injection.

produced at the end of 2 PVI was around 4 cc (0.03 PV) giving around 31 % recovery of remaining oil in place (ROIP). The pressure drop was around 4 psi at the end of flood, see Figure 6.23f.

6.2.3.2 Immiscible Flue Gas Injection at 1000 psi and 100°F

Figure 6.24 summarizes flue gas gravity assisted drainage displacement experiment (core initialization, waterflood and gasflood) on 1-ft Berea core at 1000 psi. After the core was ndecane flooded connate water saturation was determined to be 0.4. Figure 6.24a, shows the amount of water recovered as oil was injected in the core during nC_{10} injection.

Figure 6.24c shows the amount of oil recovered and water injected in the core during waterflood, secondary recovery, as a function of pore volume injected. Total produced oil at the end of waterflood was 24 cc(0.25 PV), presenting 41 % of original oil in place (OIIP). Pressure drop is shown in Figure 6.24d.

Flue gas was continuously injected at 1000 in a core on gravity mode, tertiary recovery mode. Figure 6.24e shows a tertiary flue flood: flue gas vertical immiscible injection and pressure drop during the flue gas-Assisted gravity drainage. Total oil produced at the end of 2 PV was around 13.5 cc (0.14 PV) giving around 40 % recovery of remaining oil in place (ROIP). The pressure drop was around 4 psi at the end of flood, pressure drop is illustrated in Figure 6.22f.

6.2.3.3 Immiscible Flue Gas Injection at 2000 psi and 100°F

Figure 6.25 summarizes flue gas gravity assisted drainage displacement experiment (core initialization, waterflood and gasflood) on 1-ft Berea Core at 2000 psi. After the core was n-decane flooded, pore volume and the connate water saturation were

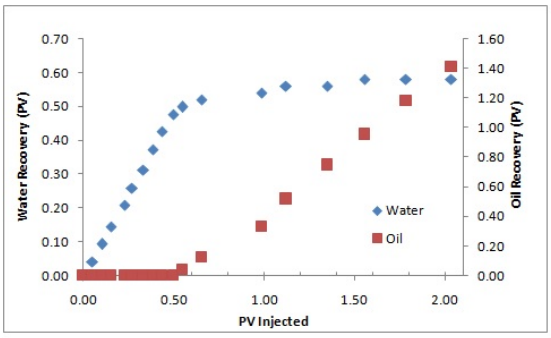

(a) Oilflood, cumulative oil and water production

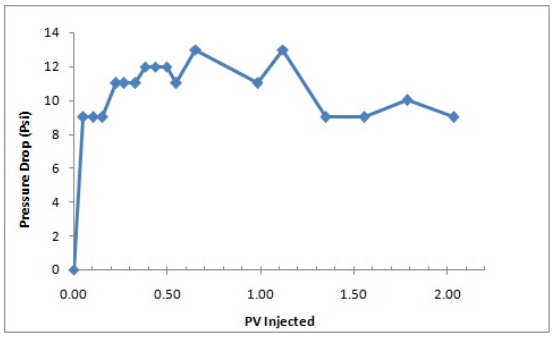

(b) Oilflood pressure drop

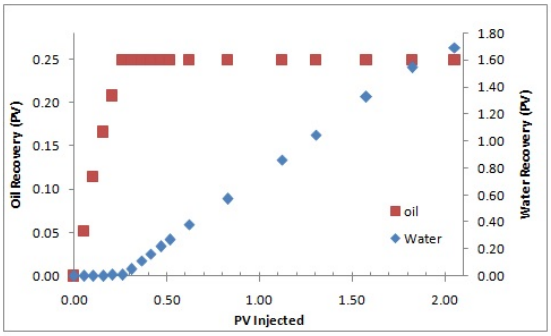

(c) waterflood, cumulative oil and water production

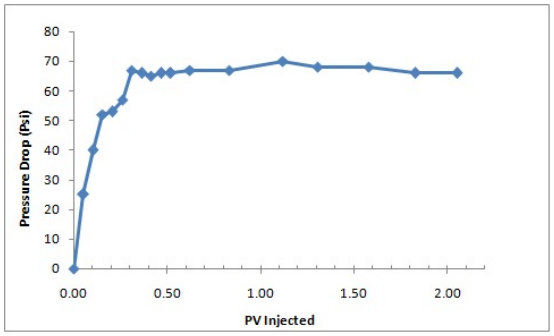

(d) waterflood pressure drop

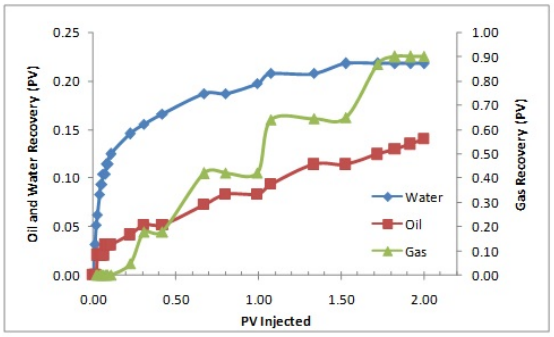

(e) gasflood, cumulative liquid and gas production

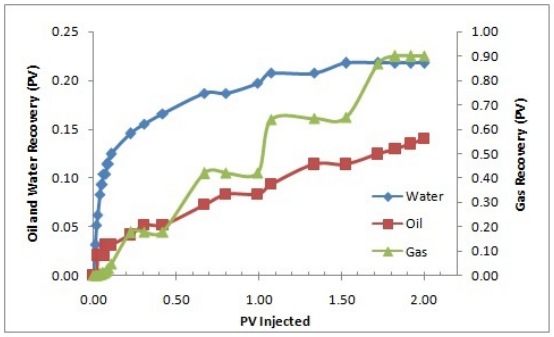

(f) gasflood pressure drop

Figure 6.24: Immiscible flue gasflood: 1-ft Berea core, using nC_{10} for oil and using flue gasflood for gas injection. Brine has 5 % NaCl concentration. Core pressure is 1000 psi and 100°F . a) Drainage Cycle: Oilflood with nC_{10}. b) Imbibition Cycle: waterflood with brine. c) Tertiary flue gasflood: flue gas continuous vertical immiscible injection.

as follows xx and 0.45. Figure 6.25a, shows the amount of water recovered as oil was injected in the core during nC_{10} injection.

Figure 6.25c, shows the amount of oil recovered and water injected in the core during waterflood, secondary recovery, as a function of pore volume injected. Total produced oil at the end of waterflood was 24 cc (0.23 PV), presenting 41 % of original oil in place (OIIP). pressure drop at the end of the flood was 66 psi, see Figure 6.25d.

Flue gas was continuously injected at 2000 in a core on gravity mode, tertiary recovery mode. Figure 6.24e shows a tertiary flue flood: flue gas vertical immiscible injection and pressure drop during the flue gas-Assisted gravity drainage. Total oil produced at the end of 2 PV was around 15 cc giving around 49 % recovery of remaining oil in place (ROIP). Here pressure drop is not reported because one of the two gauges gave faulty values.

6.2.4 Discussion

Based on the experimental results presented in this chapter the following are discussed:

1. Effect of injecting CO_2 on GAGD performance.
2. Effect of injecting N_2 on GAGD performance.
3. Effect injecting flue gas on GAGD performance.
4. Comparison between the performance of different gas types on GAGD mode.
5. IFT and GAGD recovery efficiency.
6. Comparison between flue gas injection using GAGD and other injection modes.
7. Dimensionless number and mechanisms involved.

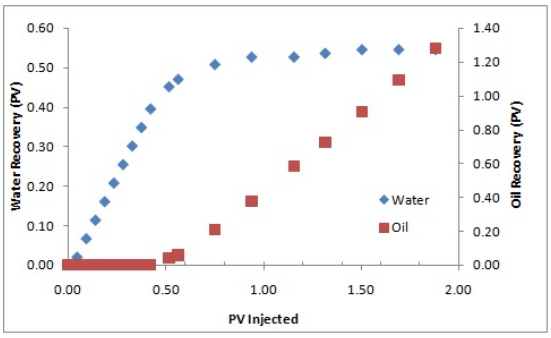

(a) Oilflood, cumulative oil and water production

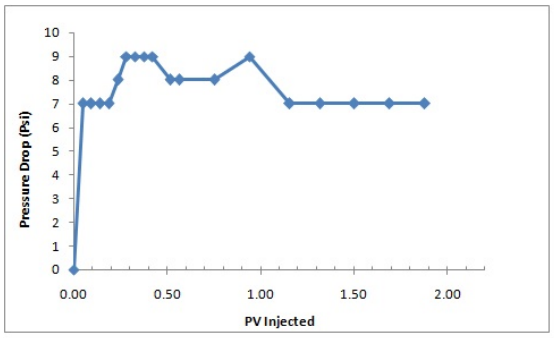

(b) Oilflood pressure drop

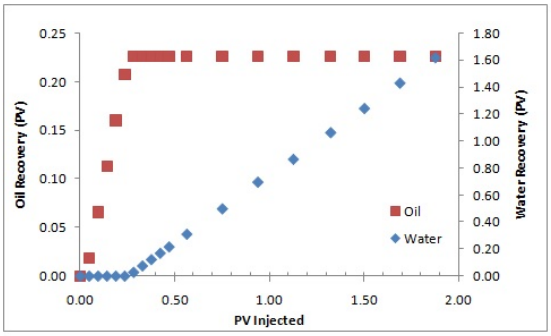

(c) waterflood, cumulative oil and water production

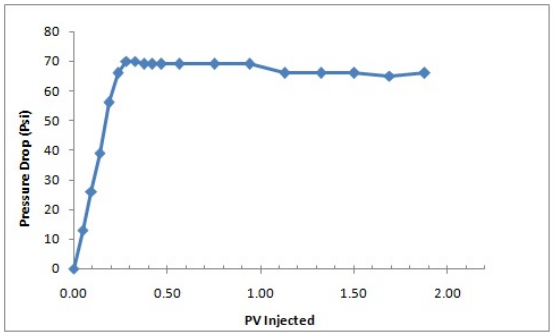

(d) waterflood pressure drop

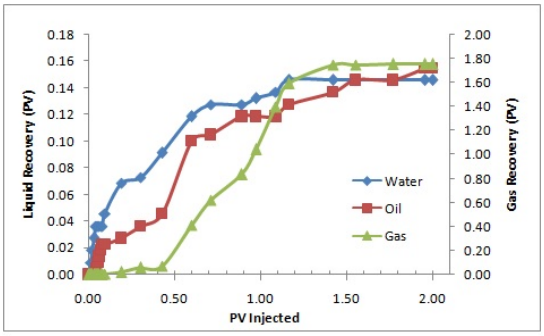

(e) gasflood, cumulative liquid and gas production

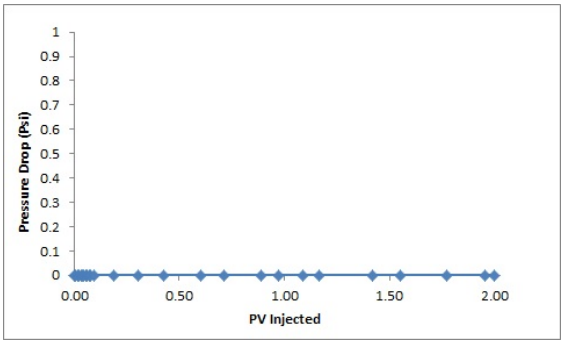

(f) gasflood pressure drop

Figure 6.25: Immiscible flue gasflood: 1-ft Berea core, using nC_{10} for oil and using flue gas for gas injection. Brine has 5 % Nacl concentration. Core pressure is 2000 psi and 100°F. a) Drainage Cycle: Oilflood with nC_{10}. b) Imbibition Cycle: waterflood with brine. c) Tertiary flue gasflood: Pure flue gas continuous vertical immiscible injection.

Table 6.7: Rock, fluid and recovery data for GAGD Core floods in this study

	Ptest	Abs Permeability	Core PV	WF Recovery	GF Recovery	Inc GF Recovery	Inc GF Recovery
				OIIP	OIIP	OIIP (2PV)	ROIP (2PV)
CO_2-nC_{10}	500	54	115	0.54	0.67	0.16	0.35
CO_2-nC_{10}	1000	54	120	0.47	0.97	0.55	0.94
CO_2-nC_{10}	2000	100	94	0.61	0.98	0.40	1.00
N_2-nC_{10}	500	127.74	116	0.38	0.58	0.20	0.30
N_2-nC_{10}	1000	150	118	0.36	0.65	0.21	0.31
N_2-nC_{10}	2000	200.56	119	0.38	0.60	0.22	0.36
Flue gas	500	25.55	110	0.68	0.80	0.12	0.31
Flue gas	1000	95.19	96	0.41	0.65	0.23	0.40
Flue gas	2000	100.28	106	0.41	0.69	0.29	0.49

6.2.4.1 Effect of Injecting CO_2 Gas on GAGD Performance

The effect of using CO_2 on GAGD floods was evaluated and reported previously, see section 2.7 for more details. Here the gasfloods were repeated in tertiraty mode and complemented with experimental IFT measurement. Figure 6.26 compares the different CO_2 assisted gravity drainage corefloods conducted in this study (at pressure 500, 1000 and 2000 psi). The Figure shows the oil recoveries at pressures 500 psi (immiscible condition), 1000 psi (immiscible condition but low IFT) and 2000 psi (above miscibility condition). The following can be summarized:

1. At 2000 psi, above miscibility pressure, the flood was the most efficient among the the three, followed by 1000 psi, near miscibility condition and 500 psi, immiscible run, the least efficient. The recoveries for the 500, 1000 and 2000 psi floods are 35, 94 and 100 % ROIP respectively.

2. The observation here agree with previous reported observations (Kulkarni 2005).

3. Low IFT pressure (1000 Psi) offers comparable recovery to the above miscibility run for CO_2-nC_{10} system. In other words, high oil recovery (more than 90 % of ROIP) was achieved even at gas-oil IFT of 4 mN/m.

4. CO $_2$ GAGD in Immiscible condition (here IFT pressure of 500 psi and IFT of 13.5 mN/m) offers atleast 35-40 % ROIP, incremental recovery after waterflood, which is considered high.

6.2.4.2 Effect of Injecting N_2 Gas on GAGD Performance

The effect of using N_2 gas for gravity stable GAGD floods is shown in figure 6.27. The following can be summarized:

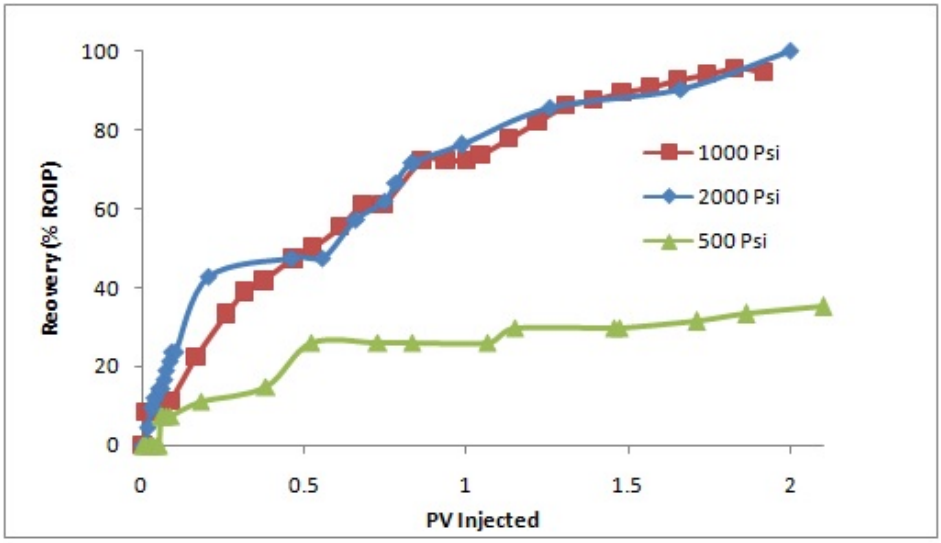

Figure 6.26: Comparison between CO_2 assisted gravity drainage floods for 500, 1000 and 2000 psi at 100°F.

1. The 2000 psi run was slightly better, followed by 1000 psi and 500 psi. All N_2 floods were at immiscible condition, however the difference in recoveries is attributed to increase in pressure (decrease in IFT).

2. The 1000 psi run took some time to recover oil, this is because initially the gas filled some empty void in the core.

3. Recoveries could be improved further increasing pressure(further reduction in IFT).

4. The oil recoveries resulted using N_2 are between 30-35 % ROIP, incremental recovery after waterflood, at pressure 500, 100 and 2000 psi. These recoveries are lower than CO_2 GAGD floods.

6.2.4.3 Effect of Injecting Flue Gas on GAGD Performance

The effect of using flue gas for gravity stable GAGD floods is shown in Figure 6.28.

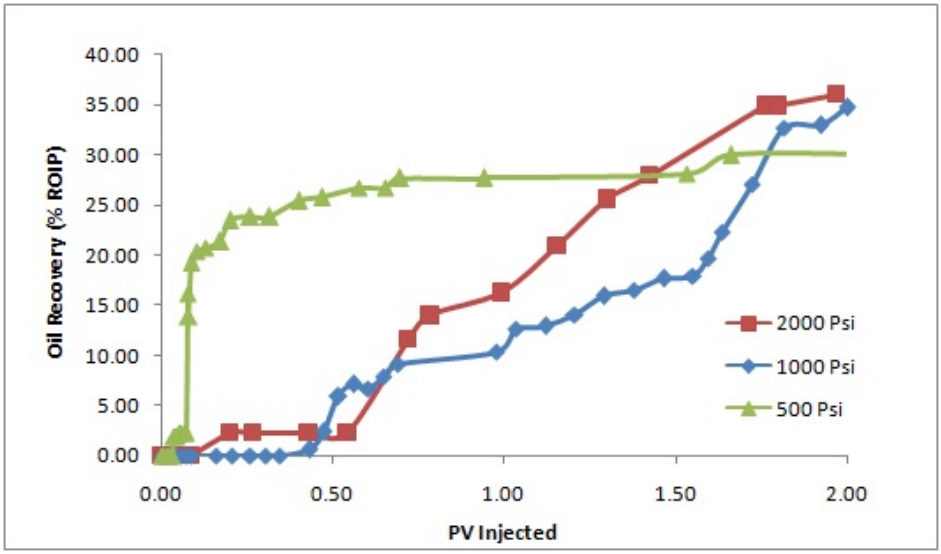

Figure 6.27: Comparison between N_2 assisted gravity drainage floods, 500, 1000 and 2000 psi at 100°F.

1. Similar to the other floods, the 2000 psi flue gas assisted gravity run was more efficient, followed by 1000 psi and 500 psi. Since all the runs were at immiscible condition the difference in recoveries was also be attributed to increase in pressure.

2. The 500 psi run took some time to recover oil, this is because initially the gas filled some empty void in the core before oil production.

3. The oil recoveries are 40-50 % ROIP. These recoveries are higher then the N_2 GAGD associated floods (recoveries or 30-35 % ROIP). This can be explained in terms of IFT, the flue gas-nC_{10} systems has lower oil-gas IFT at the corefloods compared to N_2 floods.

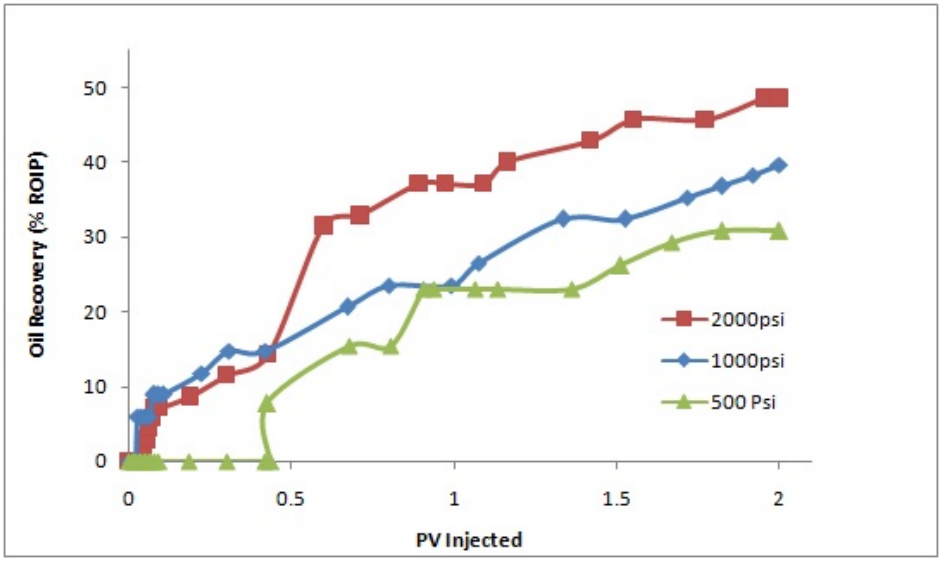

Figure 6.28: Comparison between flue gas assisted gravity drainage floods, 500, 1000 and 2000 psi at 100°F.

6.2.4.4 Comparison Between Different Injection Gases on GAGD

The performance of different gas types used in GAGD mode was compared at different pressures and fixed temperature. Figure 6.29 compares the oil recoveries as a function of pore volume injected of different gases, CO_2, N_2 and flue gas at 500 psi. The following can be summarized.

- The three gases are slightly different in recovery, CO_2 and flue gas resulted being slightly better compared to N_2 after 2 PVI.
- There was an early oil recovery for CO_2 and N_2 but the flue gas run started to recover oil after around 0.4 injected PV.
- Most of the recovery occurred around 0.5 PVI, $CO_2$and N_2, around 0.5-1.5 for the flue gas run.

Figure 6.30 compares the oil recoveries as a function of pore volume different gases, CO_2, N_2 and flue gas at 1000 psi. The following can be summarized:

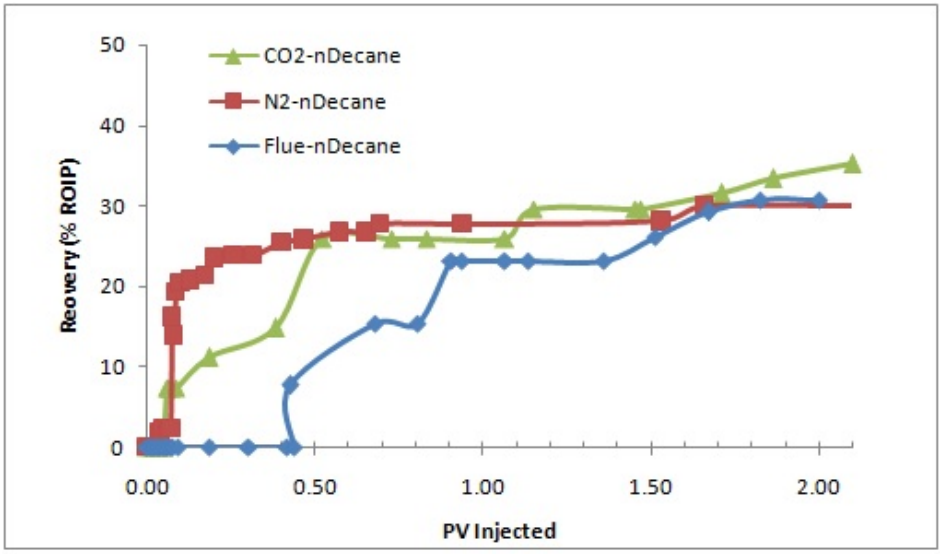

Figure 6.29: Comparison between different injection gases performance, CO_2, N_2 and flue gas on GAGD at 500 psi

- CO_2 flood recovered more oil compared to the two other gases. This is attributed to low gas-oil IFT flood.
- Flue gas is second better followed by N_2 gas in terms of recovery efficiency.
- Both CO_2 and flue gas runs started recovering oil immediately after injection.
- N_2 run started recovering oil after injecting more than 0.5 PVI of gas.
- The flue gas and N_2 profiles (still positive slope)indicate that more oil can be recovered if more gas was injected.

Figure 6.31 compares the oil recoveries as a function ed pore volume different gases, CO_2, N_2 and flue gas at 2000 psi. The following can be summarized:

- CO_2 in a better recovery compared to the two other gases, that is attributed to lower gas oil ratio IFT when CO_2 is used.
- Flue gas is second better followed by N_2 gas run in terms of recovery efficiency.

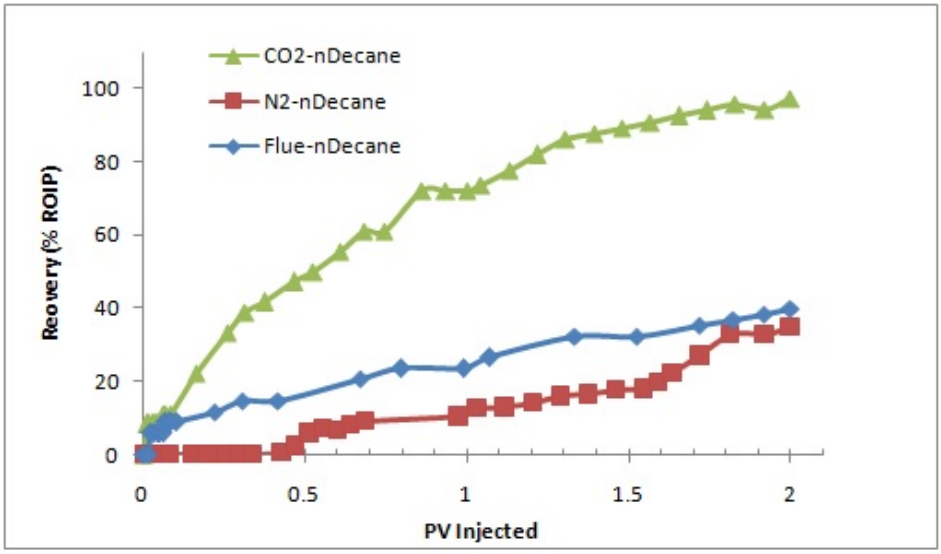

Figure 6.30: Comparison between different injection gases performance, CO_2,N_2 and flue gas on GAGD at 1000 psi

- Both CO_2 and flue gas runs started recovering oil almost at the beginning of the flood.
- N_2 run started recovering oil after injecting more than 0.5 PV of gas.
- The flue gas and N_2 profiles indicate that more oil can be recovered if we injected more gas.

6.2.4.5 IFT and GAGD Recovery Efficiency

This section relates IFT measurement presented in section 6.1.2 and the oil recovery efficiency of Tertiary-GAGD process. Figure 6.32, correlates the recoveries from corefloods with the IFT measured using pendent drop method. The following can be observed:

- The lower the IFT the higher the recovery. This statement agrees with all CO_2, N_2 and flue gas runs conducted in this study.

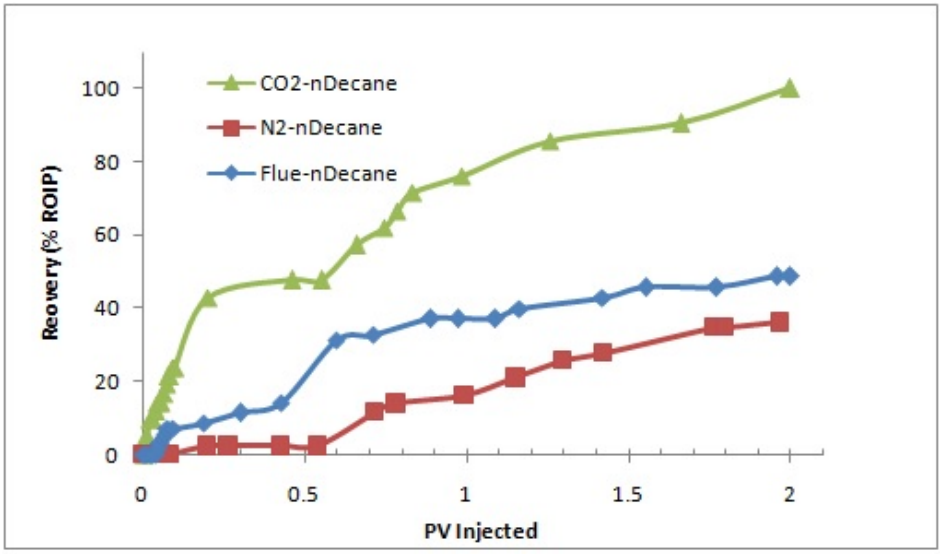

Figure 6.31: Comparison between different injection gases performance, CO_2,N_2 and flue gas on GAGD at 2000 psi

- Recoveries resulted from CO_2 are the highest among the cases tested in this study. This is because CO_2- nC_{10} offers (blue circle markers) low gas-oil IFT compared to the other gases used here.

- The more CO_2 in the gas-oil system the better is the recovery. So it can be inferred the recovery of flue gas GAGD can be enhanced if the percentage of CO_2 is increased.

6.2.4.6 Injection Pressure and GAGD Recovery Efficiency

Similarly this section relates injection pressure to the oil recovery efficiency of Tertiary-GAGD process. Figure 6.33 correlates the oil recoveries from corefloods with injection pressures. The following can be observed:

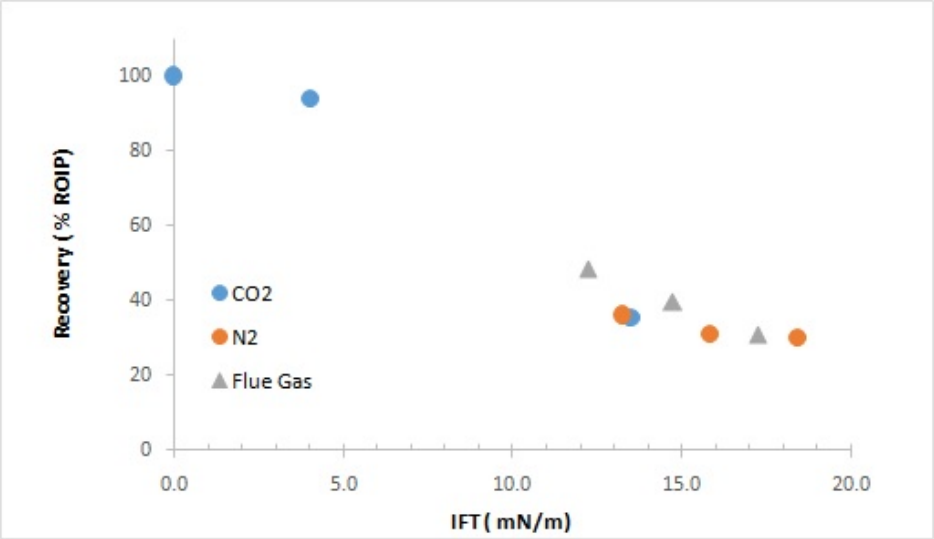

Figure 6.32: Oil recovery as a function of interfacial tension for system used in this study. Blue circle markers refer to CO_2- nC_{10} runs, orange circle markers refer to N_2- nC_{10} runs and triangle markers refer to flue gas- nC_{10} runs

- At low pressures of 500 psi all the runs were conducted at immmiscble condition, however, the CO_2 and the flue gas run resulted slightly in better oil recoveries than the N_2 run.
- At 1000 psi, the CO_2, was far better then the other two runs, due to gas-oil IFT being much lower then the other two cases at 1000 psi. This also proves the advantage of using CO_2 in gas injection.
- Flue gas run was better than the N_2 run in terms of recoveries.
- At higher pressure, the CO_2 is miscible nC_{10} and the recovery is 100 % in GAGD mode. The flue gas is the second best compared to N_2 flood.
- The recoveries due to N_2 and flue gas tend to increase with pressure and expected to result in 100 % recoveries at miscible conditions too.
- The incremental increase recoveries using flue gas is slightly higher than N_2.

Table 6.8: Summary of IFT data and GAGD coreflood recoveries using three different gas, CO_2, N_2 and flue gas.

	Pressure	IFT	Oil Recovery
	psi	mN/m	ROIP (2PV)
CO_2-nC_{10}	500	13.5	35.2
CO_2-nC_{10}	1000	4.1	95.8
CO_2-nC_{10}	2000	0.00	100
N_2-nC_{10}	500	18.4	30.0
N_2-nC_{10}	1000	15.9	31.0
N_2-nC_{10}	2000	13.3	36.0
Flue gas	500	17.2	31.0
Flue gas	1000	14.7	39.7
Flue gas	2000	12.2	48.6

6.2.4.7 Flue Gas Assisted Gravity Drainage in Secondary Mode

All GAGD floods presented earlier (nine cases using different injection gases)were on tertiary mode (cores were water flooded before GAGD runs). Kulkarani tested secondary GAGD using CO_2 and saw higher incremental when GAGD was implemented in secondary mode (see chapter 2). Therefore here it was decided to evaluate the recovery of GAGD in secondary mode using flue gas and compare it to reported results. The procedure described in section (5.3.2) were modified in such that the core was flooded with nDecane to determine connate water, skipped water flood and directly gas flooded the core (GAGD mode) using flue gas at 1000 psi for only 1PV. The secondary GAGD flue gas coreflood was compared with the tertiary flue gas mentioned earlier (for the p = 1000 psi case). Figure 6.34 compares between secondary and tertiary GAGD using flue gas, P=1000 psi and T= 100 ^oC. Y-axis represents recovery of remaining oil in place and x-axis pore volume injected (PVI).

The following can be summerised about the comparison seen in Figure 6.34:

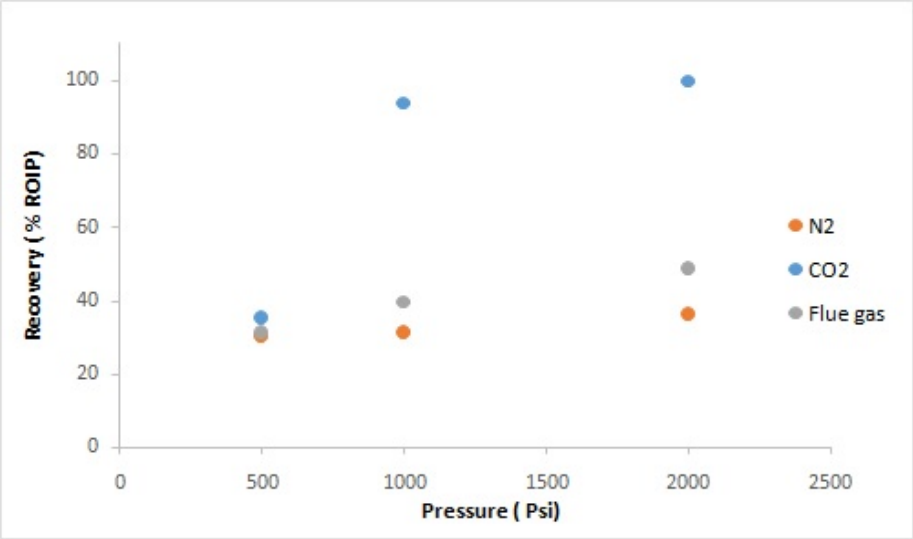

Figure 6.33: Oil recovery as a function of pressures for the systems used in this study. Blue circle markers refer to CO_2- nC_{10} runs, orange circle markers refer to N_2- nC_{10} runs and gray circle markers refer to flue gas- nC_{10} runs

- Secondary GAGD using flue gas achieved recovery of more than 41 % ROIP as opposed to 24 % ROIP in tertiary mode. In other words the secondary GAGD recovers an addition of 21 % oil recovery supporting the potential of flue GAGD.
- The recoveries at secondary model are comparable to what has been seen in other studies see the following section.
- The incremental can make flue gas Assisted gravity drainage attractive in the absence of other gases.

6.2.4.8 Comparison Between Secondary Flue Gas GAGD and Other Flue Gas Injection Mode

Literature survey on flue gas injection studies was summarized in chapter 2. This subsection compares GAGD performance using flue gas (thsi study) with reported results from Shokoya (2005) and Rivera (2010).

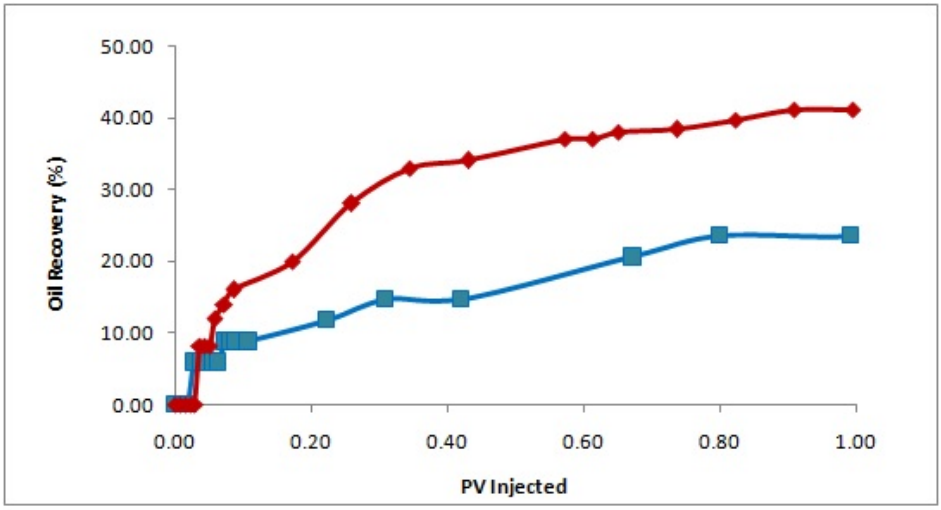

Figure 6.34: Comparison between Secondary and Tertiary GAGD using flue gas at 1000 psi and 100 °C. The comparisons only covered 1PVI. Blue curve is GAGD in tertiary mode and red curve is GAGD in secondary mode

Figure 6.35 compares the oil recovery reported by (Shokoya et al. 2005), using flue gas with different mode. The different cases reported are as follows:

- (WAG1a) WAG using (FG1) and Oil A at 27.7 Mpa
- (WAG1b) WAG using (FG2) and Oil A at 27.7 Mpa
- (WAG2a) WAG using (FG1) and Oil B at 17.6 Mpa
- (WAG2b) WAG using (FG1) and Oil B at 17.6 Mpa

The following can be summarized about the results reported by Shokoya (2005):

1. All gas injection runs were performed in secondary recovery mode. The core was initially saturated with water, then water was displaced by oil and finally three different injection gas types were used to displace oil, N_2, flue gas 1 (FG1) and flue gas-2 (FG2). FG1 contained 16 CO_2 and FG2 contained 30 % CO_2.

2. Two different reservoir oils were used (Oil A and B), with different composition, see section (2.8).

3. All floods were stopped at around 1 PV.

4. Total oil (B) recovery was 38 % using FG1 and 41 % using FG2 at 27.7 MPa (4017.5 psi).

5. Total oil (A) recovery was 45 % using FG1 and 50 % using FG2 at 17.6 MPa (2552.7 psi).

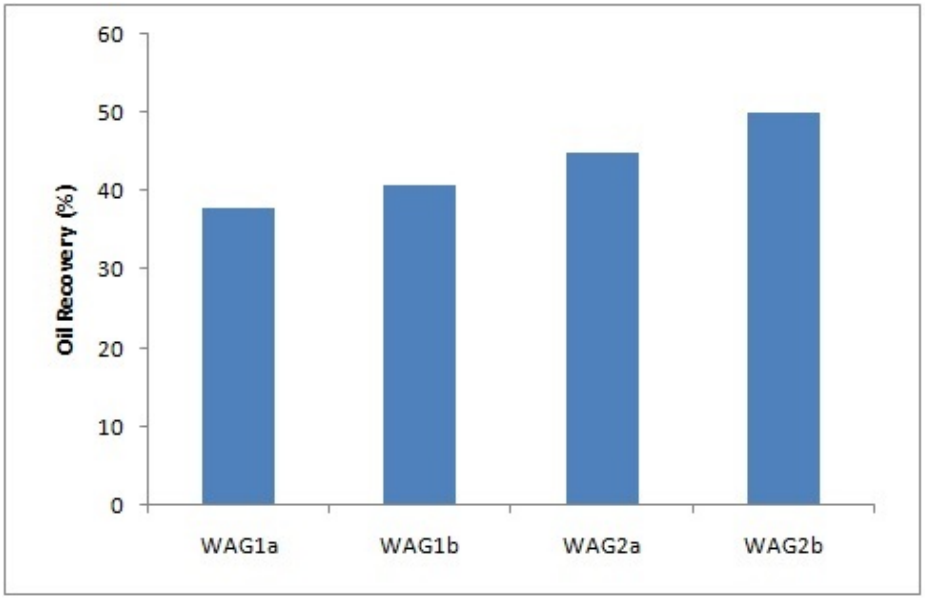

Figure 6.35: Shakoya Flue gas results(Shokoya et al. 2005).

Figure 6.36 compares the oil recovery reported by (Rivera et al. 2010), using flue gas with different mode. The different injection modes are as follows:

- Case-1 refer to contentious gas injection (CGI) at injection rate = 1 cc/min (CGI1).

- Case 2 refers to CGI at injection at pressure 4700 psi = 1 cc/min (CGI2).
- Case 3 CGI at injection at pressure 3600 psi = 1 cc/min (CGI3)
- Case 4 Slug gas injection 0.3 PV+ waterflood (WF) at 4700 = 1 cc/min (Slug1)
- Case 5 Slug gas injection 0.3 PV+ WF at 3600 = 1 cc/min (Slug1)
- Case 6 Injection Alternating of flue gas/water ratio (1:3) to complete 0.3 PV followed waterflooding at P =4350 psi (WAG-1).
- Case 7 Injection Alternating of flue gas/water ratio (1:1) to complete 0.3 PV followed waterflooding at P =4350 psi (WAG-2).

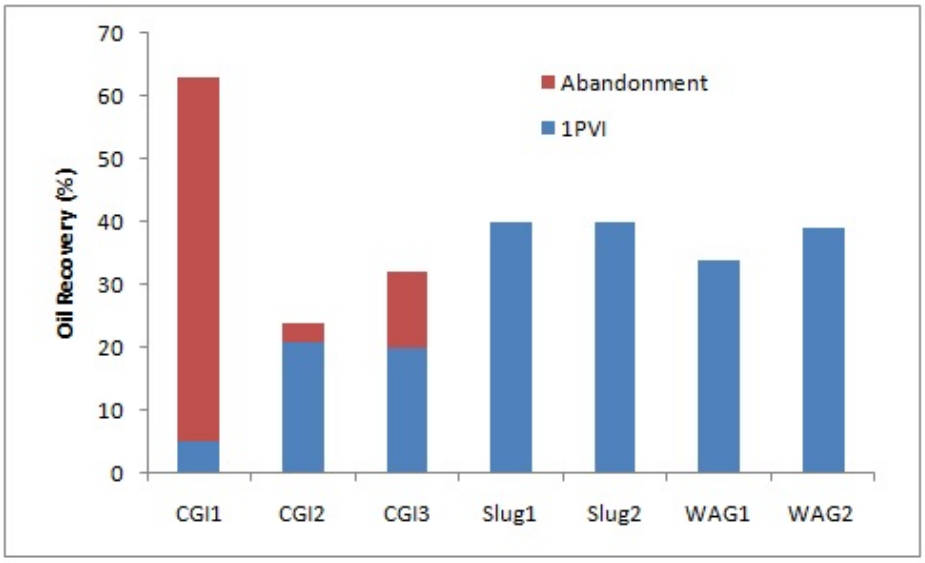

Figure 6.36: Rivera Flue gas results(Rivera et al. 2010).

The following can be summarized about the results:

1. All gas injection runs were performed in secondary mode, similarly to the other reported experiment.

2. Injection flue gas consisted of (15 % CO_2, 80 % N_2, 3.27 % O_2,0.06 % CH_4 and 1.69 % CO_1).

3. Live reservoir oil was considered at pressure of 2350 psi, see section (2.8).

4. The floods were stopped at different injection pore volume, mostly under 2 PVI.

5. The study reported different gas injection mode (contentious gas injection, slug gas injection and alternating of flue gas/water), all immiscible and in horizontal mode.

6. Total oil recovery recoveries ranged from 25-40 % ROIP (for less the 2 PVI).

Figure 6.37 compares the reported results of flue gas injection with this work, the following can be observed:

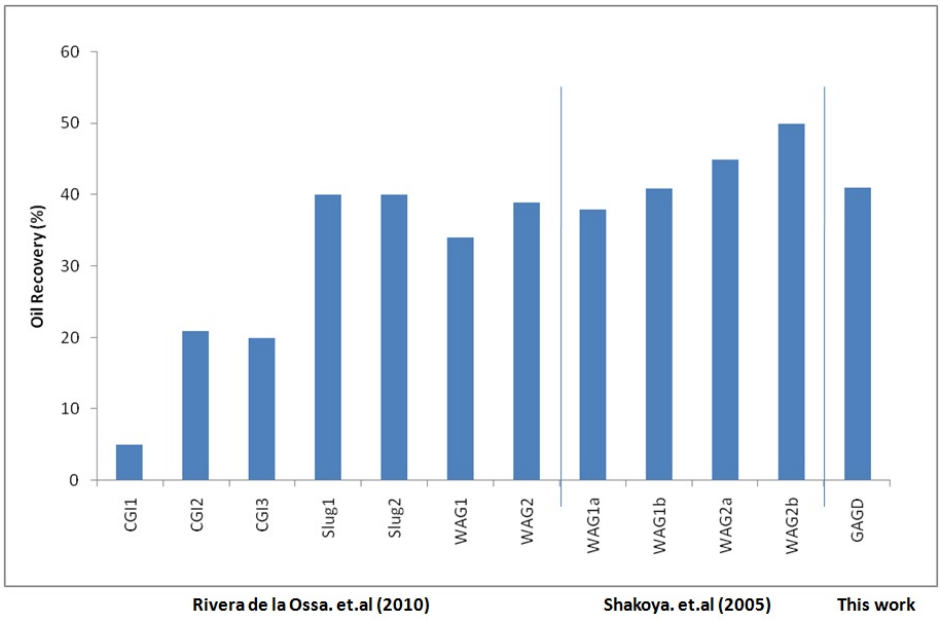

Figure 6.37: Comparison between, Rivera, Shakoya and this Flue GAGD results

1. The two reported studies are reporting gas injection (CGI, WAG, slug gas) in secondary mode and the recoveries are ranging between 20 to 50 % ROIP (less then 2 PVI) depending on gas injection type.

2. The two reported studies injected flue gas in horizontal mode and different injection type varying from CGI, WAG and slug gas.

3. Flue gas injection result in recovery up to 50 % ROIP, using either horizontal or vertical mode, depending on CO_2 percentage in flue gas.

6.2.4.9 Dimensionless Groups

To generalize the results dimensionless group numbers were calculated based on GAGD floods presented in this study. Three numbers are discussed in this section: capillary number (N_C), bond number (N_B) and gravity number (N_G),for more details refer to chapter 3. Capillary number compares viscous forces to capillary forces. Bond number compares buoyancy forces to capillary forces. The gravity number compares buoyancy forces to viscous forces. The objective here is to understand and evaluate mechanism involved.

Capillary Number: Capillary numbers of the nine core floods presented in this work were calculated and correlated to their respected remaining oil recovery after tertiary GAGD flood. This was done to assess the effect of viscous force to capillary force. Figure 6.38 shows capillary number values in x-axis and the experiment recoveries in the vertical axis. Nine experimental points were used, three flue gas immiscible gas injection run, three N_2 immiscible gas injection run and, two CO_2 immiscible gas injection run and one near miscible (low IFT) CO_2 gas injection run. The following can be seen clearly from the graph:

1. All the immiscible tertiary GAGD floods covered N_C range of 7.09 E-8 to 1.07 E-7 and recoveries of 30-49 %.

2. The low IFT CO_2 run, resulted in N_C of 3.22 E-7.

3. Similar experiment condition result in almost the same N_C results, since injection rate and viscosity are fixed and only depended on the IFT.

4. The data seem to show a trend, weather the near miscible run was included or not.

5. The data obtained through GAGD floods showed a correlation suggesting that the recoveries of GAGD can be predicted via capillary numbers assuming immiscible conditions.

6. All data can be combined and produce the following correlation,

$$\text{Oil recovery (with low IFT run)} = 3.68\ \text{E+8}\ N_p + 8.696$$

$$\text{Oil recovery (without low IFT run)} = 5\ \text{E+8}\ N_p - 9.161$$

7. Miscible GAGD does not follow the trend suggesting here. Here 2000 psi CO_2 is completely miscible, data is not shown in the graph.

Figure 6.39 shows capillary number values in y-axis and remaining oil saturation in the x- axis after GAGD floods. Nine experimental points were used, three flue gas immiscible gas injection run, three N_2 immiscible gas injection run and, two CO_2 immiscible gas injection run and one near miscible (low IFT) CO_2 gas injection run.

Bond Number: Similarly bond numbers of the nine core floods were calculated and correlated to their respected remaining oil recovery after tertiary GAGD flood. this was to assess the effect of buoyancy forces to capillary forces. Figure 6.40 shows bond

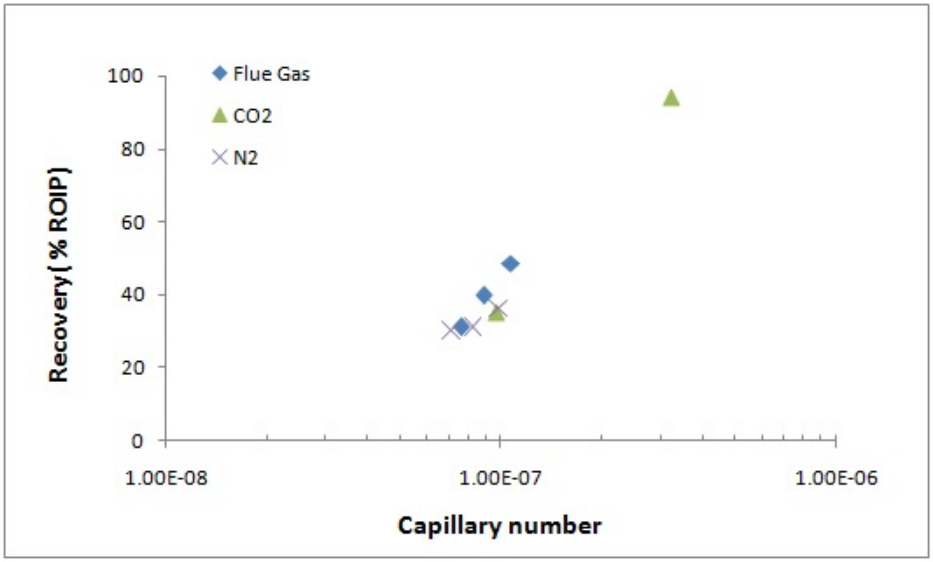

Figure 6.38: Capillary number vs. experimental recovery for GAGD core floods, using three different gas types. Pressure covered is 500-2000 psi. Gas used were flue gas, CO_2 and N_2. All floods were performed at 100 F and injection rate, 0.167 cc/min

number values in x-axis vs the experiment recoveries in the vertical axis. Eight experimental points were used, three flue gas immiscible gas injection run, three immiscible N_2 injection run and two immiscible CO_2 injection run. The following can be seen clearly from the graph:

1. All the immiscible tertiary GAGD floods covered N_B range of 5.8 E-8 to 4.04 E-7 and recoveries of 30-49 %.

2. CO_2 assisted gravity runs covered N_B range of 1.39 E-7 to 3.71 E-7 and recoveries of 35-40 %.

3. N_2 assisted gravity runs covered N_B range of 2.3 E-7 to 4.04 E-7 for recoveries of 30-36 %.

4. Flue gas assisted gravity runs covered N_B range of 5.8 E-8 to 2.4 E-7 for recoveries of 39-49 %.

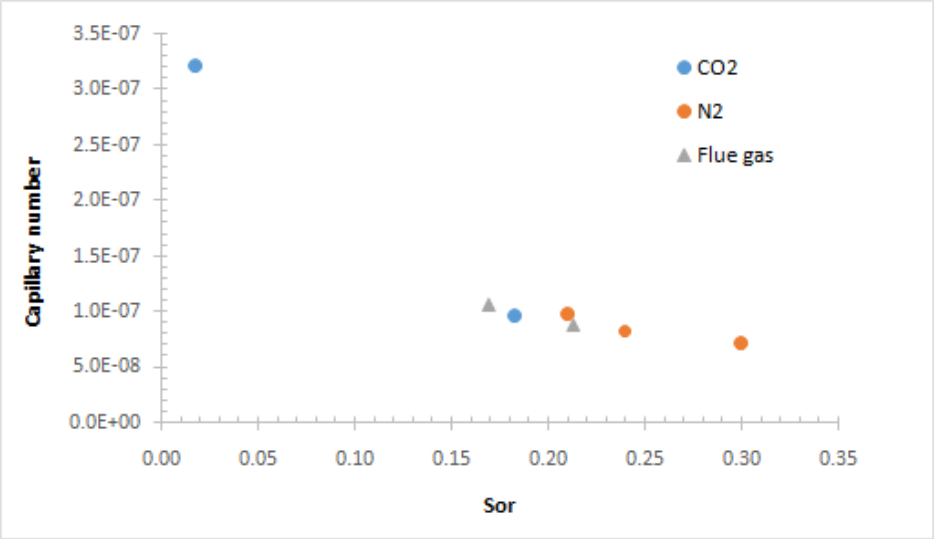

Figure 6.39: Capillary number vs. remaining oil saturation after GAGD core floods, using three different gas types. Pressure covered is 500-2000 psi. Gas used were flue gas, CO_2 and N_2. All floods were performed at 100 F and injection rate, 0.167 cc/min

5. The near miscible CO_2 run or miscible run were not considered here.

6. AT 500 psi, the first data point on the left of each gas type, the bond number varies per gas, highest being N_2 then CO_2 then flue gas. That is due to core permeability, which had the following values respectively 128, 54 and 26 md. The oil recoveries are slightly lower for N_2 run due to high IFT.

7. AT 1000 psi, we are only showing The N_2 and flue gas data since the CO_2 run was near miscible (recovery 94 % ROIP). The middle data point of N_2 and flue gas type, the bond number varies slightly since there was a small change in permeability of the core between the two cores, the recovery for N_2 was lower than the flue gas run, due to CO_2 content in the flue gas and subsequently a lower IFT.

8. AT 2000 psi, we are only showing The N_2 and flue gas data. The bond number varies due to change in permeability of the core between the two cores. Similar to the 500 and the 1000 psi cases the recovery for N_2 was lower than the flue gas run, due to CO_2 content in the flue gas and subsequently a lower IFT.

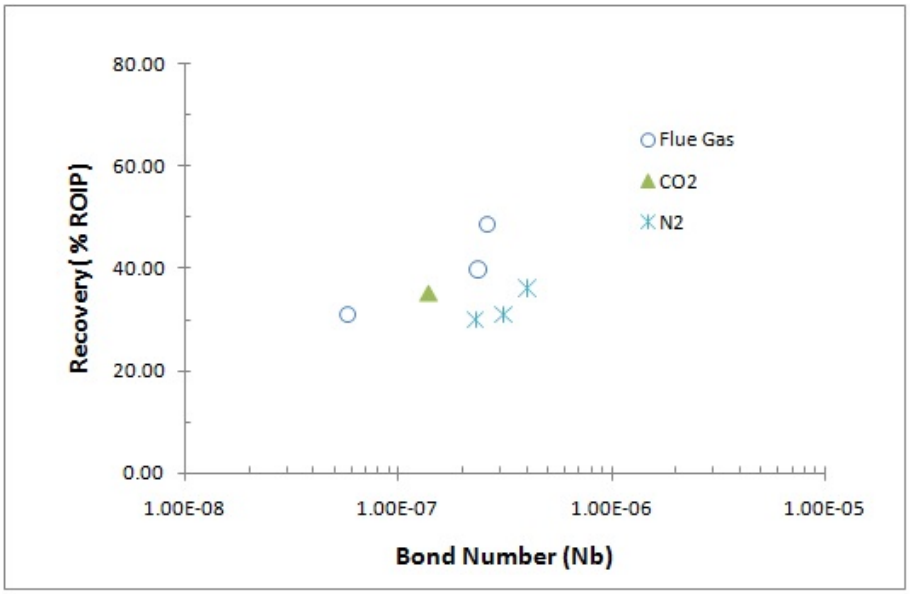

Figure 6.40: Bond number vs. experimental recovery for GAGD core floods, using three different gas types. Pressure covered is 500-2000 psi. Gas used were flue gas, CO_2 and N_2. All floods were performed at 100 F and injection rate, 0.167 cc/min

Gravity Number: Gravity numbers of the nine corefloods were calculated and correlated to their respected remaining oil recovery after tertiary GAGD flood. this was done to assess the effect of buoyancy forces to viscous forces. Figure 6.41 shows the gravity number values in x-axis vs the experiment recoveries in the vertical axis. Eight experimental points were used, three flue gas immiscible gas injection run, three N_2 immiscible gas injection run and two CO_2 immiscible gas injection run.

The following can be seen clearly from the graph:

1. All the immiscible tertiary GAGD floods covered N_G range of 0.8 to 4.1 and recoveries of 30-49 %.

2. CO_2 assisted gravity runs covered N_G range of 1.2 to 1.4 and recoveries of 35-94 %.

3. N_2 assisted gravity runs covered N_G range of 4 to 4.9 for recoveries of 30-36 %.

4. Flue gas assisted gravity runs covered N_G range of 0.8 to 2.5 for recoveries of 31-49 %.

5. The near miscible CO_2 run or miscible run were not considered here.

6. Similar variation is seen here, in the gravity number changes due to permeability change, since most of the parameters are fixed and their is small density change.

6.2.5 Summary

This section presents a summary of the GAGD experiments using three different gas mixtures-oil systems CO_2-nC10, N_2-nC10, (15 %) CO_2- (85 %) N_2- nC10 and. The experiments were designed to meet the following research objective: 1)asses the effect of different gas type on GAGD. 2) Asses the injection mode and injection type. 3) Asses dimensionless groups and suggest recommendations. The following are a summary of the main findings:

1. Nine GAGD core flood experiments were successfully performed at high pressure at 100 ^oF, miscible and immiscible modes.

2. Three different gas types were used in GAGD coreflood experiments, CO_2, N_2 and flue gas. Three sets of GAGD corefloods were performed and presented suc-

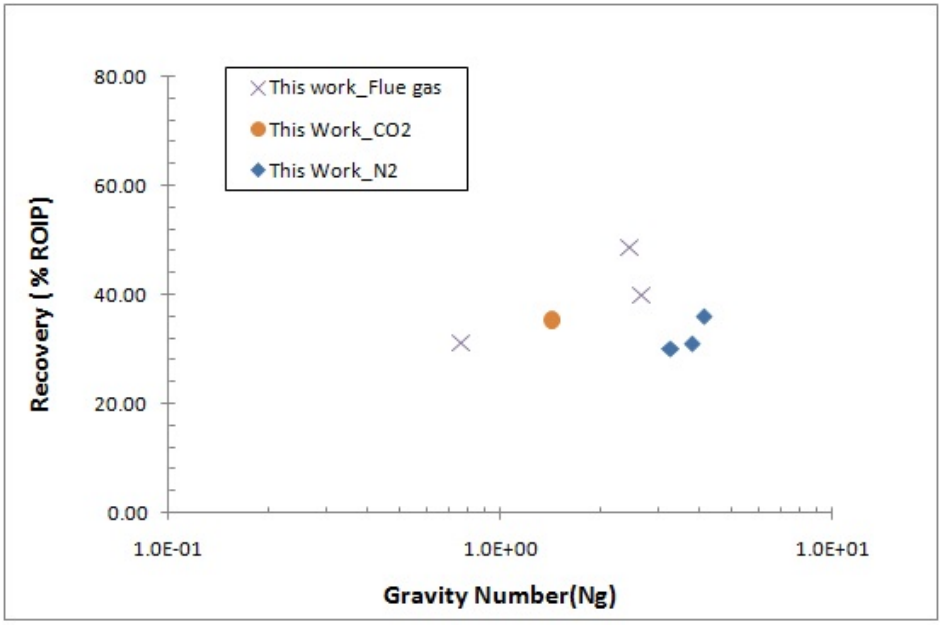

Figure 6.41: Gravity number vs. experimental recovery for GAGD core floods, using three different gas types. Pressure covered is 500-2000 psi. Gas used were flue gas, CO_2 and N_2. All floods were performed at 100 F and injection rate, 0.167 cc/min

cessfully. Each set is using a different injection gas, CO_2, N_2 and flue gas. For each set, three different pressures were tested, 500, 1000 and 2000 psi.

3. For the CO_2 runs, one was at immiscible condition, 500 psi, one was low IFT condition, 1000 psi, and the third was above miscibility condition, 2000 psi. The tertiary GAGD run resulted in the following recoveries 35.2, 95.8 and 100 % injected at 500, 1000 and 2000 psi respectively.

4. For the N_2 runs, all three runs were immiscible at P= 500, 1000 and 2000 psi. The tertiary GAGD run resulted in the following recoveries 30, 31 and 36 % at 500, 1000 and 2000 psi respectively.

5. For the flue gas runs, all three runs were immiscible at P = 500, 1000 and 2000 psi. The tertiary GAGD run resulted in the following recoveries 31, 40 and 49 % at 500, 1000 and 2000 psi respectively.

6. Miscible or near miscible injection is desirable in GAGD injection mode, as it leads to nearly 100 % oil recovery after water flood.

7. Flue gas offer better recoveries than N_2 and comparable to CO_2, that could be attributed to combination of GAGD displacement and CO_2 content in flue gas.

8. The lower the IFT the better the recovery in all the runs, that agrees with previous work (Kulkarni 2005) and with the notion of VIT.

9. Flue gas recoveries on GAGD mode were compared to the recoveries of flue gas on other injection mode, like WAG and CGI.

Chapter 7
Conclusions and Recommendations

7.1 Conclusions

7.1.1 Effect of Gas-Oil Ratio on VIT-MMP

1. VIT technique can be simulated by calculating densities and compositions using PR-EOS and calculating IFTs using Parachor model.
2. Adopting proper gas-oil IFT calculation procedure that reflects actual VIT experimental procedures, made it possible to obtain reliable prediction of gas-oil zero IFT pressure that agrees closely with VIT technique and other independent experimental IFT measurements.
3. Constant volumetric, constant molar gas-oil ratio or variable gas-oil ratio result in similar zero-IFT pressure of the gas-oil system which also agrees with the miscibility pressures from VIT experiments.
4. All analysis in this chapter and prior reported experiments (Sequeira, Ayirala, and Rao 2008; Ayirala and Rao 2011) suggest zero-IFT pressure is independent of GOR.
5. The resulting zero-IFT pressures based on the analysis are suggesting the robustness on the VIT technique in determining miscibility pressure.
6. This work provides more clarity to the ongoing discussion on VIT in addition to confirming the robustness of VIT method in estimating miscibility pressures for gas injection EOR projects.

7.1.2 Interfacial Tension method for detremintion Near Miscibility Pressure (NMP)

1. An IFT based approach was proposed here to estimate NMP of gas-oil systems. The method involves calculating densities and composition using and equation of state (EOS) and calculating interfacial tension using a Parachor model. The method is simple, robust and faster than the conventional slim tube simulation or the actual slim tube experiment.
2. A sensitivity analsyis was performed on Zicks fluids system to asses the influence of, Pc, Tc, IFT cutoff, Mw and Parachor constant on the IFT based method to estimate NMP. The analysis showed that the most prominent parameter on the proposed method is the IFT cutoff.
3. 12 reservoir fluid systems of varying compositions were tested using the proposed method and the estimated MMPs agreed with slim tube MMPs within about 7%.
4. The agreement of IFT-based NMP estimate to ST-MMPs indicate that the slim tube actually yields near miscibility pressure (at gas-oil IFT of 0.3 mN/m) rather than true miscibility pressure (MMP) which occurs at zero IFT pressure.

7.1.3 MMP of CO_2- N_2 Gas Mixture (Flue Gas)-Oil System

1. VIT technique, which is based on measuring interfacial tension at varying pressures to determine miscibility pressure, was successfully used to asses the miscibility of different mixtures gas with nC_{l0}.
2. Minimum miscibility pressure MMP for the nC_{10} with CO_2 and N_2 as injection gases were determined using VIT technique. The MMP of N_2 nC_{l0} system of 1465 psi was significantly higher then than the CO_2-nC_{l0} system of 1215 psi at 100 ^oF.

3. Minimum miscibility pressure MMP for the nC_{l0} with mixtures of CO_2 and N_2 as injection gases were determined using VIT technique. The MMP of CO_2 (15%)- N_2 (85%)- nC_{l0} system and CO_2 (85%)- N_2 (15%)- nC_{l0} system at 100 °F were, 4556 psi and 4687 psi respectively.
4. It was also shown that VIT method was fast and reliable in measuring miscibility pressures for different gas-oil system for gas injection purposes.
5. The Parachor model was used successfully to predict IFTs of the system used in this study.
6. The calculated VIT MMP, were close to the measured values, supporting the usage of calculation technique especially if you have experimental data to tune your EOS and use the method to test other affects (e.g. temperature and composition).

7.1.4 GAGD Corelfloods

1. Nine GAGD core flood experiments were successfully performed at high pressures and at 100 °F.
2. Three different gas types were used in GAGD core flood experiments, CO_2, N_2 and Flue gas. Three sets of GAGD core floods were performed and presented successfully. Each set is using a different injection gas, CO_2, N_2 and flue gas. For each set, three different pressures were tested, 500, 1000 and 2000 psi.
3. For the CO_2 runs, one was at immiscible condition, 500 psi, one was near miscible condition, 1000 Psi, and the third was above miscibility condition, 2000 psi. The tertiary GAGD run resulted in the following recoveries 35.2, 95.8 and 100% injected at 500, 1000 and 2000 psi respectively.

4. For the N_2 runs, all three runs were immiscible at P= 500, 1000 and 2000 psi. The tertiary GAGD run resulted in the following recoveries 30, 31 and 36 % at 500, 1000 and 2000 psi respectively.
5. For the flue gas runs, all three runs were immiscible at P= 500, 1000 and 2000 psi. The tertiary GAGD run resulted in the following recoveries 31, 40 and 49% at 500, 1000 and 2000 psi respectively.
6. Miscible injection is desirable in GAGD injection mode, as it leads to nearly 100% oil recovery after water flood.
7. Flue gas offers better recoveries than N_2 and comparable to CO_2, that could be attributed to combination of GAGD displacement and CO_2 content in flue gas.
8. The lower the IFT the better the recovery in all GAGD runs, that agrees with previous work (Kulkarni 2005) and with the notion of VIT.
9. Flue gas recoveries on GAGD mode were compared to the recoveries of flue gas on other injection mode, like WAG and CGI.

7.2 Recommendations for Future Work

Based on literature review and the study conducted here, the following recommendation are suggested:

7.2.1 Further VIT Laboratory Experiments

1. Measure miscibility pressure using different MMP experiments, VIT, slim tube and others for a good comparison. The following should be considered to get a valid comparison: 1) All experiment conditions should be fixed, pressure, temperature and oil composition. 2) The experiments should be simulated before conducting them to anticipate any limitation or difficulties. 3) GOR in VIT should

be controlled to enable a valid comparison between the methods. 4) live oil, multi-component oil, should be used. This set of experiments will provide a clear comparison, data that can be utilized to understand and maybe correlate the different MMP measurements.

2. VIT experiments should be conducted using Nitrogen and different multi-component oil, light medium and heavy viscosity. This will provide good data to evaluate further Parachor models, VIT models and other IFT prediction methods.
3. VIT experiments should be conducted conducted using flue gas and different multi-component oil, light medium and heavy viscosity. similarly, it will provide data to improve and test the IFT, Parachor, MMP and VIT prediction tools.
4. More controlled VIT experiments should designed to study different multi-component miscibility mechanisms using live oil.

7.2.2 Interfacial Tension Modeling and Determining Miscibility Pressures and Near Miscibility Pressure

1. Modeling concepts used in this work should be evaluated using different new equation of states available in literature.
2. Modeling concepts used in this work should be coded and designed to be used more efficiently.
3. Modeling concepts used in this work should further be developed and validated using experimental data.

7.2.3 Further GAGD Laboratory Experiments

1. Evaluate GAGD concept in carbonate rocks, dolomite and limestone. This should be investigated systematically to understand the impact of the following param-

eters: 1) heterogeneity. 2) Kv/Kh. 3) Miscibility effect, injection mode. 4) Wettability and IFT.

2. Evaluate GAGD concept in fractured rocks, sandstone or carbonate. This should also be investigated systematically to understand the impact of the following parameters : 1) heterogeneity. 2) Kv/Kh. 3) Miscibility effect, injection mode. 4) Wettability and IFT.
3. Design core floods to evaluate the effect of different fracture orientation on GAGD performance.
4. Corefloods experiments conducted in this study should be repeated using N_2 and different multi-component oil, light medium and heavy viscosity at different reservoir conditions.
5. Corefloods experiments conducted in this study should be repeated using flue gas and different multi-component light medium and heavy oil at different reservoir conditions.

,

Bibliography

Ahmadi, K, and R T Johns. 2011. "Multiple-Mixing-Cell Method for MMP Calculations." *SPE* 16 (4): 733–742 (Decemeber). SPE 116823-PA.

Alvarado, V, and E Manrique. 2010. "Enhanced Oil Recovery: An update review." *Energies* 3 (9): 1529–1575 (August).

Awari-Yusuf, I O. 2013. "Measurement of crude oil interfacil tesnion to determine minimum miscbility in carbon dioxide and nitrogen." Master thesis, Dalhousie University, Halifax, Nova scotia.

Ayirala, S, and D N Rao. 2006. "A new mechanistic Parachor model to predict dynamic interfacial tension and miscibility in multicomponent hydrocarbon systems." *Journal of Colloid and Interface Science* 299:321331.

Ayirala, S C. 2005. "Measurement and Modeling of Fluid-Fluid Miscibility in Multicomponent Hydrocarbon Systems." PhD Dissertaion, LSU, Baton Rouge, Lousiana.

Ayirala, S C, and D Rao. 2011. "Comparative Evaluation of a New Gas/Oil Miscibility-Determination Technique." *J.Canadian Pet. Tech* 50 (9): 71–81 (Septemebr/October). SPE 99606-PA.

Ayirala, S C, and D N Rao. 2007. "Misbility determination from gas-gil interfacil tension and P-R equation of state." *The canadian Journal of Chemical Engineering* 85 (9): 302–312.

Blaskovich, F T. 2000, April. "Historical Problem with Oil Field Rejuvenation." *Proceedings of SPE Asia Pacific Conference on Integrated Modelling for Asset Management*. Yokohama, Japan. SPE 62518,.

Christensen, J R, E H stenby, and A Skauge. 2001. "Review of WAG Field Experience." pp. 97–106.

Christiansen, R L, and H H Haines. 1987. "Rapid Measurement of Minimum Miscibility Pressure With the Rising-Bubble Apparatus." *SPE RE* 20 (November): 523–527.

Danesh, A. 1998. *PVT and phase behaviour of petroleum reservoir fluids*. Volume 47. New York : Elsevier.

Dindoruk, B, F M Orr, and R T Johns. 1997. "Theory of Multicomponet Miscible Displacement with Nitrogen." *SPE* 2 (3): 268–297 (September). SPE 30771-PA.

D. W. Green, G. P. Willhite. *Enhanced Oil Recovery*. Volume 6. SPE.

Elsharkawy, A M, F H Poettmann, and R L Christiansen. 1996. "Measuring Minimum Miscibility Pressure: Slim-Tube or Rising-Bubble Method?" *Energy and Fuels* 10:443–449. SPE 99606-PA.

Ghorbani, M, A Momeni, S Safavi, and A Gandomkar. 2014. "Modified vanishing interfacila tension(VIT) test for CO2-oil minimum miscibility pressure(MMP) measurement." *Journal of Natural Gas Science and Engineering* 20:92–98.

Girifalco, L A, and R J Good. 1957. "Good A Theory for the Estimation of Surface and Interfacial Energies. I. Derivation and Application to Interfacial Tension." *J. Phys. Chem*, p. 904912.

Guggenheim, E A. 1945. "The principle of corresponding states." *J. Chem. Phys.*, p. 253261.

Hearn, C L, and C H Whitson. 1995. "Evaluating Miscible and Immiscible Gas Injection in the Safah Field, Oman." *Proceedings of th 13th SPE Symposium on reservoir simulation*. San Antonio, Texas. SPE 25115.

Holm, L W. 1986. "Miscibility and miscible Displacement." *Petroleum Technology* 38 (8): 817–818 (August).

Hough, E W, and G L Stegemeir. 1961. "Correlation of surface and interfacial tension of light hydrocarbons in the critical region." *SPEJ*, vol. 259.

Jadhawar, P S. 2010. "Co-assisted gravity drainage EOR: numerical simulation and scaling models study." PhD Dissertaion, University of Adelaide, Australian School of Petroleum.

Jaubert, J-N, L Avaullee, and J-F Souvay. 2002. "A crude oil data bank containing more than 5000 PVT and gas injection data." *J. Petroleum Science and Engineering* 34 (1-4): 65–107 (June).

Jessen, K, and F M Orr. 2008. "On interfacial Tension Measurements to estimate minimum miscibility pressure." *SPE. Res. Eval. Eng* 11 (5): 933–939 (October). SPE-110725-PA.

Johns, R T, and F M Orr. 1996. "Miscible Gas Displacment of Multicomponent Oils." *SPE* 1 (1): 39–50 (March). SPE 30798-PA.

Kulkarni, M M. 2005. "Multiphase Mechanisms and Fluid Dynamics in Gas Injection Enhanced Oil Recovery Processes." PhD Dissertaion, LSU, Baton Rouge, Lousiana.

Kuo, S S. 1985. "Prediction Of Miscibility for the Enriched Gas drive process." *Proceedings of SPE Annual Technical Conference and Exhibition.*

Lake, L. *Enhanced Oil Recovery.* Volume 6. SPE.

Lee, S T, and M C Chien. 1984. "A new Multicomponent surface Tension correlation based on scaling theory." *Proceedings of SPE improved Oil Recovery Sympsium.* Tulsa, Oklahoma.

Luks, K D, E A Turek, and L E Baker. 1987. "Calculation of Minimum Miscibility Pressure." *SPERE* 2 (4): 501–506 (November). SPE 14929-PA.

Maclead, D B. 1923. "On a realtion Between Surface Tension and Density." *Faraday.*

Mahmoud, T N. "Demonstration and Performance Characterization of the Gas Assisted Gravity Drainage (GAGD) Process Using a Visual Method." Master's thesis, LSU.

Metcalf, R S, D D Fussel, and J L Shelton. 1973. "A Multicell Equilibrium Separation Model for the study of Multiple Contact Miscibility in Rich Gas Drives." *SPE* 13 (3): 147–155 (June). SPE 3995-PA.

Metcalfe, R D, and L Yaborough. 1979. "The effect of Phase Equilibiria on teh CO2 Displacment Mechanism." *SPE* 19 (4): 242–252 (August).

Nagarajan, N, K A Gasem, and R L Robinson. 1990. "A Framework for the Prediction of Densities and Interfacial Tensions for CO2 + Hydrocarbon Systems. 6. CO2 + n-Butane + n-Decane." *SPE*, pp. 228–231. review.

Nour, A, and D L Lock. 1988. "Prediction of the Minimum Miscibility Pressure of Vaporizing Gas Drive." *SPERE* 3 (1): 182–198 (February). SPE 15075-PA.

Orr, F M., and K Jessen. 2007. "An analysis of vanishing interfacial tension technique for Determination of minimum miscibility pressure." *Fluid Phase Equilibria* 255 (July): 99–109.

Paidin, W. 2013. "Evaluation Of Gas-Assisted Gravity Drainage Eor Process Applicability In A Louisiana Oil Field Through Experiments And Reservoir Simulation." PhD Dissertaion, LSU, Baton Rouge, Lousiana.

Paidin, W R. "Physical model experiments to evaluate the effect of wettability and fractures on the The gas assisted gravity drainage (GAGD) performance." Master's thesis, LSU.

Peng, D Y, and D B Robinson. 1976. "A new Two-Constant Equation of State." *Ind. Eng. Chem. Fundamen* 16 (1): 59–64 (February).

Rao, D. 2001. "Gas Injection EOR- A New Meaning in the New Millennium." *J. Canadian Pet Technology* 40 (2): 11–18.

Rao, D N. 1997. "A new Vanishing Interfacial Technique for Miscibility Determination." *Fluid Phase Equilibria* 139 (December): 311–324.

Rao, D N, S C Ayirala, and M M Kulkarani. 2004. "Development of Gas Assisted Gravity Drainage (GAGD) Process for Improved Light Oil Recovery." *Proceedings of SPE/DOE Symposium on Improved Oil Recovery.* Tulsa, Oklahoma. SPE 89357.

Rao, D N, and J Lee. 2003. "Determination of gasoil miscibility conditions by interfacial tension measurements." *Journal of Colloid and Interface Science* 262 (June): 574–482.

Rao, D N, and J I Lee. 2002. "Application of the New Vanishing Interfacial Tension Technique to Evaluate Miscibility Conditions for the Terra Nova Offshore Project." 35:247–262.

Rivera, J E, A Bejarano, A Anaya, and N Santos. 2010. "Experimental Evaluation of the Flue-Gas Injection of Barrancabermeja Refinery as EOR Method." *SPE International Conference on CO2 Capture, Storage, and Utilization.* New Orleans, Louisiana, USA. SPE-139715.

Rotenberg, Y, L Boruvka, and L Neumann. 1983. "Determination of surface tension and contact angle from the shapes axisymmetric fluid interfaces." *Journal of Colloid and Interface Science* 93:169.

Saini, D, and D Rao. 2010, May. "Experimental Determination of Minimum Miscibility Pressure (MMP) by Gas/Oil IFT Measurements for a Gas Injection EOR Project." *Proceedings of PE Western Regional Meeting.* Anaheim, California, USA. SPE 132389.

Schechter, D S, and B Guo. 1998. "Parachor Based on Modern Physics and Their Uses in IFT Prediction or reservoir Fluids." *SPE. Res. Eval. Eng* 1 (3): 207–217 (June). SPE 30785-PA.

Sequeira, D S. "Reservoir condition Measurements of Compositional Effects On Gas Oil Interfacial Tension and Miscibility." Master's thesis, LSU.

Sequeira, D S, S C Ayirala, and D N Rao. 2008. "Reservoir condition Measurements of Compositional Effects On Gas Oil Interfacial Tension and Miscibility." *Proceedings of SPE improved Oil Recovery Sympsium.* Tulsa, Oklahoma. SPE 113333.

Sharma, A P. "Physical model experiments of the gas-assisted gravity drainage process." Master's thesis, LSU.

Shokoya, O S, S A Mehata, R G Moore, and B B Maini. 2005. "Effect of CO2 Concenrtaion on Oil Recoevry in Enriched Flue Gas Flood." *Proceedings of SPE Annual Technical Conference and Exhibition*. Dallas, Texas. SPE 97262.

Stalkup, F I. 1983. *Miscible Displacement*. Volume 8 of *Henry L. Doherty series*. Henry L. Doherty Memorial Fund of AIME, Society of Petroleum Engineers of AIME. SPE Monogrph.

Stalkup, F L. 1987. "Displacement behavior of the condensing/vaporizing gas drive process." *Proceedings of SPE Annual Technical Conference and Exhibition*. Dallas, Texas. SPE 16715.

Walsh, P, and L Lake. 2008. "Enhanced Oil recovery Field Data Literature search." Technical report, University of Texas at Austin, Austin, TX.

Wang, Y, and F M Orr. 1997. "Analytical Calculation of Minimum Miscibility Pressure." *Fluid Phase Equilibria* 139 (December): 101–124.

Weinaug, C F, and D L Katz. 1943. "Surface Tension for Methane-Propane Mixtures." *Industrial and Engineering Chemistry*.

Whitson, C, and M Brule. 2000. *Phase Behavior*. Volume 20 of *Henry L. Doherty series*. Henry L. Doherty Memorial Fund of AIME, Society of Petroleum Engineers of AIME. SPE Monogrph.

Whitson, C H, and M Michelsen. 1989. "The Negative Flash." *Fluid Phase Equilibria* 53 (December): 51–71.

Winprop. 2013. *version 7.10.0 (R2010a)*. Calgary, Cananda: Computer Modeling Group.

Xiang, Z, and E H. Stenby. 1997. "Calculation of interfacial tensions with gradient theory." *Fluid phase equilibria*, pp. 139–158.

Zhou, D, and F m Orr. 1998. "Analysis of rising-bubble experiments to determine minimum miscibility pressures." *SPEJ*, pp. 19–25.

Zick, A A. 1986, October. "A Combined Condensing/Vaporizing Mechanism in the Displacement of Oil by Enriched Gases." *Proceedings of SPE Annual Technical Conference and Exhibition*. New Orleans, Louisiana. SPE 15493.

Vita

Mohamed Al Riaymi was born in Dubai, United Arab Emirates. After completing high school in Oman in 1997, Mohamed attended Loughborough college, UK. Then he attended Leeds University and received a Bachelor of Science in Physics in 2002 and a Master in science in petroleum engineering from Imperial College of London, UK. After graduation, Mohamed joined Petroleum Development of Oman (PDO)as a reservoir engineer, where he worked over 5 years. During which he was involved in number of field development projects exposing him to wide range of petroleum skills. Mohamed later joined the PhD graduate program in Louisiana State University (LSU).